Mechanistic Investigation of Oxygen Activation and *cis*-Dihydroxylation by Rieske Dearomatizing Dioxygenases

A DISSERTATION

SUBMITTED TO THE FACULTY OF

UNIVERSITY OF MINNESOTA

BY

Brent Stuart Rivard

IN PARTIAL FULFILLMENT OF THE REQUIREMENTS

FOR THE DEGREE OF

DOCTOR OF PHILOSOPHY

ADVISOR: JOHN D. LIPSCOMB

March 2016

Acknowledgements

First, I give great thanks to my advisor John D. Lipscomb for the dedication and effort he put into my graduate level training as a scientist. His wisdom and guidance was truly invaluable. John's tutelage has made me a better scientist and person. Thank you for sticking with me and for the fantastic wine along the way.

I am deeply grateful for the support of family and friends. I thank my parents, to whom I dedicate this work. I also thank my brother (Todd Rivard) and sister (Stephanie Caves), and their respective families, for their love and support. I would like to especially thank the Caves family for taking me in during a turbulent crossroads in my life and graduate career. Your kindness and generosity helped me stay the course. I started graduate school with a wonderful cohort of fellow students who I thank for many fun times. Without the frequent gatherings, graduate school would have been a lonelier and more frustrating place. I wish you all great success in your future endeavors.

I thank the current and past members of the Lipscomb lab for all of the help and guidance. It has truly been an honor to work with such helpful and knowledgeable people. Thank you to Dr. Melanie Rogers for everything she does to keep the lab running smoothly. Melanie contributed greatly to the research presented herein and it would not have happened without her. I thank Prof. Tom Makris for his formative mentorship and subsequent friendship. I also acknowledge Anna Komor, working with her on the CmlI project has greatly enriched my graduate school experience.

Thanks to the collaborators who have contributed to this work. Thanks to Daniel Marell and Prof. Christopher Cramer of the University of Minnesota for providing computational analysis (Chapter 3). I thank Kyle Sutherlin, Dr. Lei Liu, and Prof. Edward Solomon of Stanford University for collection and analysis of the NRVS data (Chapter 4). I thank Prof. Yisong (Alex) Guo of Carnegie Mellon University for providing Mössbauer analysis (Chapter 4). I also thank Prof. Larry Que for accepting me as an adopted member of the Que group during group meeting and other lab events.

Last, but certainly not least, I want to thank Charlie Parr for playing at the Turf Club (St. Paul MN) the fateful Sunday evening in August I meet my wonderful wife. Hannah, I love you beyond words. I cannot thank you enough for your support and understanding. You are, by far, the best "result" I have gotten during graduate school.

Dedication

To my parents, Stuart and Diane Rivard.

No matter what mountaintop I have set out to summit, your response has always been, "we believe in you, take these new boots."

Thanks you for your steadfast love and support.

Abstract

Rieske dearomatizing dioxygenases are multicomponent enzymes that catalyze a biochemically unique regio and stereospecific *cis*-dihydroxylation of aromatic compounds. The active site of the terminal oxygenase component contains a nonheme mononuclear iron and a [2Fe-2S] Rieske cluster. The isolated oxygenase component (hereafter RDD) can rapidly form product in a single turnover (STO) reaction after stoichiometric reduction of the metal centers and exposure to substrate and O_2. After product formation, both metal centers are oxidized, indicating that two non-substrate-derived electrons are required for the reaction. The normal O_2-driven STO reaction is complete in $\ll$1 second and no reaction cycle intermediates have been detected. Past studies have also shown that the fully oxidized RDDs can form product by utilizing H_2O_2 as the source of both oxygen and electrons. In the specific case of the RDD benzoate 1,2-dioxygenase, product formation during H_2O_2-driven reactions is much slower (completion requires $\geq$ 60 min), and a kinetically competent Fe^{3+}-hydroperoxo species has been detected. These results, combined with several other logical and experimentally supported arguments, engendered the hypothesis that an Fe^{3+}-hydroperoxo or an electronically equivalent Fe^{5+}-oxo/hydroxo was the initial substrate oxidant of the RDD reaction. This thesis presents the most complete presteady-state kinetic analysis of O_2-driven RDD *cis*-dihydroxylation to date. In contrast to the previous mechanistic hypotheses, the results support a model in which an Fe^{3+}-superoxo-like species is the initial substrate oxidant. The use of this oxidant significantly changes the predicted reaction coordinate utilized by RDD for *cis*-dihydroxylation under O_2-driven conditions. Additionally, the structure of the Fe^{3+}-hydroperoxo species formed during H_2O_2-driven turnover and the conditions that allow its formation are further defined. In total, the new insights gained from the studies herein provide the first evidence that O_2- and H_2O_2-driven turnover reactions utilize different reaction coordinates, but nevertheless lead to formation of the same unique *cis*-diol product.

Table of Contents

List of Tables

List of Figures

List of Abbreviations

(alphabetical)

3,4,5-FB	3,4,5-trifluorobenzoic acid
3,4,5-FB *cis*-diol	the product resulting from BZDO turnover with 3,4,5-FB, (1*S*,6*S*)-3,4,5-trifluoro-1,6-*cis*-dihydroxycyclohexa-2,4-diene-1-carboxyic acid
3,5-FB	3,5-difluorobenzoic acid
3,5-FB *cis*-diol	the product resulting from BZDO turnover with 3,5-FB, (1*S*,6*S*)-3,5-difluoro-1,6-*cis*-dihydroxycyclohexa-2,4-diene-1-carboxyic acid
4-FB	4-fluorobenzoic acid
4-FB *cis*-diol	the product resulting from BZDO turnover with 4-FB, (1*S*,6*R*)-4-fluoro-1,6-*cis*-dihydroxycyclohexa-2,4-diene-1-carboxyic acid
AAD	aromatic amino-acid dioxygenase
alkyl$^{\bullet+}$peroxo	alkylperoxo with a cation radical on the alkyl group
apoBZDO	BZDO without mononuclear iron
benzoate *cis*-diol	the product resulting from BZDO turnover with benzoate, (1S,6R)-1,6-*cis*-dihydroxycyclohexa-2,4-diene-1-carboxy acid
BPMEN	*N,N'*-dimethyl-*N,N'*-bis(2-pyridylmethyl)-1,2-diaminoethane
BZDO	benzoate 1,2-dioxygenase oxygenase
^{ox}BZDO-Fe^{2+}	benzoate 1,2-dioxygenase oxygenase with an oxidized Rieske cluster oxidized and ferrous mononuclear iron
^{ox}BZDO-Fe^{3+}	benzoate 1,2-dioxygenase oxygenase with an oxidized Rieske cluster oxidized and ferric mononuclear iron
^{red}BZDO-Fe^{2+}	benzoate 1,2-dioxygenase oxygenase with a reduced Rieske cluster oxidized and ferrous mononuclear iron
$BZDO_O$	structurally uncharacterized intermediate observed during the BZDO peroxide shunt
$BZDO_{OX}$	oxidized BZDO (^{ox}BZDO-Fe^{3+}) without bound product
$BZDO_P$	the Fe^{3+}-hydroperoxo intermediate observed during the BZDO peroxide shunt reaction

$BZDO_{PS}$	$BZDO_P$ with substrate bound in a chemically competent position
BZDR	benzoate dioxygenase reductase
BZDOS	benzoate 1,2-dioxyenase enzyme system composed of the terminal oxygenase and accessory redox protein
$BZDO_T$	the oxidized product complex of BZDO
CarDO	carbazole 1,9a-dioxygenase oxygenase
cytP450	cytochrome P450
DFT	density functional theory
EPR	electron paramagnetic resonance spectroscopy
HOMO	highest occupied molecular orbital
(H)peroxo	peroxo ligand of unknown protonation state
HPCD	homoprotocatechuate 2,3-dioxygenase
HPLC	high performance liquid chromatography
IDO	indolamine 2,3 dioxygenase
MCD	magnetic circular dichroism spectroscopy
NBDO	nitrobenzene 1,2-dioxygenase
NDO	naphthalene dioxygenase oxygenase
$^{ox}NDO\text{-}Fe^{2+}$	naphthalene dioxygenase oxygenase with an oxidized Rieske cluster oxidized and ferrous mononuclear iron
$^{ox}NDO\text{-}Fe^{3+}$	naphthalene dioxygenase oxygenase with an oxidized Rieske cluster oxidized and ferric mononuclear iron
$^{red}NDO\text{-}Fe^{2+}$	naphthalene dioxygenase oxygenase with a reduced Rieske cluster oxidized and ferrous mononuclear iron
NDOS	naphthalene dioxygenase enzyme system composed of the terminal oxygenase and accessory redox proteins
NDF	naphthalene dioxygenase ferredoxin

NHE	normal hydrogen electrode
NDR	naphthalene dioxygenase reductase
NO	nitric oxide
NRVS	nuclear resonance vibrational spectroscopy
PCD	protocatechuate 3,4-dioxygenase
RDD	Rieske dearomatizing dioxygenase oxygenase
^{ox}RDD-Fe^{2+}	Rieske dearomatizing dioxygenase oxygenase with an oxidized Rieske cluster oxidized and ferrous mononuclear iron
^{ox}RDD-Fe^{3+}	Rieske dearomatizing dioxygenase oxygenase with an oxidized Rieske cluster oxidized and ferric mononuclear iron
^{red}RDD-Fe^{2+}	Rieske dearomatizing dioxygenase oxygenase with a reduced Rieske cluster oxidized and ferrous mononuclear iron
RDDS	Rieske dearomatizing dioxygenase enzyme system composed of the terminal oxygenase and accessory redox protein(s)
RO	Rieske oxygenase
RRT	reciprocal relaxation time
sMMO	soluble methane monooxygenase
TauD	taurine dioxygenase
TDO	tryptophan 2,3-dioxygenase
TMC	tetramethylcyclam
TPA	tris(2-pyridylmethyl)amine

Chapter 1

Introduction

Note: Parts of this chapter are reprinted or adapted with permission from Rivard, B. S., Rogers, M. S., Marell, D. J., Neibergall, M. B., Chakrabarty, S., Cramer, C. J., and Lipscomb, J. D. (2015) Rate-Determining Attack on Substrate Precedes Rieske Cluster Oxidation during Cis-Dihydroxylation by Benzoate Dioxygenase, Biochemistry 54(30), 4652-4664.

The Evolution of Biological Iron/Oxygen Chemistry

From Life's Origins to the Great Oxidation Event.

Iron (Fe) and diatomic oxygen (O_2) have greatly shaped life on Earth, and it is hard to devise evolutionary pathways to the present biomes of complex and diverse multicellular plants and animals without both. At the dawn of life on this planet, the abundance of iron in Earth's crust and the reducing anoxic atmosphere made soluble forms of iron widely available in the primordial oceans. Early life exploited the multivalency of the iron cation as one way to establish the far from equilibrium conditions inherent to all living systems. As a result of this availability and utility, iron has been indelibly incorporated into the many enzymatic processes that orchestrate the flow of energy and matter within a living cell collectively known as metabolism.

All life ultimately depends on a constant influx of energy and biologically relevant matter, preeminently carbon. Many metabolic strategies have evolved utilizing different sources for each. Heterotrophic organisms obtain energy and carbon by ingesting other organisms and catabolizing the carbohydrates therein. Ultimately, autotrophic organisms produce all of the organic carbon required for themselves and heterotrophs by reductively converting inorganic forms of oxidized carbon into reduced organic carbohydrates. Photosynthetic autotrophs use solar photon energy to oxidize an otherwise stable reductant for carbon fixation. The first photosynthetic organisms probably oxidized gasses present in the early atmosphere or reduced and soluble metals and minerals.[1]

Around 3 billion years ago, evolution began to tinker with processes utilizing water as the electron source for photosynthesis.[2] During this novel process called oxygenic photosynthesis, each of two water molecules is oxidized by two electrons resulting in the diatomic gas O_2. Using water was advantageous because it was much more abundant and available than previous electron sources. By 2.5 billion years ago, oxygenic photosynthesis had become efficient and prevalent enough to produce a spike in the O_2 concentrations of earth's biosphere, known as the Great Oxidation Event.[2] This increase in planetary O_2 oxidized the hitherto reducing atmosphere, was inescapably toxic for much of Earth's early life, but enabled the proliferation of new life forms that evolved into complex multicellular organisms.[2]

Oxygen: The Life-energizing Gas with Masked Reactivity.

O_2 is a simple molecule with complex reactivity. Oxidation reactions can be grouped into two broad types, electron-transfer and atom-transfer reactions. Electron-transfer reactions only involve electrons and protons and can result in multiple intermediate reduction states between O_2 and $2H_2O$ (Figure 1-1). Atom-transfer reactions are those bonding at least one of the oxygen atoms of O_2 to a heteroatom. Both electron and atom-transfer reactions are exergonic in a biological environment. The $\Delta G°$ values for the reduction of O_2 to water with 4 electrons and 4 protons and for atom-transfer forming phenol from benzene and O_2 are -315 and -180 kJ/mole, respectively. If oxidation reactions are so thermodynamically favorable, how can Earth's atmosphere be 20% O_2 and why does a biological unit (a bacterium, a plant, or the next animal you see) simply not "burn-up" to H_2O and CO_2 in the highly oxidizing atmosphere of earth environment?

Oxygen is an ideal oxidant for use in biological systems because its high thermodynamic reactivity is tempered by two intrinsic chemical characteristics. The first can be identified by inspection of the reduction potential reported in Figure 1-1. The one electron reduction of O_2 to the superoxide anion is thermodynamically unfavorable (negative reduction potential vs. NHE) compared to the two or four electron process (positive reduction potentials vs. NHE). Concerted transfer of multiple electrons is rare in uncatalyzed reactions, thus the low redox potential for superoxide formation provides a thermodynamic barrier that limits the initiation of the otherwise favorable O_2 reduction process. The second mask of O_2 reactivity is a consequence of its ground state electronic structure. O_2 has a paramagnetic ground state. The two degenerate $2p\pi^*$ HOMOs each contain one electron with the same spin resulting in a triplet S=1 spin state (Figure 1-2). The HOMOs of biological molecules have paired electrons of opposite spins resulting in a singlet S= 0 spin state. The reaction of triplet and singlet molecules violates a quantum mechanical selection rule for reactivity, the conservation of spin angular momentum, and is thus called spin forbidden. If a spin inversion occurs in the HOMO electrons of O_2, the resulting singlet O_2 is very reactive, but the activation energy required is very large at ambient conditions resulting in a kinetic barrier to O_2 reactivity with biological molecules.

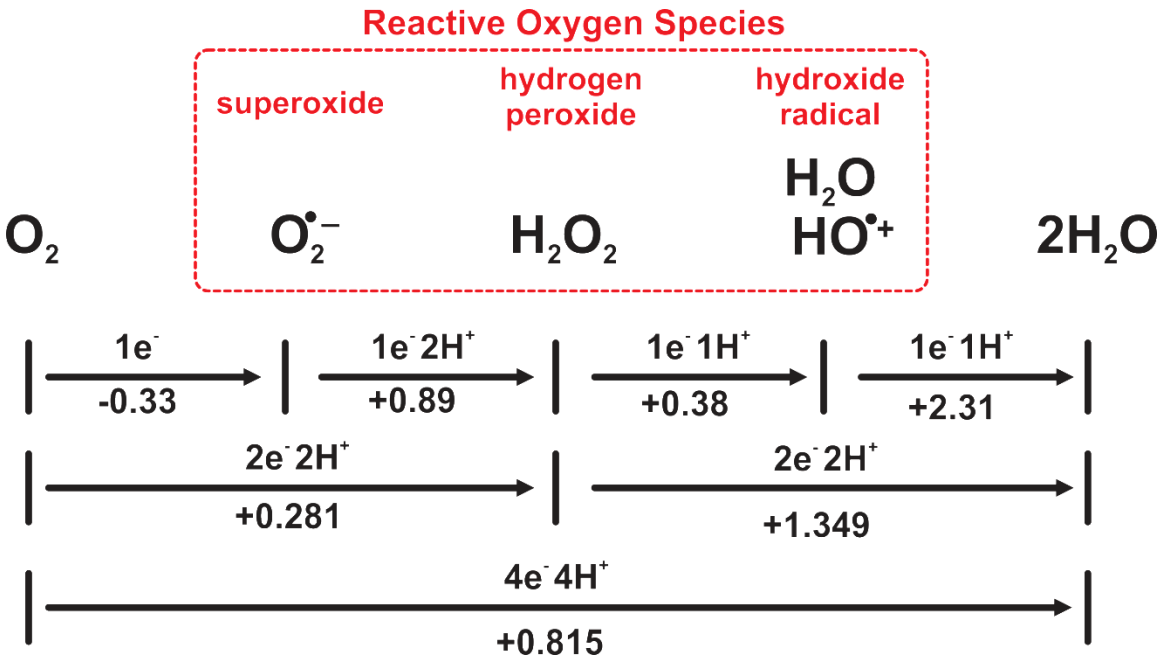

Figure 1-1: Standard state potentials (vs NHE) of O_2 reduction in pH 7.0 water at 25° C. Figure adapted from Wood 1988.[3]

Life has evolved two general strategies, often used together in highly coordinated ways, to release the latent reactivity of O_2. The first is to use electron donating cofactor(s) for multielectron reduction bypassing the thermodynamically unfavorable formation of superoxide (Figure 1-1). The second is to use the d-orbitals of transitions metals to lower the activation energy required for the O_2 activating spin conversion. These strategies are employed in both biological electron and atom-transfer reactions. Most familiar and important for higher plants and animals is the reduction of O_2 back to water by cytochrome-c oxidase (the terminal component of the mitochondrial electron transport chain) that drives oxidative phosphorylation during cellular respiration. However, oxygen atom-transfer reactions are widely used in nature. In the 1950s the first such enzymes, called dioxygenases and monooxygenases, were described by Hayaishi and Mason respectively.[4-6] Dioxygenases incorporate both oxygen atoms of O_2 into a substrate or into a substrate and a cosubstrate (*vide infra*). In most cases, all four electrons required for O_2 reduction are provided by the substrates(s), but this is not universal as the dioxygenase studied in this thesis does not follow this paradigm. In monooxygenase chemistry, only one oxygen atom of O_2 is incorporated into the

substrate while the other is reduced to water. In general two of the electrons for O-O bond cleavage are provided by the substrate and the other electrons are provided by an external source such as NAD(P)H.

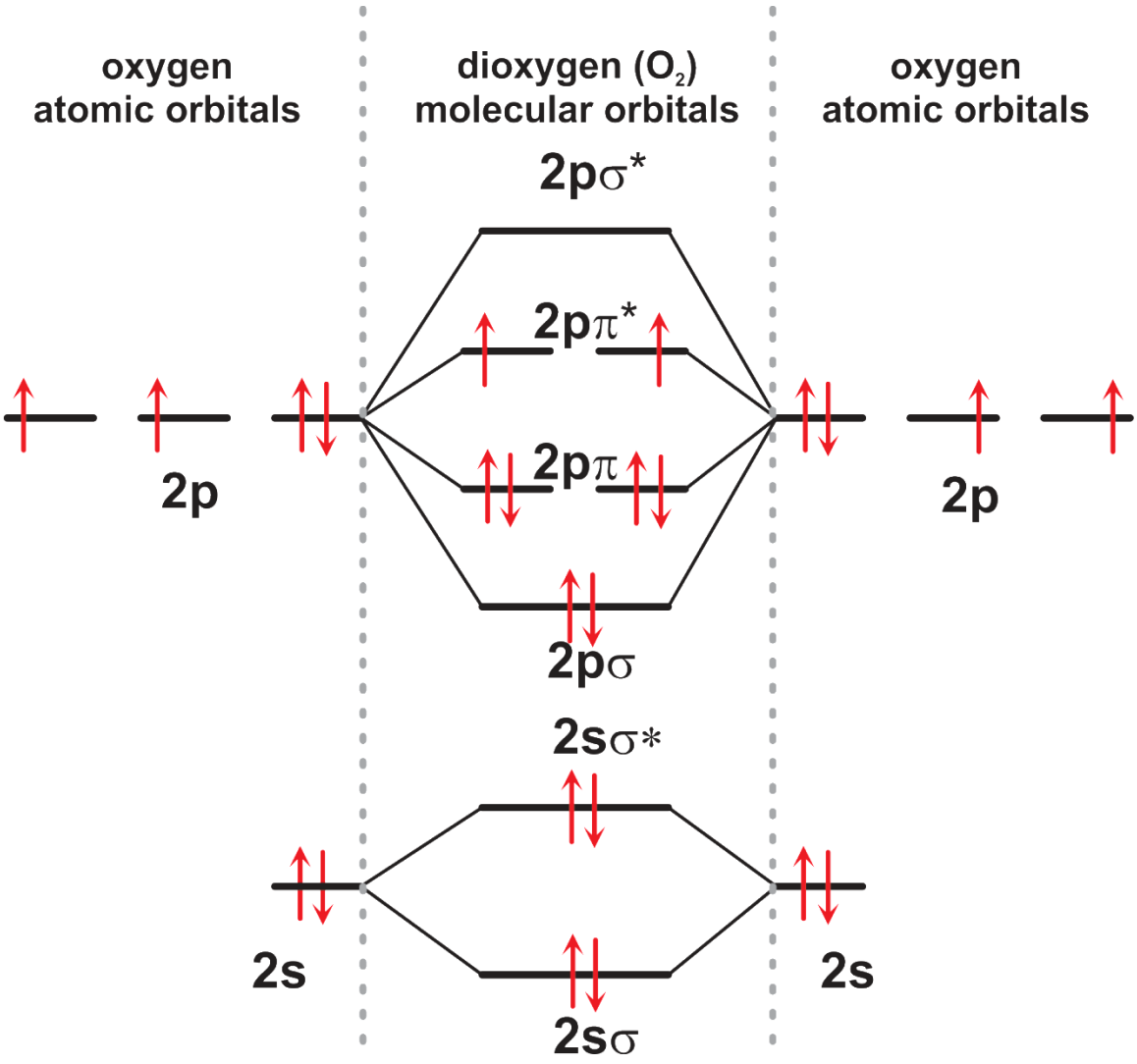

Figure 1-2: Molecular orbital diagram of triplet O_2.

In the ~60 years since the discoveries of Hayaishi and Mason, the landscape of oxygenase chemistry has greatly expanded and continues to be a lively research field. For some enzymes, there are well-supported consensus models for exactly how nature reductively activates oxygen and performs the intended chemistry. These established models are supported by detailed kinetics and corroborating identification of transient reaction intermediates described with spectroscopy and, occasionally, crystallography. In others cases, comparatively little is known about a reaction's kinetics and reactive intermediates, and research continues moving toward a well-supported consensus model. Rieske oxygenases are an example of the latter and are the focus of research presented in this thesis.

Rieske Oxygenases: Chemical Landscape and Research Justifications

The Rieske oxygenase (RO) family of enzymes catalyze a remarkable array of oxidative chemistries via reductive activation of O_2 at a nonheme mononuclear Fe^{2+} bound within each active site.[7] As shown in rows 2-8 of Table 1-1, the catalytic diversity of ROs is reported to include monooxygenation, O-demethylations, N-demethylations, desaturation, N-oxygenation, and C-C bond formation, all reactions also performed by other metal-dependent mono and dioxygenases. In contrast to the above chemistries, a subset of ROs called the Rieske dearomatizing dioxygenases (RDDs) are the only known enzymes that catalyze dearomatizing *cis*-dihydroxylations, transforming aromatic moieties to cyclic alkenes with vicinal O_2-derived *cis*-diols (Table 1-1, row #1). As illustrated for each transformation, two NADH derived electrons are used to activate and split the O-O bond, but the fate of each oxygen atom of O_2 depends on the chemistry performed.

Table 1-1: Chemistry performed by Rieske oxygenases.

	Reaction Type	Example Reaction	References by substrate[a]
1	dearomatizing *cis*-dihydroxylation	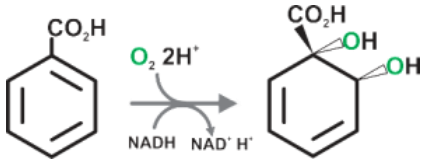	**benzoate**[8-10], naphthalene[11-13], toluene, biphenyl, phthalate, anthranilate, benzene, nitrobenzene, carbazole
2	aromatic monooxygenation	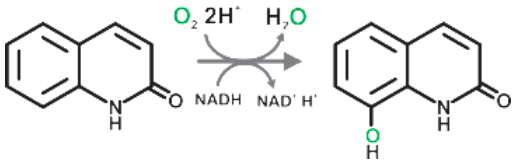	**2-oxoquinoline**[14], salicylate[15]
3	aliphatic monooxygenation	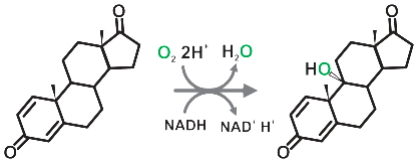	**sterols**[16, 17], promysalin precursors[18], alkanes[19], short chain alcohols[20, 21], chlorophyll *a*[22], choline
4	O-demethylation	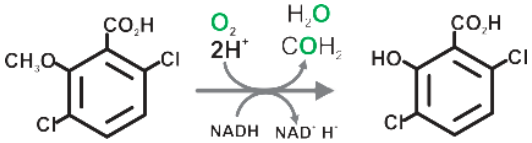	**dicamba**[23-25], vanilliate[26], 4-methoxybenzoate[27-32]
5	N-demethylation	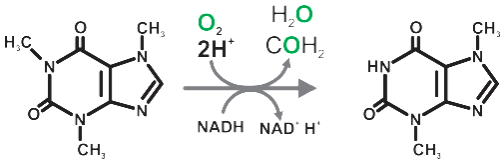	methylated xanthines (**caffeine**)[33-35], N,N-dimethyl phenylurea herbicides[36], stachydrine[37]
6	desaturation	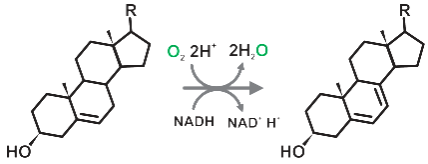	**sterols**[38-40], short chain alcohols[20, 21]
7	N-oxygenation	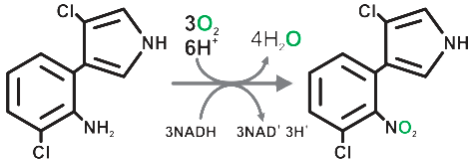	**pyrrolinitrin precursor**[41-43]
8	C-C bond formation	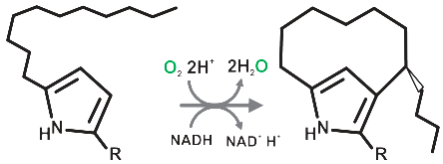	**undecylprodigiosin**[44, 45]

[a] substrate in bold illustrated as example reaction

The applications of ROs have historically focused on two areas utilizing the unique *cis*-hydroxylation chemistry of RDDs. The degradation of aromatic compounds is an important thread in the global carbon cycle that frees organic carbon otherwise trapped in the high stability of aromatic bonds. Two significant sources of environmental aromatics are the structural polymers of plants (lignin) and human industrial processes. The intrinsic biochemistry of neither plants nor humans has the ability to degrade these types of aromatics that they input into the environment, and this is accomplished instead by bacteria and fungi. The aromatic compounds from human industry are all too often noxious pollutants and can damage the health of ourselves and the environment. Because all characterized RDDs are within bacterial pathway for the mineralization of aromatic compounds (*vide infra*), they have use as agents of bioremediation, removing these pollutants from contaminated environments. [46-48]

The second established application for RDDs is as a green catalysts for the production of *cis*-diols. Enantiomerically pure *cis*-diols can be produced chemically via the Sharpless dihydroxylation reaction with catalytic amounts of an osmium based reagent, but the highly toxic reagent and its proclivity to overoxidize and/or cleave the resulting diols is problematic.[49, 50] In contrast, RDDs can produce large quantities of regio and stereospecific *cis*-diols from aromatic or olefinic substrates in mild and nontoxic conditions.[51] RDD generated *cis*-diols have played important roles in many complex chemoenzymatic synthesis procedures including the first total synthesis of the antibiotic tetracycline and several other biomedically relevant compounds.[52, 53] Moreover, RDDs are engineerable, thereby enhancing their utility as green catalyst. Early indications of this came from reactivity studies with the RDD naphthalene dioxygenase (NDO) from *Pseudomonas sp* NCIB 9816-4 by demonstrating the wild-type enzymes ability to perform desaturations, dealkylations, monooxygenations, and sulfoxidations depending on the substrate type.[54] Furthermore, RDD regiospecificity can be altered with modest active site mutations suggesting that the aromatic and olefinic substrates accessible to *cis*-dihydroxylation may only be limited by the research community's ambition, motivation, and creativity.[50, 55-57]

Although ROs are often pigeonholed as catabolic bacterial enzymes for degradation of environmental aromatic compounds, discoveries over the last decade have greatly expanded their biological roles. ROs have been identified in many anabolic

pathways performing crucial functionalizations of antibiotics,[18] fungicides,[41-43] and antimalarial compounds.[45] The Rieske monooxygenase KshAB is essential for cholesterol utilization by the human pathogen *Mycobacterium tuberculosis,* likely increasing virulence.[16, 17] While the monooxygenation chemistry and its catabolic role may be similar to the canonical ROs, this is the first example of the use of an RO by a human pathogen. KshAB and possibly other ROs yet to be characterized in pathogens could be potential targets for the development of future antibiotics that block catalysis and/or uncouple the reaction, resulting in damaging oxidative stress. CntAB is the first RO identified within the human microbiota and highlight ROs in another biological sphere of consequence to human health.[58] CntAB produces trimethylamine from the hydroxylation of dietary carnitine. Trimethylamine is known to promote atherosclerosis and ultimately heart disease and the direct inhibition CntAB could help in its prevention. As with KshAB and pathogens, CntAB could be a harbinger of other ROs within the human microbiome with direct consequences to human health.

A complete understanding of the chemical mechanisms of ROs will aid in further development of current and future applications, however, it is important to stress the importance of ROs for basic research. ROs provide the only opportunity to study enzymatic *cis*-dihydroxylation. Like several other iron oxygenase families, ROs allow study of how structurally homologous enzymes control and direct activated oxygen species during diverse chemical transformations.

Rieske Dearomatizing Dioxygenases

The Role of RDDs in the Aerobic Degradation of Aromatics.

The biochemical logic for aerobic aromatic degradation is to funnel the diverse environmental aromatics into a small number of “hub” compounds, two pertinent examples being catechol and protocatechuate.[59] The hub compounds then undergo ortho or meta-cleavage by intradiol or extradiol dioxygenases before further processing into TCA cycle intermediates or other metabolites as dictated by the needs of the organism (upper panel of Figure 1-3). Both intra- and extradiol dioxygenases are

nonheme mononuclear iron containing enzymes and their reaction cycles are further discussed below (Figure 1-12 and Figure 1-13).

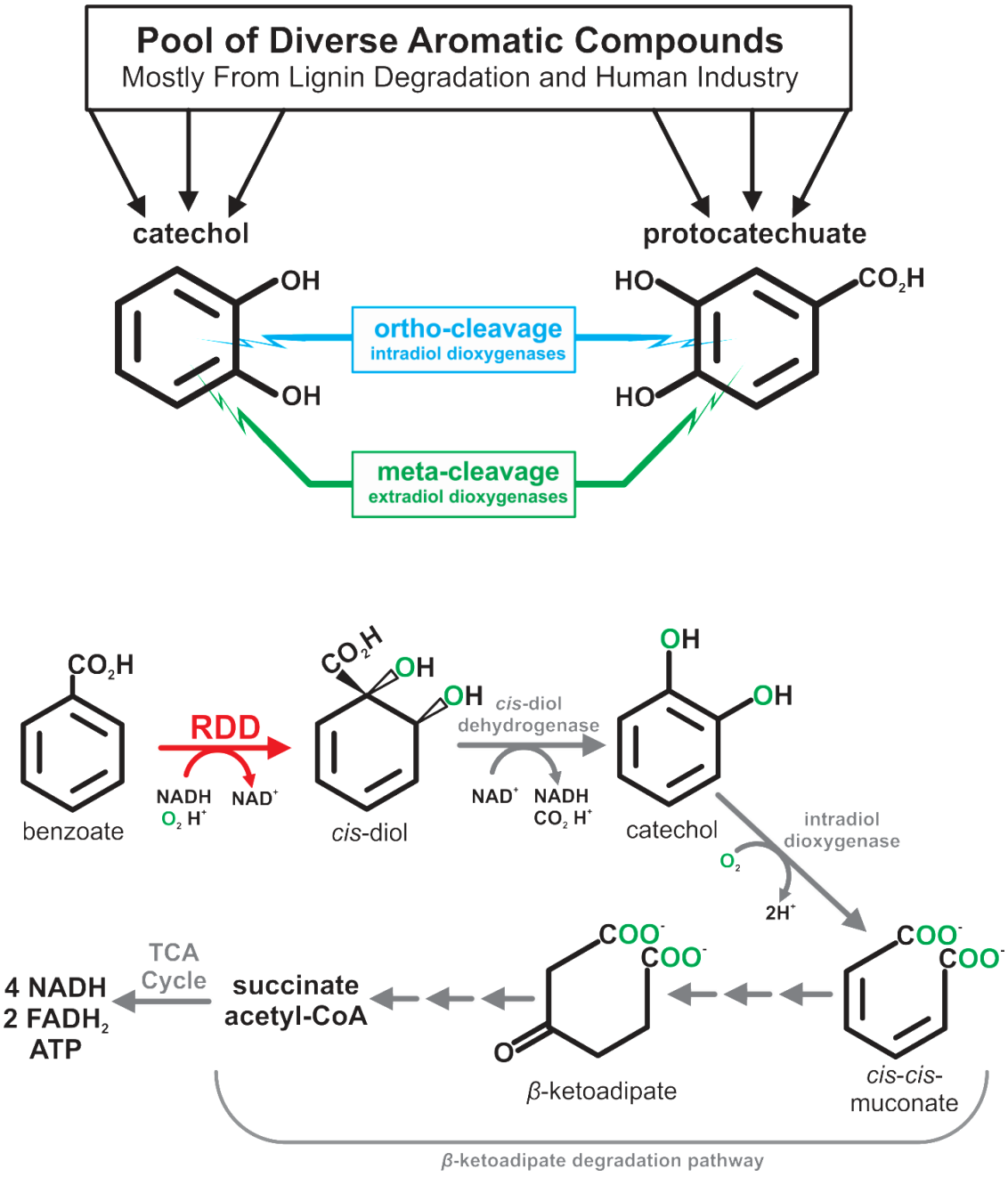

Figure 1-3: Aerobic degradation of aromatic compounds.

The lower panel of Figure 1-3 illustrates the aerobic catabolism of benzoate via ortho-cleavage and the *β*-ketoadipate pathway.[59] The RDD Benzoate 1,2-Dioxygenase (BZDO, highlighted in red) performs the initial reaction of this pathway, activating the otherwise stable aromatic by addition of two hydroxyl groups. The resulting dearomatized *cis*-diol is rearomatized via a NAD^+ dependent dehydrogenase to catechol. After oxidative ring cleavage of catechol, degradation via the *β*-ketoadipate pathway results in succinate and acetyl-CoA.[59] Oxidative decarboxylation of succinate and acetyl-CoA within the TCA cycle results in 4 NADH, 2 $FADH_2$, and 1 ATP. The 6 reduced nucleotides cofactors can be used to drive oxidative phosphorylation, the process at the center of aerobic metabolism, for ATP production.

RDDs are Part of a Multicomponent Enzyme Systems.

RDDs are not directly reduced by NADH, but are instead the terminal electron accepting oxygenase in a multicomponent enzyme system (designated RDDS) with one or two additional redox proteins (Figure 1-4).[60] In two component systems such as BZDOS (Figure 1-4 A), only a reductase (benzoate dioxygenase reductase, BZDR) is used for electron transfer to the RDD. In three component systems such as NDOS, both a reductase (naphthalene dioxygenase reductase, NDR) and a ferredoxin (naphthalene dioxygenase ferredoxin, NDF) are used in the electron transfer chain (Figure 1-4 B). Multiple redox cofactors including flavins, glutathiones, and [2Fe-2S] clusters are used to access the range of reduction potentials required for electron flow through the system.[60] RDD reductases contain two redox active cofactors, usually a flavin mononucleotide and a [2Fe-2S] cluster, and are capable of storing and transfer two electrons directly to the oxygenase. The ferredoxins used in three component systems only contain a single [2Fe-2S] cluster and are only capable of transferring one electron at a time to the oxygenase.

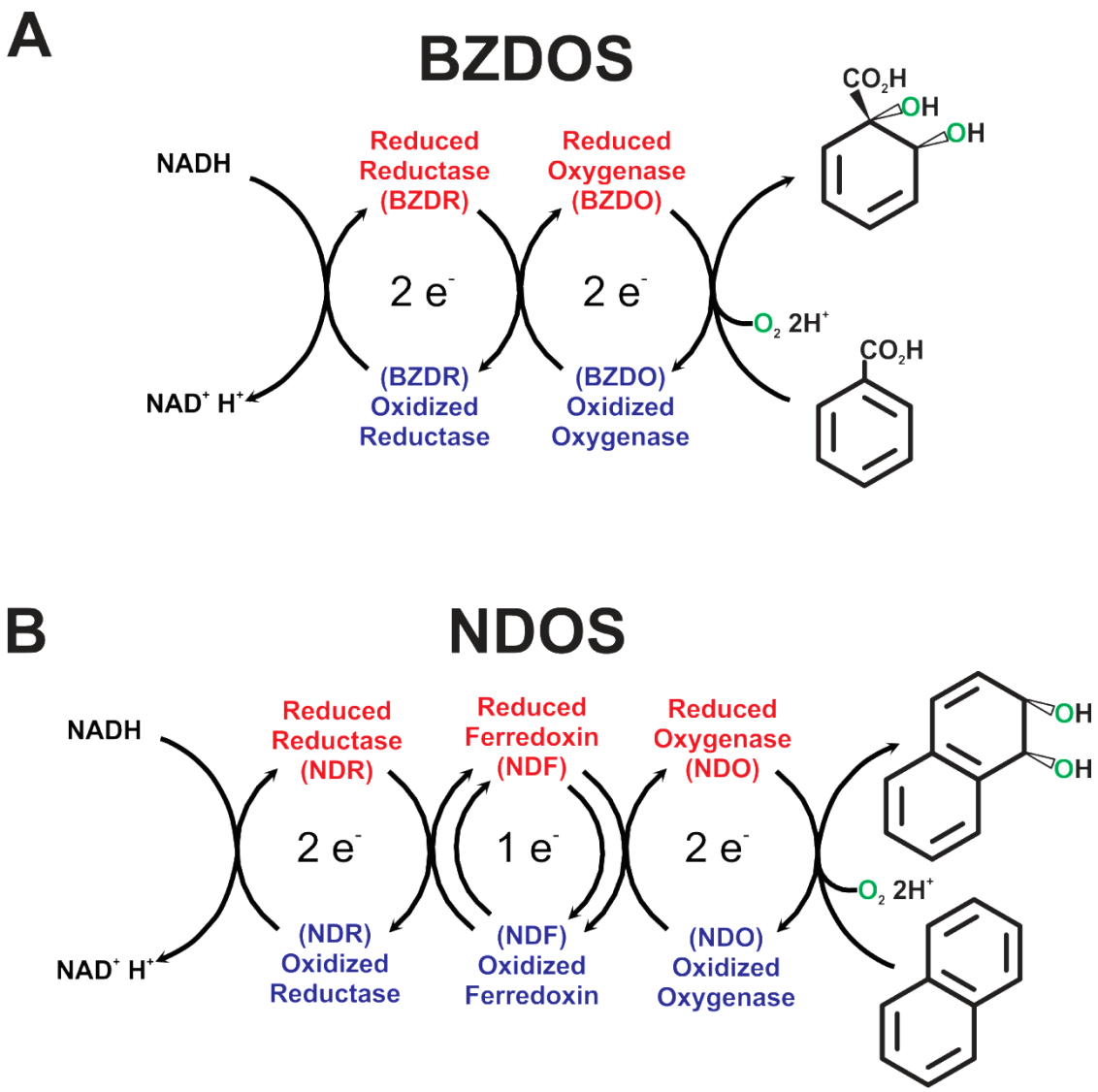

Figure 1-4: Electron transfer chain for RDDs

Structure of RDDs.

RDDs have either an α_3 homotrimer or a α_3/β_3 heterohexamer quaternary structure with three-fold symmetry(Figure 1-5).[60] The α and β-subunits are approximately 50 and 20 kD respectively, and the α-subunit is where catalysis occurs. In α_3/β_3 enzymes, the β-subunits is required for catalysis, but the exact role is not known.[61] Generally, the β-subunit is thought to provide structural stability, but experiments expressing chimeric RDDs composed of α and β-subunits from different enzymes have

demonstrated altered catalytic properties.[60, 62-64] Phylogenetic analysis indicate the α_3/β_3 structure mostly occurs only in a small subset of RDDs and a majority of ROs enzyme family has α_3 structures (*vide infra*).[65]

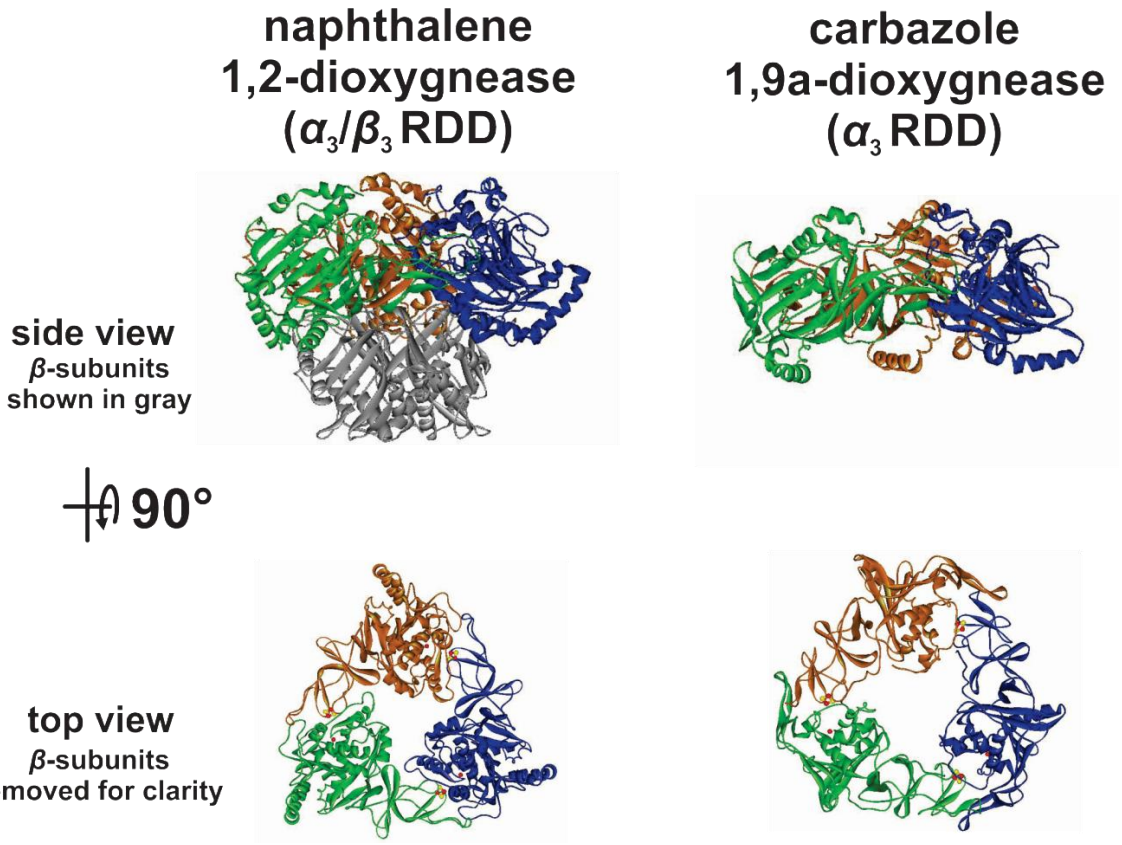

Figure 1-5: Quaternary structure of α_3/β_3 and α_3 RDDs.

Each catalytic *α*-subunit is composed of an N-terminal an C-terminal domains harboring the eponymous [2Fe-2S] Rieske cluster and the nonheme mononuclear iron respectively.[60] The Rieske cluster is ligated by two His and two Cys residues within the conserved sequence motif **C**X**H**X_{17}**C**X_2**H**. The mononuclear iron is coordinated two His and one Asp residues (a 2-His-1-carboxylate facial triad)[66] in addition to 1 or 2 solvent molecules.[60, 67] Substrates binds near (but not to) the mononuclear iron, showing that this is the site of O_2 activation and *cis*-dihydroxylation (Figure 1-6).[12, 68-70] Spectroscopic

analysis and molecular dynamics simulations suggests that the Asp is maintained as bidentate but several crystal structures indicate monodentate binding. [14, 24, 25, 60, 70, 71]

The distance between the Rieske cluster and the mononuclear iron within one *α*-subunit is ~44 Å, but the trimeric quaternary structure positions the metals centers of adjacent subunits at ~15 Å (Figure 1-6). The shorter distance between the intersubunit Rieske cluster and mononuclear iron suggests this pair comprise the functional unit of the enzyme.[60, 72] A conserved carboxylate residue (Asp or Glu) provides a cross subunit bridge by hydrogen bonding with His ligands of the adjacent Rieske cluster and mononuclear iron (Figure 1-6). The carboxylate appears to both mediate the electron transfer from the Rieske cluster to the mononuclear iron during catalysis and contribute to the regulation of oxygen activation as described below. [72-74]

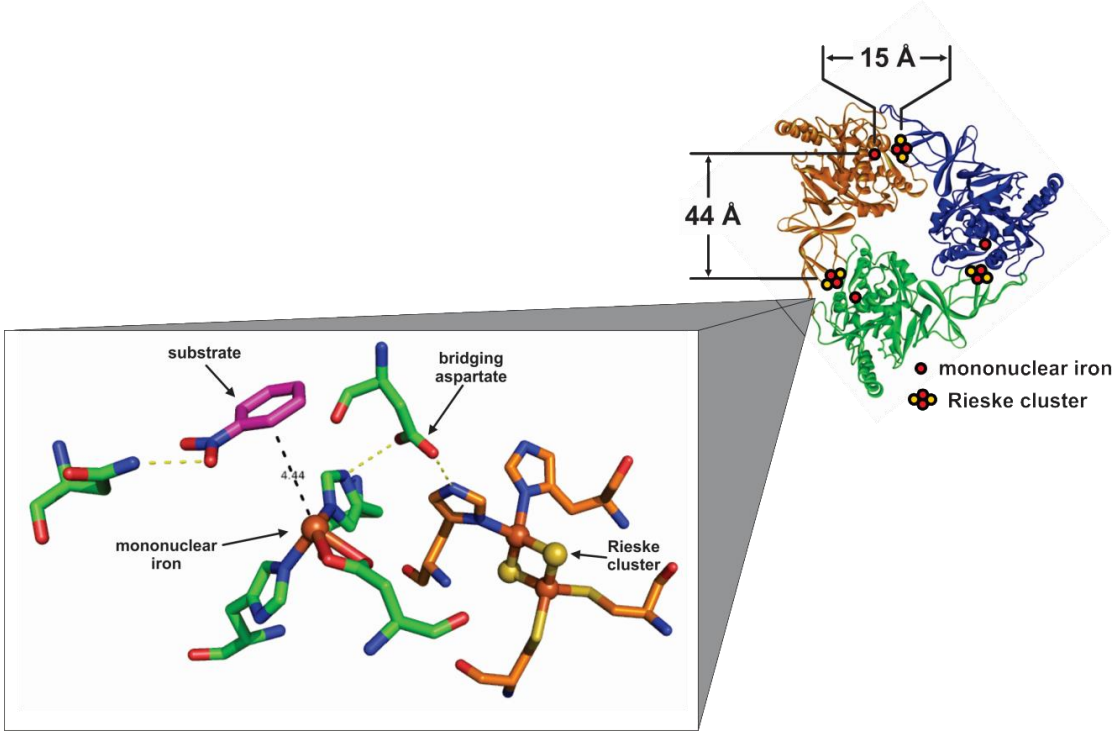

Figure 1-6: Active site structure of RDDs as illustrated with nitrobenzene 1,2-dioxygenase (NBDO).[69]

Classification and Phylogenetics of ROs and RDDs.

Multiple classifications schemes have been proposed for RDDs and the broader RO family of enzymes. The first classification scheme was based on the differences in the number and properties of the accessory redox proteins in each system (Figure 1-4), and while useful in many ways, does not provide information about phylogenetic relatedness.[65, 75] Following classifications relied on sequence similarity, but had multiple shortcomings including working in a small sequence space, not selecting sequences encompassing the diversity of ROs, and problems aligning highly divergent sequences containing many insertions and deletions.[65, 76-78] The latest phylogenic study conducted by Capyk *et.al.* avoided these problems by analyzing the largest most diverse dataset to date and by only using conserved structural elements for multiple sequence alignment and phylogenetic analysis.[65] The results of this study showed that ROs divide into two phylogentic groups based on the sequence of the N-terminal Rieske domain. The authors interpret this as evidence of two distinct protein fusion events between the Rieske and catalytic domains in the evolutionary history of ROs. This study also showed that while the majority of research has been conducted with α_3/β_3 RDDs, ROs with operonically associated β-subunit were only present in one of the two groups and comprised ~5 % of the total representative sequences.

Electron Stoichiometry During Single-turnover Reactions.

RDDs are stable in multiple electronic configurations defined by the redox states of the Rieske cluster and mononuclear iron. Figure 1-7 illustrates the three stable electronic states and the naming convention used throughout this work to denote each. The superscripted prefix and the hyphenated suffix identify the redox state of the Rieske cluster and mononuclear iron respectively. For example, NDO with a ferrous mononuclear iron and an oxidized Rieske cluster would be designated ^{ox}NDO-Fe^{2+}. The mononuclear iron has a much higher redox potential than the Rieske cluster making electron transfer between the reduced Rieske cluster and oxidized mononuclear iron fast and effectively irreversible. This makes the fourth possible state, a reduced Rieske cluster and oxidized mononuclear iron, unstable. The two oxidized forms of RDDs can be fully reduced to ^{red}RDD-Fe^{2+} by addition of electrons from either NADH via native redox protein(s) (Figure 1-4) or by a strong chemical reductant such as dithionite.

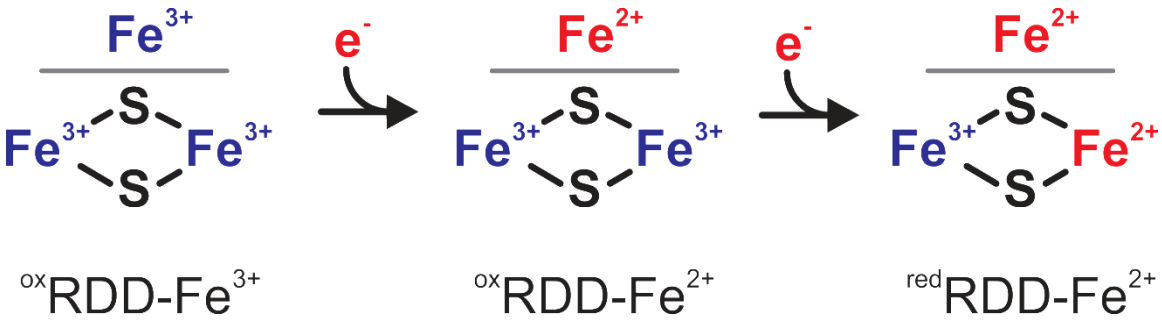

Figure 1-7: Electronic configurations of RDDs.

The majority of RDD research has been done using whole cell assays and steady-state kinetics, but single-turnover experiments with purified enzymes have been, and continue to be, crucial for gaining mechanistic insights into the individual steps within the catalytic mechanism of RDDs. The first single turnover experiments were done with NDO and BZDO and provided foundational observations that guide mechanistic research of RDDs to this day.[8, 11] RDD single turnovers are done by stoichiometric chemical reduction to ^{red}RDD-Fe^{2+} followed by addition of excess O_2 and substrate, resulting in formation of ^{ox}RDD-Fe^{3+} and the *cis*-diol product. Even in the presence of excess O_2 and substrate, only a single turnover occurs because there is no additional reductant present for reduction back to ^{red}RDD-Fe^{2+}. After the single turnover, product remains bound within the enzyme active site, and the enzyme must be reduced in order for product to dissociate.[8] The retention of product could be caused by binding of the *cis*-diol product to the ferric mononuclear iron, a closed configuration of the enzyme that blocks the active site entrance, or a combination thereof. In summary and to emphasize a very important observation, the single turnover studies demonstrated the catalytic cycle starts ^{red}RDD-Fe^{2+}, ends ^{ox}RDD-Fe^{3+}, established a two electron per *cis*-diol stoichiometry, and shows that the two required electrons come from the reduced metal centers of the oxygenase.[8]

The two metal centers within RDDs make them spectroscopically rich and enable investigation of the electronic structure of various electronic states. Both the reduced and oxidized Rieske clusters have a broad optical absorbance spectrum covering the majority of the visible spectrum. The absorbance of the oxidized Rieske clusters is

distinct from that of the reduced cluster, having a larger extinction at all wavelengths (Figure 1-8). The Rieske cluster is oxidized during single turnovers and monitoring this change in absorbance provides a convenient signal to monitor reaction kinetics.

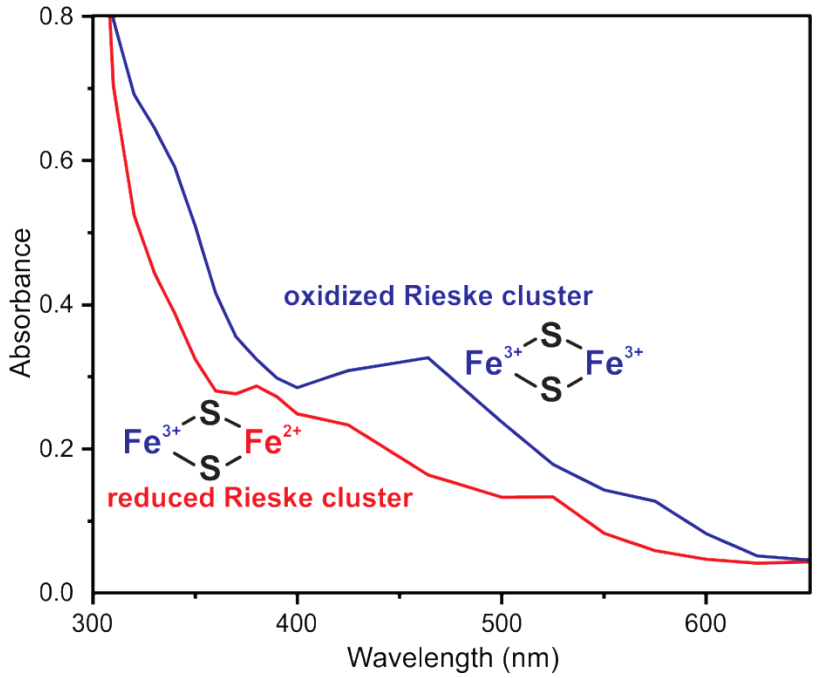

Figure 1-8: The optical changes during a single turnover with benzoate. The optical spectra observed after reduced BZDO (100 µM) was mixed with an O_2-saturated reaction buffer containing benzoate (20 mM) at 4 °C in a stopped-flow spectrophotometer. The spectra are combinations of 21 single wavelength time courses collected from 300 -725 nm.

Regulation of O_2 Activation by RDDs and Other Nonheme Dioxygenases.

Nonheme mononuclear iron dioxygenases follow a common regulatory paradigm that ensures substrate and any required cosubstrates or cofactor are bound and the cofactors are in the correct redox state before initiation of O_2 activation.[79] The regulation prevents enzyme catalyzed uncoupling, the incomplete reduction of O_2 resulting in release of reactive oxygen species (Figure 1-1). Uncoupling is damaging to the protein matrix, potentially causing irreversible enzyme inactivation, and can cause oxidative stress at the cellular level. The central strategy of the regulation mechanisms is to prevent O_2 from associating with the mononuclear iron until the enzyme is in the

chemically competent state for coupled product formation. This is accomplished by keeping the mononuclear iron in a 6-coorindinate state with protein and water/hydroxo ligands until the chemically competent state of the enzyme is established. In a 6-coorndinate state, the ligand field of the mononuclear iron is saturated and formation of an Fe-O_2 complex is sterically inhibited. After the chemically competent state is achieved, one of the aqua ligands dissociates, resulting in a 5-coordinate mononuclear iron. This opens a place for O_2 to interact with the mononuclear iron and initiate the processes of reductive activation and product formation.

The first insights into the regulation of O_2 activation in RDDs came from the initial single-turnover studies with NDO and BZDO. ^{red}RDD-Fe^{2+} enzyme would not bind the spectroscopically active O_2 analog nitric oxide (NO) until substrate was present, an observation in accord with the general regulation mechanism described above. Further spectroscopic and crystallographic studies have expanded the regulation mechanism as illustrated with NDO in Figure 1-9.[14, 67, 80, 81] Starting in the as-isolated ^{ox}NDO-Fe^{2+} state, the mononuclear iron was assigned as 6 coordinate by MCD spectroscopy, but one of the two aqua ligands appears to be weakly bound.[67] Reduction of the Rieske cluster triggers a structural reorganization of the active site resulting in three important changes. First, an Asp residue from the subunit containing the mononuclear iron repositions such that it forms a cross-subunit hydrogen bond between the His ligands of the Rieske cluster and the mononuclear iron. Second, a change in the position of the helix containing the two His ligands of the mononuclear iron results in the mononuclear iron moving ~ 0.5 Å away from the substrate. This change in the position of the mononuclear iron relative to the substrate has been observed both crystallographically and spectroscopically.[14, 80, 81] Third, the affinity of the water for the mononuclear iron increases making it unequivocally 6-coordinate. In this state of the enzyme (Figure 1-9, ^{red}RDD- Fe^{2+} without substrate), the coupled metal centers can facilitate rapid electron transfer, but Rieske cluster oxidation in this unproductive state is avoided because the 6-coordinate mononuclear Fe is unable to bind O_2 (or NO). Substrate binding results in loss of a water molecule and opens a spot for O_2 to ligate and be activated for catalysis (Figure 1-9, ^{red}RDD- Fe^{2+} with substrate).[67]

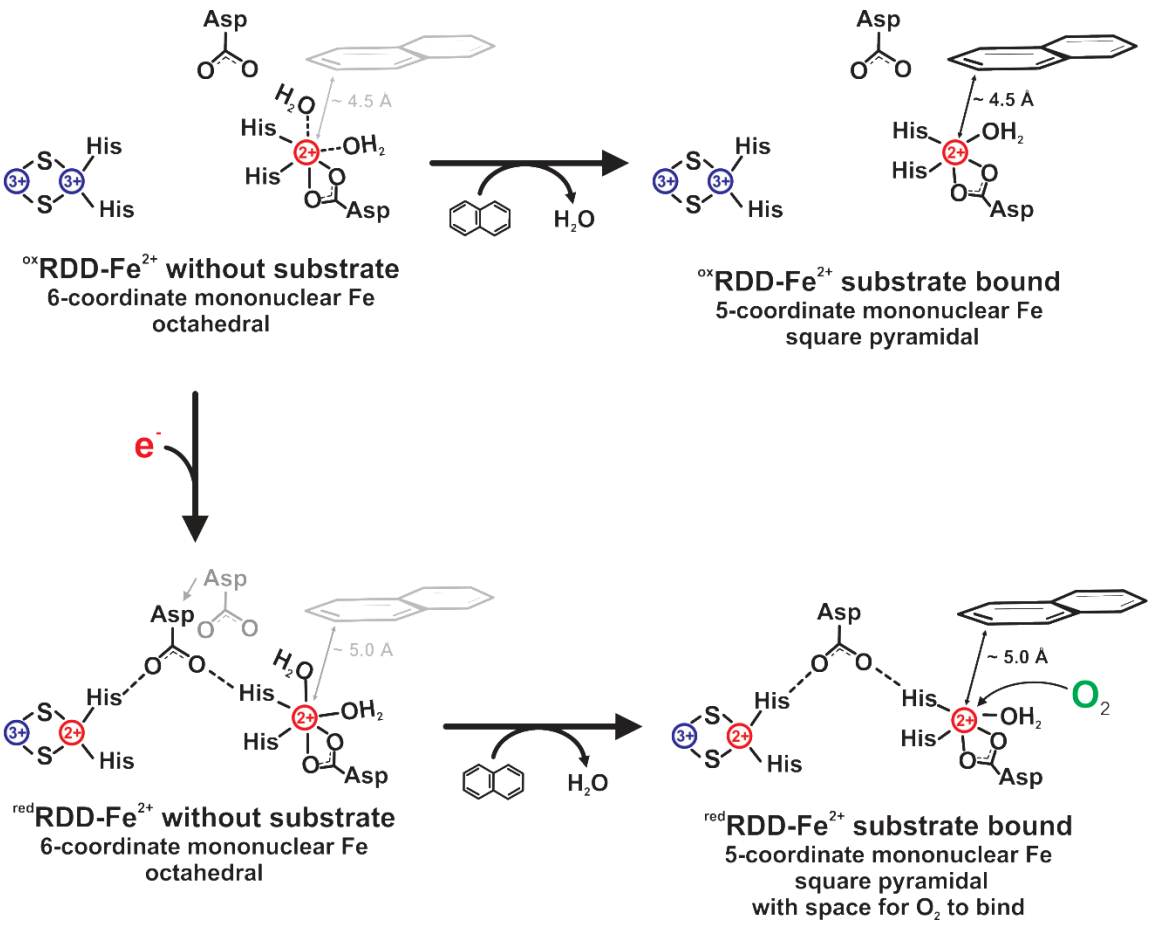

Figure 1-9: Regulation of O_2 activation by RDDs.

Enzymatic Fe/O_2 Activation: Perspective and Overview

To contextualize the following mechanistic hypotheses' for RDD *cis*-dihydroxylation, the catalytic mechanisms of multiple iron-dependent oxygenases will now be surveyed. Three of the enzymes are nonheme mononuclear dioxygenases utilizing the 2-His-1-carboxylate ligation as in RDDs, however, a heme monooxygenase (cytP450), diiron monooxygenase (sMMO), and a nonheme mononuclear dioxygenase with a different ligand environment are also presented. Each system uses a distinct method to active O_2, and Table 1-2 compiles characteristics of each system for ease of comparison.

Heme Monooxygenases:

Cytochrome P450 (cytP450).[82, 83]

Because of its many important biological roles in animals, and the spectroscopic richness of the heme cofactor, cytP450s are a frequently studied iron oxygenase. The catalytic cycle (Figure 1-10) of cytP450 begins as a ferric low-spin heme with water bound as the sixth ligand ($P450_{ox}$). Substrate binding causes the water ligand to dissociate and the heme to go high-spin. As a result of this, the redox potential of the heme increases enabling one electron reduction by the protein reductase putidaredoxin and results in a ferrous form of enzyme ($P450_{red}$). O_2 binds end-on to the ferrous heme (oxyP450) and second putidaredoxin mediated reduction occurs. Protonation of the distal oxygen forms an end-on ferric hydroperoxo, and completes the sequence required for heterolytic O-O bond cleavage following a “push/pull” type mechanisms first described in the related heme peroxidases. The electron rich thiolate ligated heme pushes electron density into the antibonding orbitals of the ferric peroxo while a second protonation of the distal oxygen atom provide the pull to the distal oxygen. O-O bond cleavage results in formation of compound I, an Fe^{4+}-oxo with a porphyrin based π-cation radial (compound I), that performs the substrate oxidation via hydrogen atom abstraction. Radical rebound of the hydroxyl back to the substrate results in product formation, and the system returns to the low-spin ferric resting state after product release.

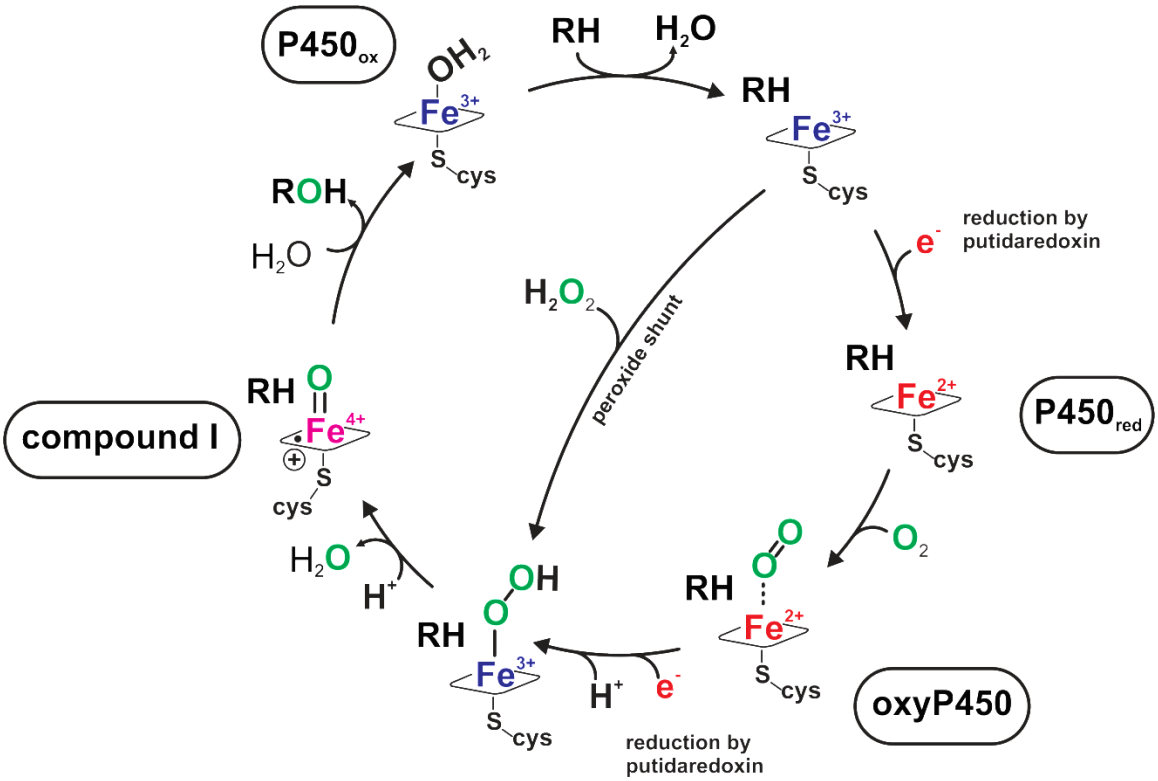

Figure 1-10: Monooxygenase mechanism of cytochrome P450 as illustrated by P450cam.

Nonheme Diiron Monooxygenases:

Soluble Methane Monooxygenase (sMMO).[84-86]

sMMO catalyzes the oxidation of methane to methanol allowing methanotrophs to use methane as their sole carbon and energy source. sMMO is a multicomponent bacterial monooxygenase composed of a reductase (sMMO-R), a small regulatory effector protein (sMMO-B), and a hydroxylase (sMMO-H) that contains the catalytic diiron center. The catalytic cycle of sMMO (Figure 1-11) starts by enzymatic or chemical reduction of the oxidized enzyme (H^{ox}) forming the diferrous H^{red}. Binding of O_2 within the active site but not to either of the iron atoms of the diiron center results in formation of the intermediate labeled O. Intermediate P* forms when O_2 initially binds to the diiron center, perturbing its electronic structure, but not oxidizing it. Next, one electron from each ferrous iron of the diiron center reduces O_2 to a peroxo forming intermediate P

which is best described as a dinuclear Fe^{3+}-μ-1,2-peroxo. Cleavage of the O-O leads to formation of intermediate Q, the unique and highly oxidizing dinuclear Fe^{4+}-μ-oxo species capable of hydroxylating methane despite its high C-H bond strength 105 kcal/mole. After hydrogen atom abstract by Q, product is formed via a radical rebound of the iron bound hydroxide, resulting in the product complex known as T. Product release returns the system to the H^{ox} resting state.

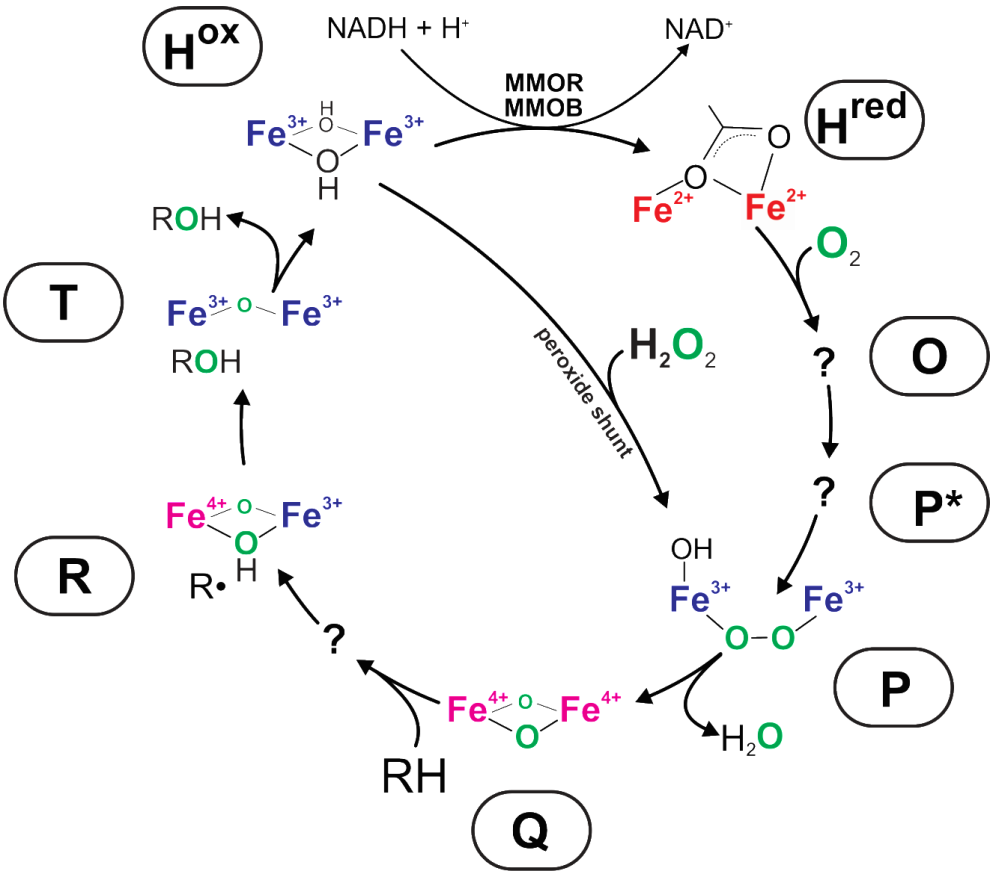

Figure 1-11: Mechanism of methane hydroxylation by sMMO.

Extradiol Ring-cleaving Dioxygenases:

Homoprotocatechuate 2,3-Dioxygenase (HPCD).[87]

HPCD catalyzes the oxidative meta ring-cleavage of protocatechuate (Figure 1-3) with a 2-His-1-carboxylate-ligated mononuclear Fe^{2+}. A defining characteristic of

both extradiol and intradiol ring-cleaving dioxygenases is binding of the substrate hydroxyls directly to the monocular iron. During turnover with HPCD (Figure 1-12) the substrate chelates the iron with one of the hydroxyls deprotonated. Following the common regulation paradigm, substrate binding causes dissociation of an iron bound water molecule, opening a spot for O_2 binding. After O_2 binding, electron density is transferred from the bound substrate to O_2 via the mononuclear iron such that a superoxo/substrate radical pair is formed. Rapid radical recombination forms a Fe^{2+}-alkyperoxo and protonation of the oxygen atom proximal to the mononuclear iron results in heterolytic O-O bond cleavage and formation of lactone by a Criegee rearrangement. Lastly, the lactone is hydrolyzed by the iron bound hydroxide, resulting in the ring cleaved product the ferrous resting state.

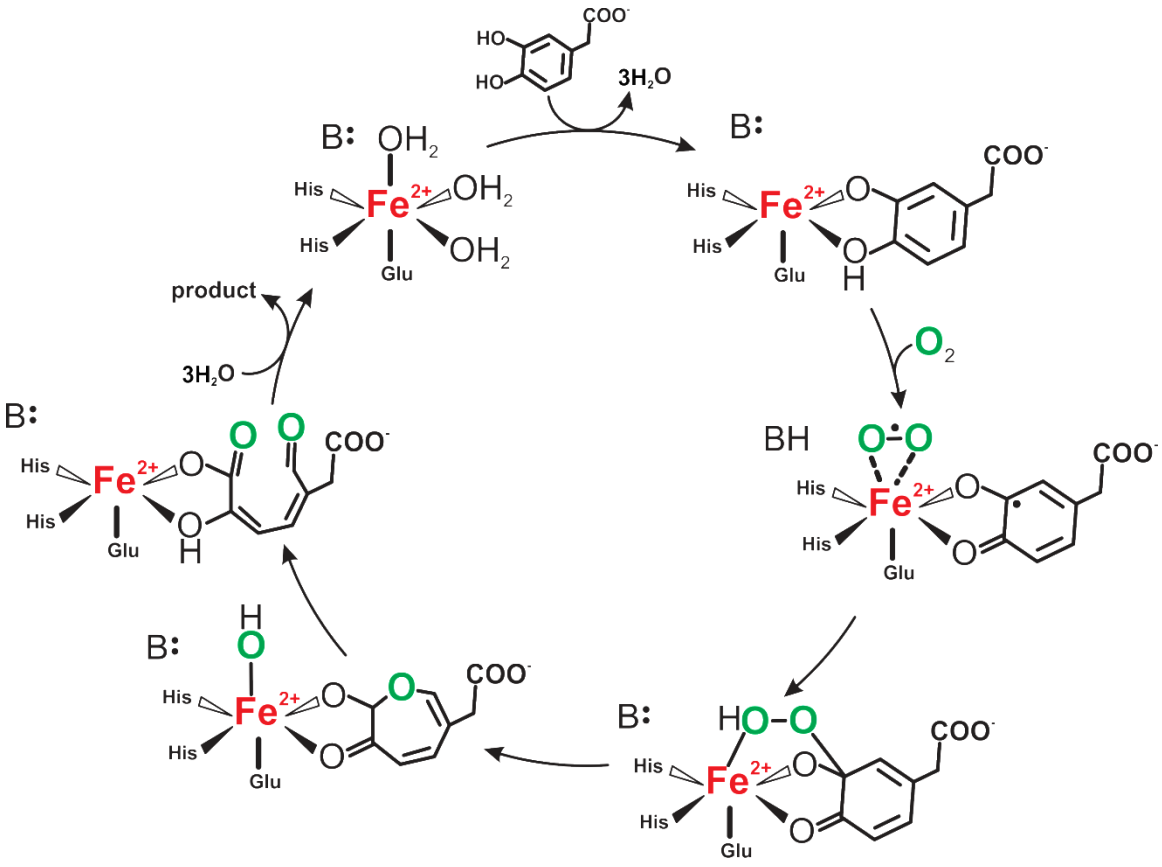

Figure 1-12: Mechanism of meta ring cleavage by the extradiol HPCD.

Intradiol Ring-cleaving Dioxygenases:

Protocatechuate 3,4-Dioxygenase (PCD).[88]

PCD is an intradiol dioxygenase that catalyzes oxidative ortho-cleavage (Figure 1-3). In contrast to the extradiol dioxygenases, catalysis occurs with a ferric mononuclear iron within a 2-His, 2-Tyr ligand set. Catalysis starts in the ferric resting state with a bound hydroxide completing the iron coordination sphere (Figure 1-13). Substrate binding is a multistep process causing dissociation of the iron-bound hydroxide and the axially bound Tyr opening a coordination spot for O_2 activation. Oxygen cannot occupy this site directly because ferric ion has no affinity for O_2. Instead, O_2 reacts with the iron and the substrate in a concerted manner forming a 6-coordinate Fe^{3+}-alkylperoxo intermediate. This species undergoes a structural rearrangement to form an 5-coordinate Fe^{3+}-alkylperoxo. Rebinding of the Tyr ligand protonates the oxygen atom proximal to the mononuclear iron causing O-O bond cleavage and formation of an anhydride intermediate by a Criegee insertion reaction. Attack of the iron-bound hydroxide cleaves the anhydride, and then product dissociation returns the enzyme to the ferric resting state.

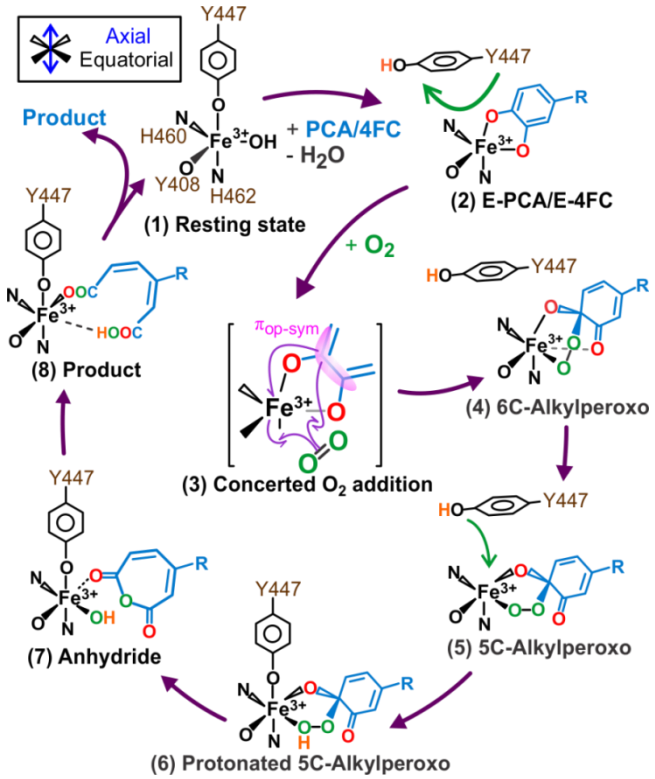

Figure 1-13: Mechanism of ortho ring cleavage by the intradiol PCD.[88]

α-Ketoglutarate Dependent Oxygenases:

Taurine (Hydroxylating) Dioxygenase (TauD).[89]

The α-ketoglutarate dependent oxygenases, like ROs, comprise an enzyme family that catalyzes a wide variety of oxidative chemistry utilizing an active site 2-His-1-carboxylate-bound nonheme mononuclear iron. α-Ketoglutarate-dependent dioxygenases provide an example of a dioxygenase that hydroxylates a substrate and incorporates oxygen into a cosubstrate during the catalytic cycle. One of the most studied reactions is the hydroxylation of taurine catalyzed by TauD (Figure 1-14). As with the monooxygenases cytP450 and sMMO, TauD turnover logically divides into two parts, formation of the high valent oxidant and the reaction of that species with the substrate. Catalysis starts with ferrous mononuclear iron and three water molecules completing the coordination sphere. The α-ketoglutarate binds equatorially and in a bidentate manner to the mononuclear iron with corresponding release of two waters. The remaining axially bound water molecule dissociates after substrate binding, opening a coordination spot for O_2 binding. There is no direct evidence for any species between O_2 binding and breaking of the O-O bond, but the following sequence is generally agreed upon based upon the chemical species formed after O-O bond cleavage. A ferric superoxo forms after O_2 binding to the ferrous mononuclear iron. This species attacks the bound α-ketoglutarate to form an iron-peroxohemiketal bicyclic intermediate. In contrast to ring cleaving dioxygenases, the breaking of the O-O bond of the iron-peroxohemiketal is not facilitated by protonation by an active site base. Instead, heterolytic O-O bond cleavage is driven by oxidative decarboxylation of the α-ketoglutarate cosubstrate. The resulting Fe^{4+}-oxo carries out hydrogen atom abstraction from the substrate, and product is formed via hydroxyl radical rebound as in cytP450 and sMMO. Release of product and succinate return the enzyme to the starting ferrous resting state.

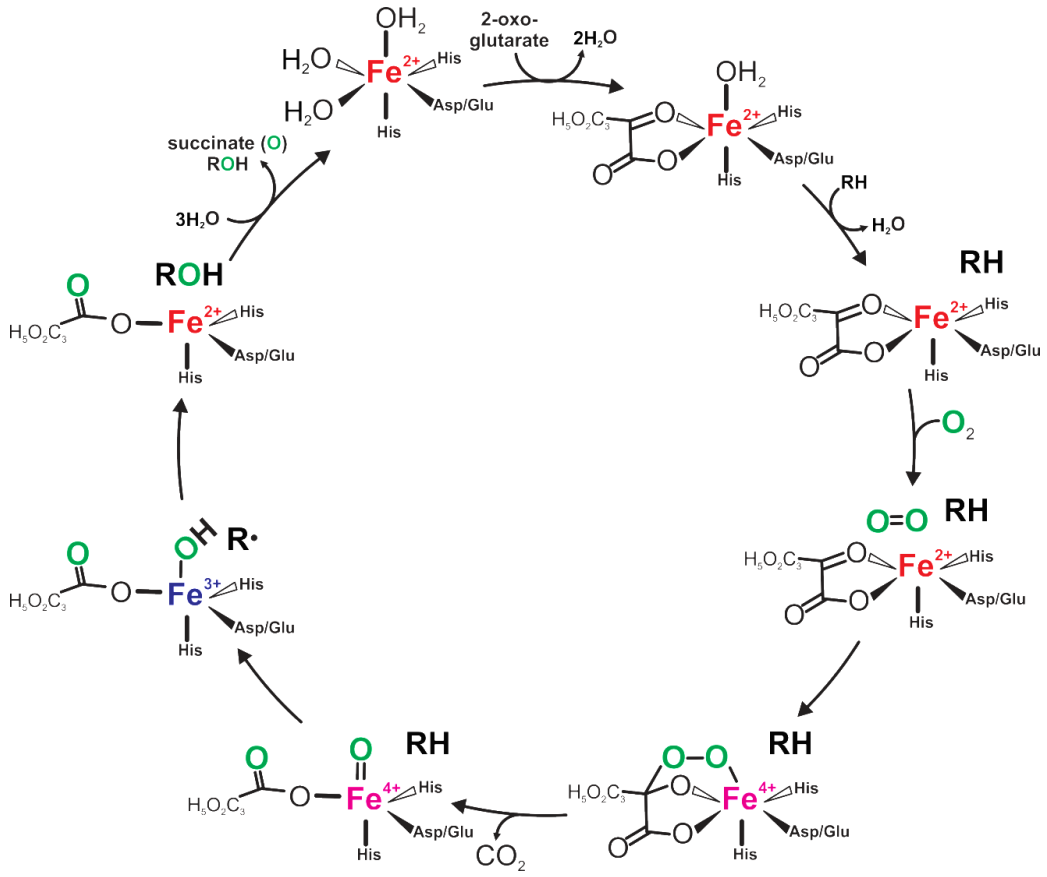

Figure 1-14: Mechanism of substrate hydroxylation by an *α*-ketoglutarate dependent dioxygenase.

Pterin Dependent Dioxygenases:

Aromatic Amino-acid (Hydroxylating) Dioxygenase (AAD).[90]

AADs catalyze the hydroxylation of multiple aromatic amino acids during biosynthesis of tyrosine and multiple neurotransmitters. Like the TauD, the dioxygenase designation of AADs can cause confusion because even though they only insert one atom of O_2 into the aromatic amino acid substrate, they also hydroxylate the tetrahydropterin cosubstrate. As in TauD, the catalytic cycle can be split in to two parts, formation of the Fe^{4+}-oxo reactive species, and hydroxylation of the substrate by the Fe^{4+}-oxo. As in the above examples, binding of the tetrahydropterin and amino acid substrate open a coordination spot for O_2 to bind to the mononuclear iron (Figure 1-15). As with TauD, there is no direct evidence of any intermediate between O_2 binding to the

resting state and the O-O bond cleavage, but it is generally accepted that the Fe^{4+}-oxo is formed via heterolytic cleavage of an Fe^{2+}-peroxypterin intermediate (Figure 1-15). The hydroxylation of aromatic amino acid by the Fe^{4+}-oxo follows a typical electrophilic aromatic substitution with NIH shift mechanism.

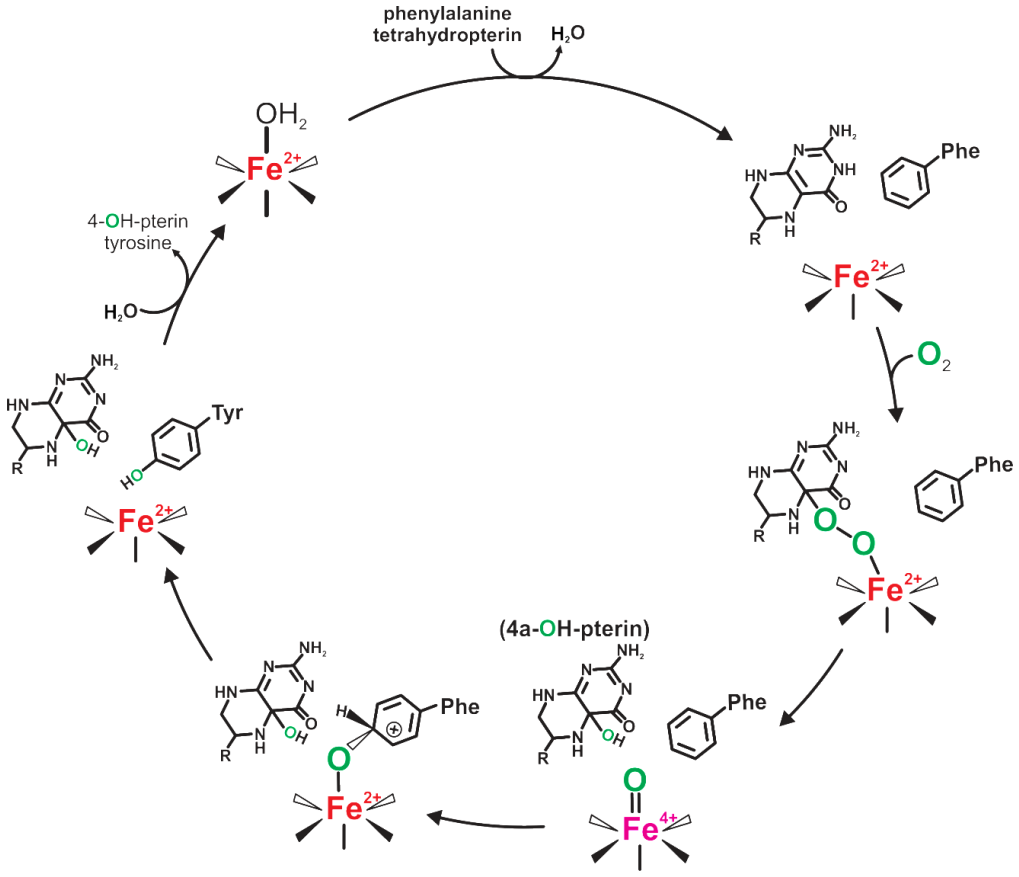

Figure 1-15: Mechanism of substrate hydroxylation by a pterin dependent dioxygenase as illustrated by phenylalanine hydroxylase.

Table 1-2: Summary of O_2 activation performed by iron oxygenases.

				source of electrons for O_2 reduction			distribution of O_2 oxygen atoms		
	enzyme	**reaction type**	**metal center**	**NADH**	**cosubstrate**	**substrate**	**water**	**cosubstrate**	**substrate**
1	RDD	dearomatizing dioxygenase	2-His-1-carboxylate mononuclear iron	2	0	2	0	0	2
2	sMMO	monooxygenase	2-His-4-carboxylate diiron	2	0	2	1	0	1
3	cytP450	monooxygenase	mononuclear heme iron	2	0	2	1	0	1
4	HPCD	ring-cleaving dioxygenase	2-His-1-carboxylate mononuclear Fe^{2+}	0	0	4	0	0	2
5	PCD	ring-cleaving dioxygenase	2-His-2-Tyr mononuclear Fe^{3+}	0	0	4	0	0	2
6	TauD	hydroxylating dioxygenase	2-His-1-carboxylate mononuclear Fe^{2+}	0	2	2	0	1	1
7	AAH	hydroxylating dioxygenase	2-His-1-carboxylate mononuclear Fe^{2+}	0	2	2	0	1	1

Mechanistic Knowledge of Rieske Dearomatizing Dioxygenases

RDDs have characteristics that make them mechanistically distinct from the other iron-dependent dioxygenases and monooxygenases described above (Table 1-2). RDDs are similar to 3 of the 4 other dioxygenases in that they are reactive in the Fe^{2+} state and utilize a 2-His-1-carboxylate facial triad (Table 1-2, rows 4, 6, and 7). However, these dioxygenases extract all four electrons required for O_2 reduction from the substrate or substrate and cosubstrate, whereas RDDs ultimately utilize two electrons from the substrate and two from NADH. The monooxygenases (sMMO and cytP450) also extract two electrons from both substrate and NADH, but the products are oxidized substrate and water rather than a dihydroxylated substrate (Table 1-2, rows 2 and 3). [91-93] It is noteworthy that well-characterized Rieske monooxygenases exists which are structurally similar to RDDs, but exhibit the same NADH and O_2 stoichiometry and single oxygen atom incorporation pattern as sMMO or cytP450.[14, 15] Working under the hypothesis that Rieske mono and dioxygenase utilize a similar mechanism, these similarities have led to mechanistic theories for RDDs along the lines of monooxygenase rather than dioxygenase enzymes.

A hypothesis for the mechanism of RDDs based on typical monooxygenase chemistry is shown in Figure 1-16 using the RDD BZDO.[8] Substrate binds to the enzyme with the Rieske cluster and mononuclear iron reduced (^{red}BZDO-Fe^{2+}), resulting in solvent release from the mononuclear Fe^{2+}. Then, O_2 binds to the Fe^{2+} and an electron from the reduced Rieske cluster is transferred to the mononuclear Fe-O_2 complex to yield a (H)peroxo intermediate similar to those proposed for all well-characterized monooxygenases.[83, 85, 94-96] The (H)peroxo species might be reactive with substrate or the O-O bond could cleave to yield a reactive Fe^{5+}-oxo-hydroxo species (red bracketed box in Figure 1-16).

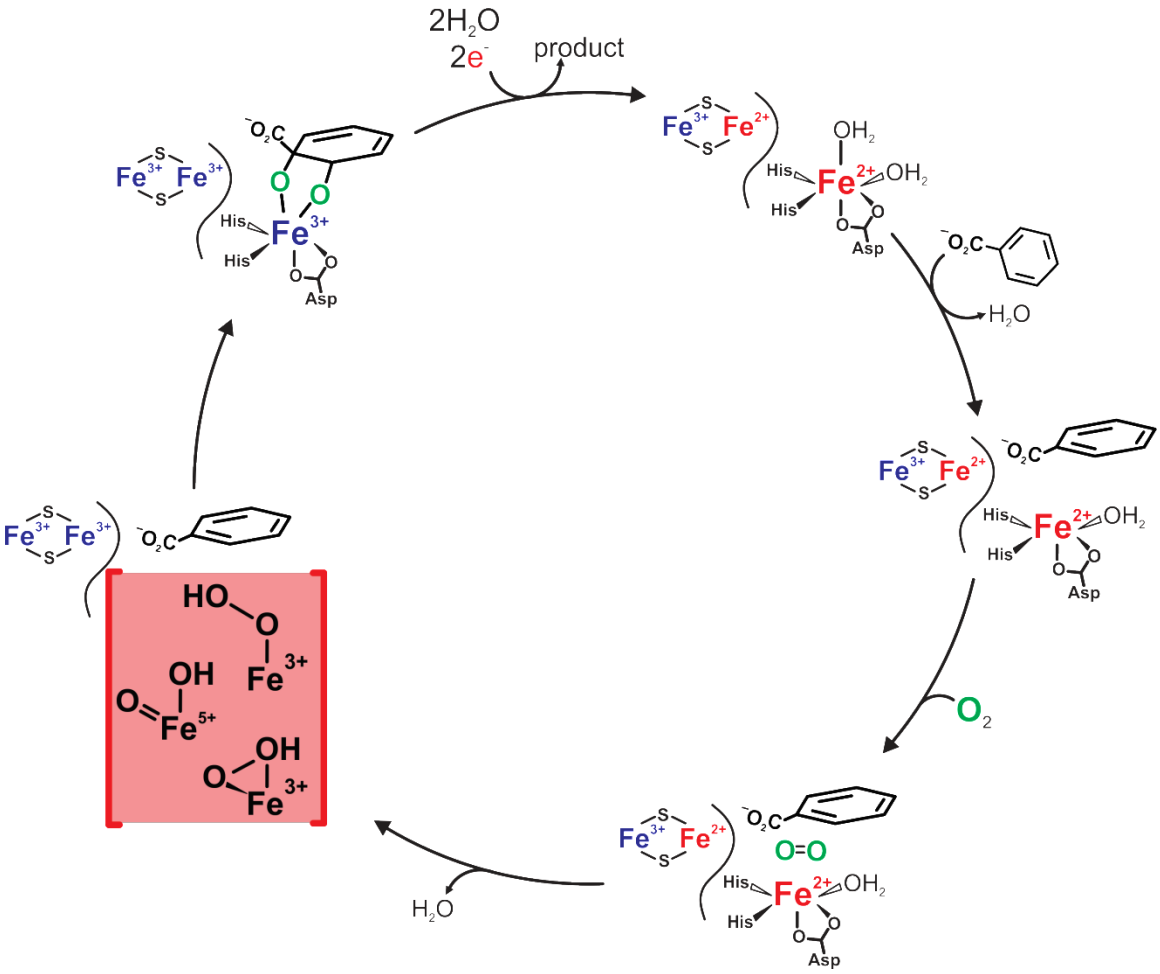

Figure 1-16: Monooxygenase-like mechanism of *cis*-dihydroxylation by RDDs.

Results from experimental and computational approaches have supported the monooxygenase-like mechanism of RDD catalysis, but have not agreed on the identity of the reactive species performing the initial substrate oxidation.[7, 97] *In crystallo* EO_2 and ESO_2 complexes have been characterized in the RDDs NDO and carbazole 1,9a-dioxygenase (CarDO) and in all cases the O_2 appears to be ligated to the mononuclear iron. [12, 70] Both the EO_2 and the ESO_2 complexes of NDO and the ESO_2 complex of CarDO have Fe-O_2 bond distances consistent with a side-on O_2 binding, but the O_2 adduct of CarDO EO_2 complex is reported as end-on. In all of these structures, it is reported that the O-O bond has lengthened to ~ 1.5 Å. This bond distance is longer than the O-O bond distance of molecular O_2 (1.2 Å) and is consistent with the bond length of

a peroxo. However, because of the small difference in the bond distances between molecular O_2 and a peroxo and the intrinsic resolutions of the crystal structures, the formation of an iron-bound peroxo cannot be confirmed using only the crystal structure. As a result, these structures may represent reactive Fe-(H)peroxo species predicted by the monooxygenase like mechanism, but they could also be iron adducts of molecular O_2 or superoxide.

The monooxygenases cytP450 and sMMO can form product in peroxide-driven reactions starting from the oxidized state of the enzyme.[98, 99] Peroxide is equivalent to O_2 reduced by 2 electrons, so the two electrons required for catalysis are supplied by the oxidant, instead of by NADH via the active site iron center(s) as with normal O_2-driven catalysis. In sMMO and cytP450, addition of H_2O_2 to the ferric form of the enzyme results in the formation of a di- or mononuclear Fe^{3+}-(H)peroxo species, respectively, skipping the steps required for O_2 reduction. In this situation, H_2O_2 addition links two nonadjacent intermediates of the normal turnover cycle, thus these reactions are known as peroxide shunt reactions (Figure 1-10 and Figure 1-11). Like these monooxygenases, both BZDO and NDO can form significant yields of the correct *cis*-diol product after addition of substrate and H_2O_2.[10, 100] Of particular interest, is the BZDO peroxide shunt. Spectroscopic analysis of this reaction revealed formation of a transient $S = 5/2$ ferric species with spectroscopic properties most consistent with a side-on Fe^{3+}-(H)peroxo species. This intermediate is apparently identical to that proposed from the *in crystallo* ESO_2 adducts of NDO and CarDO as described in the previous paragraph.

DFT studies based on active site models of the structurally homologous RDDs NDO and nitrobenzene 1,2-dioxygenase (NBDO) have reached different conclusions regarding the reaction coordinate of the proposed monooxygenase-like mechanism. The calculations with NDO showed that heterolytic cleavage of a side-on Fe^{3+}-hydroperoxo to form a Fe^{5+}-oxo/hydroxo occurred with a $\Delta G^{\ddagger}$ of 26.5 and a ΔG of ~ 15 kcal/mole. Based on the large activation energy and the endothermic nature of this reaction, the authors concluded it was unlikely to occur. An alternative reaction coordinate was calculated in which the side-on Fe^{3+}-hydroperoxo performs the initial substrate oxidation. The proposed reaction coordinate for this reaction started with a rate-limiting and concerted aromatic oxidation and O-O bond breaking, resulting in formation of an epoxide with $\Delta G^{\ddagger}$

=17.5 kcal/mole and a ΔG = -25.5 kcal/mole. The epoxide would then open aided by an interaction with the mononuclear iron resulting in a cation that is attacked by an iron-bound hydroxide to form the *cis*-diol product. All calculated steps occurring after epoxide formation are energetically favorable with low energy transitions states and near thermoneutral or exothermic intermediates. Because of the lowered activation energy for the initial substrate oxidation and the energetically favorable pathway to product, the authors concluded this mechanism was the most plausable.[101]

A separate DFT study reported conflicting results modeling the *cis*-dihydroxylation of nitrobenzene by NBDO. The calculations in this study showed the favored epoxide forming pathway from the NDO study was comparably exothermic, but had a significantly higher activation energy ($\Delta G^{\ddagger}$ ~ 20-40 kcal/mole). Furthermore, the resulting optimized structures in this study suggested that the epoxide intermediate would move away from the mononuclear iron. As a result, the epoxide intermediate would not be opened via an interaction with the mononuclear iron and an alternative lactone side product would form instead of the correct *cis*-diol. [102] Due to these differences, the authors proposed that the rate-limiting initial oxidation of the aromatic substrate occurs via an Fe^{5+}-oxo/hydroxo.

Several insights have been gained from studies with small-molecule iron-chelate complexes that mimic the active site of RDDs. Investigations of olefin oxidation using various complexes showed two distinct reactive pathways to *cis*-dihydroxylation.[103] Both types of reaction rely on the availability of two adjacent ligand sites on the iron, as is apparently the case for RRDs. In one type of reaction catalyzed by some low spin Fe^{3+}-(H)peroxo complexes within TPA (tris(2-pyridylmethyl)amine) or BPMEN (*N,N'*-dimethyl-*N,N'*-bis(2-pyridylmethyl)-1,2-diaminoethane) ligands, one oxygen from water is incorporated into the *cis*-diol product in addition to one oxygen from H_2O_2. [104] This observation and subsequent experiments have demonstrated a water assisted cleavage of the O-O bond to form an Fe^{5+}-oxo/hydroxo reactive species. [105] In contrast, both *cis*-diol oxygens were found to derive from peroxide when the reactions were carried out with high-spin TPA and BPMEN iron-chelate compounds.[103] The mononuclear iron of RDDs is high spin in both the ferric and ferrous state,[8] but whether this correlates with the type of reactive species formed is unknown. Another study using high-spin TMC-

Fe^{3+}-hydroperoxo complexes has shown that the *S* = 5/2 state increased the oxidation potential. [106] This generates a more potent species for electrophilic catalysis, thereby providing evidence that an Fe-(H)peroxo could be active in RDDs.

Research Directions for Rieske Dearomatizing Dioxygenases

As described above, a significant body of experimental and computational results support a monooxygenase-like mechanism for *cis*-dihydroxylation by RDDs utilizing an Fe^{3+}-(H)peroxo or Fe^{5+}-oxo/hydroxo as the species that performs the initial substrate oxidation (Figure 1-16). This mechanism is a valid and logical hypothesis, but the accumulated evidence is not beyond reasonable scientific criticism. Based on the above evidence, it can be concluded that Fe^{3+}-(H)peroxo species can form within an RDD active site, and these intermediates lie on a reaction coordinate capable of *cis*-dihydroxylation. No evidence for such a species has been observed during O_2-driven solution single-turnovers, so it cannot be ruled out that under the optimized conditions, RDDs uses a different chemical pathway. A similar situation has been observed in the ring-cleaving dioxygenase HPCD. Several alternative product forming pathways exist under suboptimal conditions in which an Fe-(H)peroxo can form product, but a different pathway (Figure 1-12) is kinetically favored in the optimized conditions.[87, 107]

The focus on the monooxygenase-based mechanism shown in Figure 1-16 has limited consideration of a mechanistic strategy shared by dioxygenases in the 2-His-1-carboxylate family. These systems are distinct from the monooxygenases in that cleavage of the O-O bond is preceded by formation of an iron/alkylperoxo with the substrate or cosubstrate and the electrons required for O_2 reduction are derived from oxidation of the substrate or cosubstrate. Figure 1-17 illustrates how a comparable iron/alkylperoxo could form within the established mechanistic boundaries of BZDO single-turnover. The proposed mechanisms are identical until formation of the ESO_2 complex. At this point they diverge, and instead of Rieske cluster oxidation and formation an Fe^{3+}-(H)peroxo and/or Fe^{5+}-oxo/hydroxo, a substrate oxidation that precedes Rieske cluster oxidation would result in the formation an Fe^{3+}-alkylperoxo-

cation radical (alkyl$^{\bullet+}$peroxo). The formation of this species would trigger Rieske cluster oxidation resulting in an Fe^{2+}- alkyl$^{\bullet+}$peroxo. This species, as in the analogous dioxygenase, would then undergo O-O bond cleavage and product formation.

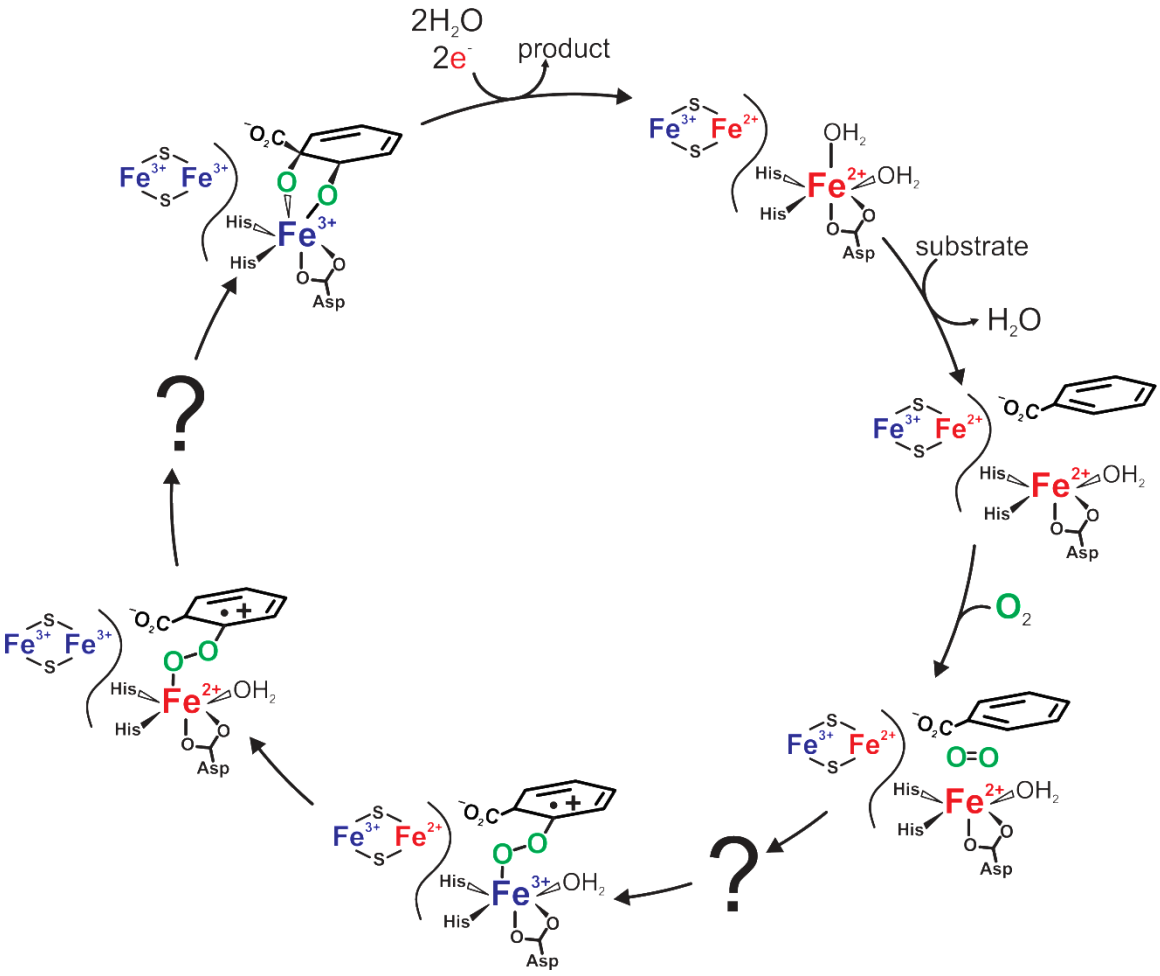

Figure 1-17: RDD *cis*-dihydroxylation based on dioxygenase chemistry.

When considered in the context of both the monooxygenase and dioxygenase-like mechanisms an experimental result reported in the original BZDO single-turnover study takes on new importance. The experiment showed that the rate of Rieske cluster oxidation is decreased when 3-methyl, 3-chloro, or 3-fluorobenzoate was used as the substrate (Figure 1-18).[8] There are two ways the addition of aromatic substituents could

affect the rate constant for electron transfer during RDD single-turnover reactions. First, adding aromatic substituents can change the size of the substrate, and the added steric bulk may alter the forward and reverse rate constants for substrate and/or O_2 binding. The formation of an ESO_2 complex is a prerequisite for electron transfer, so if the overall rate of ESO_2 formation is decreased by addition of the aromatic substituents, it would be reflected by the Rieske cluster oxidation. This explanation could cause a decrease in the rate constant of Rieske cluster oxidation in the monooxygenase and dioxygenase-like mechanism. Second, aromatic substituents alter the electronic properties of a molecule by changing the distribution of the π-electrons within the aromatic bonds. This can either activate or deactivate the substrate for the chemical reaction performed. In the proposed substrate oxidations, electron donating substituents would activate the substrate and increase the reactions rate, while electron withdrawing substituents would deactivate and slow the reaction.

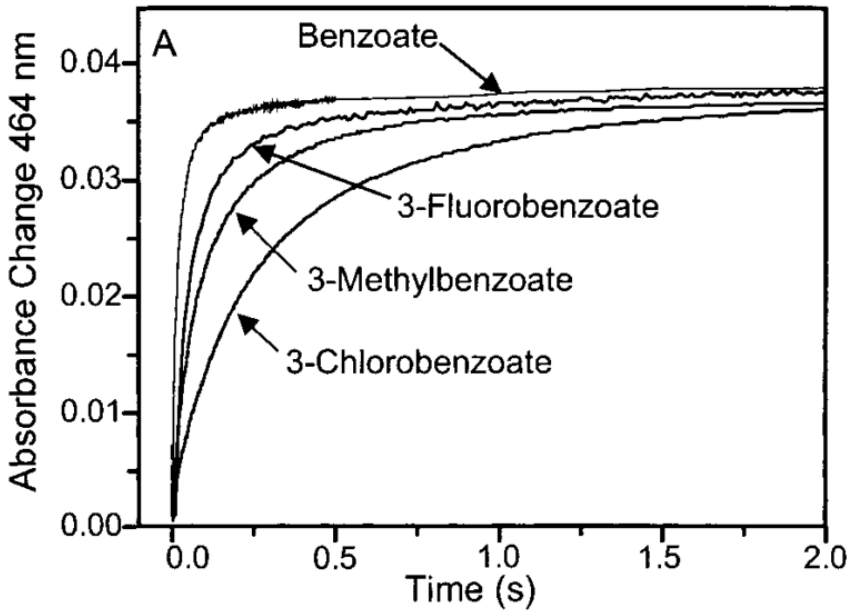

Figure 1-18: Original observation of substrate type affecting Rieske cluster oxidation. The Van der Waals radii of methyl group, chlorine, fluorine, and hydrogen are 200, 175, 147, and 125 Å, respectively.

In contrast to a binding explanation, demonstration that the reduced rate constant for Rieske cluster oxidation is caused by deactivation of the aromatic ring by inductive effects of its substituents would be evidence for the dioxygenase-like mechanism. The formation of Fe^{3+}-(H)peroxo or Fe^{5+}-oxo/hydroxo species characteristic of the monooxygenase-like mechanism requires transfer of the electron from the Rieske cluster. As a result, the reactive species is formed before the substrate is oxidized. In such a mechanism, the electronics of the substrate cannot modulate the rate constants of electron transfer because Rieske cluster oxidation occurs before the initial substrate oxidation. In the dioxygenase-like hypothesis, formation of the Fe^{3+}- alkyl$^{\bullet+}$peroxo is the initial oxidation step and triggers Rieske cluster oxidation. Because the substrate is oxidized before electron transfer, the rate constant of this transfer would be sensitive to the electronics of the substrate, assuming this initial oxidation is rate-limiting.

All three substituents in Figure 1-18 decreased the observed rate constants of Rieske cluster oxidation. This data does not support the explanation based on substituent inductive effect because the electron-donating and substrate-activating methyl substituent results in slower Rieske cluster oxidation than the deactivating fluorine. Nor is the data clearly consistent with the binding hypothesis. Based on substituent Van der Waals radii (see caption of Figure 1-18 for values), the Rieske cluster oxidation rate constant should decrease in the order fluoro > chloro > methyl. Inductive and steric effects could be occurring simultaneously and to different degrees, such that the true basis of the decrease in rate constants cannot be resolved by the data in Figure 1-18. Using these ideas as a guide, a set of experiments was designed to isolate the contributions of binding and reactivity and directly test the two hypotheses for the decreased rate constants.

We choose to use the RDD BZDO and a set of fluorinated benzoates for this study. BZDO is an archetypal α_3/β_3 RDD that utilizes the electrons from NADH to catalyze the conversion of benzoate to (1S,6R)-1,6-*cis*-dihydroxycyclohexa-2,4-diene-1-carboxy acid (benzoate *cis*-diol), inserting both atoms from O_2 into the substrate while forming the product (Table 1-1, row #1). In order to obtain information about the individual binding and chemical steps occurring during turnover, the techniques of presteady state kinetic must be used. BZDO is ideal for such a study, because (1) it is heterologously expressed in high yield, (2) the benzoic acid substrates are soluble

enough to achieve the high concentrations preferred for presteady-state analysis under pseudo-first-order conditions, and (3) a large variety of substituted benzoic acids are commercially available.

Fluorinated benzoic acids were used in this study because they are the smallest substituent, so their effects on binding should be minimized, but their electronegativity significantly perturbs the electronic structure of the aromatic substrates. Given these properties, the fluorine substituents should result in the largest substrate deactivation per change in substrate size and provide the best chance at isolating the variables in question. 4-fluorobenzoate, 3,5-difluorobenzoate, and 3,4,5-trifluorobenzoate were chosen for this study based on two criteria. First, *ortho* substituted benzoic acids were not selected to avoid an additional variable that may perturb the reaction coordinate, the rehybridization of an aromatic C-F (compared to C-H) bond that occurs during the *cis*-dihydroxylation reaction. Second, only benzoic acids symmetric about the axis defined by carbons #1 (*ipso* carbon) and #4 were selected. *cis*-Dihydroxylation can presumably occur on either side of the *ipso* carbon, so using a symmetric substrate yields only one product and greatly simplifies the possible results.

Using this experimental setup, we set out to investigate what rate limits the electron transfer step within BZDO single turnover by monitoring how the observed rate constant of Rieske cluster oxidation changes over a range of substrate and O_2 concentrations. With proper experimental setup, the trend in the observed rate constants (linear, hyperbolic, or no change) can reveal if the binding of substrate, O_2, or another step after formation of the initial ESO_2 complex rate limits the electron transfer. Doing these substrate and O_2 titrations with benzoate and each of the fluorobenzoates can show if all reactions are rate limited by the same step, or if the rate-limiting step is changed by addition of fluorine substituents.

However, there is an additional question originating from the initial single-turnover studies that needed to be addressed before the experimental plan outlined above could be implemented. Past experiments that are further supported by the results in this thesis show that the observed optical change observed during single turnover (Figure 1-8) is only caused by oxidation of the Rieske cluster and no other optically active species form during the time course. Because this optical change is caused by an

intramolecular electron transfer directly between the Rieske cluster and the mononuclear iron, logically it should occur in a single kinetic step. However, the kinetic analysis of the Rieske cluster oxidation time course shows this oxidation occurs in three to five kinetically resolved steps. The original study was not able to resolve what causes the multistep Rieske cluster oxidation or which of the kinetically resolved steps are relevant to product formation. However, this information is critical to a further understanding the *cis*-dihydroxylation mechanism and prerequisite for the proposed experimental plan.

The work done to address the outstanding questions of how RDDs perform this fascinating reaction is present here. In Chapter 2, the study of the multistep Rieske cluster oxidation process is presented. The results in this chapter provide the first evidence that only one of the multiple Rieske cluster oxidation steps is relevant to single-turnover product formation. Using the new insights gained in Chapter 2, the analysis of the binding and chemical steps occurring during BZDO single turnover was conducted using benzoate and a series of fluorinated benzoates proposed above. The results of this study provide the first kinetic evidence of a dioxygenase-like mechanism (Figure 1-17) for RDD *cis*-dihydroxylation in which the initial substrate oxidation occurs after formation of the ESO_2 complex, but before Rieske cluster oxidation. In Chapter 4 the peroxide shunt reactions are reanalyzed in light of the new mechanistic insights from Chapter 3. Chapter 5 is a perspective on the newly proposed dioxygenase-like mechanism detailing how this mechanism fits within the current biochemical landscape of RDD and nonheme iron oxygenases.

Chapter 2

Kinetic Investigation of Electron Transfer During BZDO Single Turnover with Native and Fluorinated Substrates

Summary

Rieske dearomatizing dioxygenases (RDDs) are the only enzymes that catalyze dearomatizing *cis*-dihydroxylation of aromatic compounds (Table 1-1), and this unique chemistry makes them well-suited for multiple industrial and medical applications. Missing from the RDD literature is a thorough study of the presteady-state kinetics that would provide the kinetic constants for individual binding and chemistry steps. A problem standing in the way of such a kinetic study is the complex time course of the optically monitored Rieske cluster oxidation during single-turnover reactions (Figure 1-8). The structure of the RDD active site, experimental observations, and theoretical calculations all support the prediction that the Rieske cluster should oxidize in a single kinetic step, but the experimentally obtained time courses suggest that it occurs in multiple steps. In the following chapter, the hitherto confounding multistep Rieske cluster oxidation is studied with benzoate and a series of fluorinated benzoates selected for their potential use as mechanistic probe. For all of the substrates tested, the experimental results support a model in which the Rieske cluster oxidizes in multiple independent and parallel steps, but only the fastest oxidation step leads to product formation. The insights gained from this study provide the first experimentally supported model to account for the multistep Rieske cluster oxidation, and supplies the needed information to conduct future presteady-state investigations.

Introduction

Rieske oxygenases are a family of enzymes that catalyze a diverse repertoire of chemical reactions, but a subgroup termed Rieske dearomatizing dioxygenases (RDDs) are the only known enzymes that catalyze dearomatizing *cis*-dihydroxylation of aromatic compounds (Table 1-1).[7] This unique aromatic chemistry makes RDDs of interest for their use as agents for bioremediation, and as green catalysts for production of industrially and medically relevant regio and stereospecific *cis*-diols.[52] A complete understanding of the catalytic mechanism of RDDs will aid further development and utilization of these applications and provide guiding insights for mechanistic studies of the broad class of Rieske oxygenases.

Multiple experimental techniques have been used to gain a foundational understanding of how RDDs catalyze *cis*-dihydroxylation, but absent from the RDD literature is a thorough study of the presteady-state kinetics. Such a study would provide the kinetic constants for individual binding and chemistry steps, and this information is needed to plan and interpret other experiments probing the mechanism of *cis*-dihydroxylation. In principle, the optical change resulting from Rieske cluster oxidation (Figure 1-8) provides a convenient spectroscopic handle for monitoring the events that precede it during single-turnover reactions. Past studies have provided substantial evidence that the observed optical change is only caused by oxidation of the Rieske cluster, and this conclusion is further supported by data reported in this chapter. As illustrated in Figure 1-6, the Rieske cluster and mononuclear iron are only separated ~15 Å, and a bridging aspartate residue provides a through-bond pathway to facilitate rapid electron transfer directly between the Rieske cluster and the mononuclear iron. Several lines of evidence and multiple experimental observations provide a strong argument that the electron transfer is effectively irreversible. Taken together, it is logical to predict that the electron transfer should occur as a single step process, and that the observed time course collected under pseudo-first-order conditions should be well simulated by a single exponential function.

The predicted single-exponential Rieske cluster oxidation is not what is observed experimentally. In the previous single-turnover studies, as well as every time course inspected in the current study, multiple exponentials (≥ 4) are required for a satisfactory

fit of the complete time course under pseudo-first-order conditions. This means that the Rieske cluster oxidation occurs in several kinetically resolvable steps. By comparison to k_{cat}, 2 or 3 (depending on substrate type) of the steps are catalytically relevant. Several hypotheses have been proposed for this multistep process. One possible explanation is that oxidation of the Rieske cluster occurs in a multiple sequential steps. A second explanation is that subpopulations of the enzyme result in multiple parallel electron transfer reactions each with a distinct rate constant. To further explore this longstanding conundrum, the kinetics of product formation were determined for single-turnover reactions under pseudo-first-order conditions in the presence of benzoate or one of several fluorinated benzoates.

Materials and Methods

Chemicals and Reagents.

Water used in all experiments was purified with a Millipore Super-Q system. All commercial reagents were purchased from standard vendors and used without further purification. Gases were purchased from Matheson. Unless noted, all enzymatic reactions were conducted in a standard reaction buffer of pH 6.9 MOPS (50 mM) and NaCl (100 mM).

Cloning, Heterologous Expression, and Purification of BZDO.

BZDO was cloned from genomic DNA of *Pseudomonas putida* mt-2 into the plasmid pET-29 using standard restriction enzyme-based methods. Heterologous expression utilized *E. coli* BL21(DE3) co-expressing a subset of proteins of the *Isc* pathway from the plasmid pACYC-*isc* that increased Rieske cluster loading in expressed protein.[108] The strain was grown in 2 liter flasks each containing 1 liter of LB media supplemented with kanamycin (50 µg/ml), chloramphenicol (34 µg/ml), 10 mg/ml ferrous ammonium sulfate at 30 °C and 150 RPM. When the optical density of the culture at 600 nm was 0.5, the temperature of the shaker was reduced to 20 °C. Culture growth continued while the cultures cooled to ~ 23 °C. When the OD of the culture at 600 nm reached 0.9, the protein expression was induced with IPTG (250 µM). The cells were harvested by centrifugation after 15 h of growth.

BZDO was purified using modifications to the previously reported procedure.[8] Cell paste (100 g) was lysed by sonication in 250 ml of a pH 7.5 buffered solution of HEPES (125 mM), glycerol (5%), DTT (1 mM) and 20 units DNase I (New England Biolabs) maintaining the slurry temperature < 10 °C. The lysate was centrifuged at 39,000 × g at 4 °C for 45 min to pellet the insoluble cellular debris. The cell-free extract containing soluble BZDO was loaded onto a 500 ml DEAE column (resin bed diameter ≈ 55 mm) equilibrated with pH 7.5 purification buffer consisting of HEPES (25 mM), glycerol (5%), and DTT (1 mM). Then, the column was washed with 1 liter of purification buffer supplemented with 100 mM NaCl. Protein fractionation and elution was achieved with a 5 liter linear gradient of NaCl from 100 to 250 mM in purification buffer at 15

ml/min. Coomassie stained SDS-PAGE gels were used to select pure fractions of BZDO and the resulting dilute pool was concentrated, frozen in liquid N_2, and stored at -80 °C.

The specific activity of the enzyme was assayed by monitoring O_2 consumption during steady state assays as described below. The specific activity of BZDO was ~ 12.5 units/mg (one unit of enzyme activity is equal to the amount of BZDO required to consumed 1 µmole O_2 per minute). This activity is higher than previously reported,[8] however, the assay temperature (4 °C) and concentration of BZDR (15 µM) in the present assays was different from those previously reported.

Cloning, Heterologous Expression, and Purification of BZDR.

The protein reductase required for catalytic turnover, BZDR, was cloned from genomic DNA of *Pseudomonas putida* mt-2 into the plasmid p11 (DNASU Plasmid Repository) using standard restriction enzyme-based methods resulting in an N-terminal His_6-tagged protein construct. Heterologous expression was similar to that described for BZDO, but the media was Terrific Broth containing ampicillin (50 µg/ml), chloramphenicol (34 µg/ml), 2.5 % glycerol and 10 mg/ml ferrous ammonium sulfate. The growth temperature was 35 °C.

To purify BZDR, 100 g of cell paste was lysed by sonication in 250 ml of a pH 8.0 buffered solution of sodium phosphate (50 mM) and NaCl (200 mM) containing 10 mM imidazole and 20 units DNase I (New England Biolabs) maintaining the slurry temperature below 10 °C. The lysate was centrifuged at 39,000 × g at 4 °C for 45 min to pellet the insoluble cellular debris. The cell free extract containing soluble expressed BZDR was loaded onto a 25 ml Ni-NTA column (Qiagen) equilibrated in the same buffer used during lysis. The column was washed with 250 ml of the phosphate/ NaCl buffer containing 20 mM imidazole and the expressed BZDR was eluted with the same buffer containing 250 mM imidazole. Coomassie-stained SDS-PAGE gels were used to select pure fractions of BZDR, and the resulting dilute pool was dialyzed in a pH 7.0 buffer of MOPS (25 mM), glycerol (5 %), and DTT (1 mM) and subsequently concentrated, frozen in liquid N_2, and stored at -80 °C.

BZDO Steady-State Activity Assays.

The k_{cat} was estimated by monitoring the rate of O_2 consumption during catalytic turnover using a Hansatech Oxytherm oxygen electrode at 4 °C, 50 mM MOPS buffer,

pH 6.8 plus 100 mM NaCl with the concentration of BZDR optimized and the substrates saturated. The reactions contained benzoate or a fluorobenzoate (10 mM), NADH (0.6 mM), BZDR (15 µM), O_2 (250 µM) and BZDO at 0.18 µM, 1.2 µM, 0.6 µM, or 4.8 µM when assaying with benzoate, 4-FB, 3,5-FB, or 3,4,5-FB, respectively. Reactions were initiated by addition of NADH.

Anaerobic Technique and Chemical Reduction of BZDO.

Solutions of BZDO were made anaerobic by purging the headspace of a sealed vial while stirring on ice with high purity argon gas dispensed through an additional O_2 scrubbing column (Agilent). Reduction of the mononuclear iron and Rieske cluster for single-turnover experiments was conducted in an anaerobic glove bag (Coy). After adding methyl viologen (20 µM), sodium dithionite was added from a concentrated stock until the blue color of reduced methyl viologen persisted for ≥ 20 min indicating complete reduction of BZDOs metal centers. The methyl viologen and dithionite were removed with a PD-10 desalting column (GE Healthcare) in the anaerobic chamber.

Stopped-Flow Analysis of Single Turnover Reactions.

Stopped-flow experiments were performed at 4 °C, 50 mM MOPS buffer, pH 6.8 plus 100 mM NaCl using an Applied Photophysics SX.18MV configured for single wavelength data collection at 464 nm. The instrument was made anaerobic by flushing with a dithionite solution and then anaerobic buffer. BZDO (60 µM) was reduced as described above and mixed with a solution containing varied concentrations of substrate and O_2 (see figure legends). Fitting procedures for time courses to multiexponential equations are described below.

Chemical Quench and Rapid Chemical Quench Product Analysis.

Reduced BZDO (400 µM) was mixed 1:1 with reaction buffer (50 mM MOPS buffer, pH 6.8 plus 100 mM NaCl) saturated with O_2 (1.8 mM at 4 °C) containing benzoate or a fluorobenzoate (10 mM). For time point quenches of completed reactions (> 3 min), 200 µl of the reaction mixture was pipetted into 800 µl of rapidly stirring 1 M HCl. Rapid quenches were accomplished in an identical manner except that an Update 715 Ram Syringe Controller was used to mix and dispense the reactants. Sodium formate (50 µl of 7.5 M) and NaOH (50 µl of 10 M) were added to the quenched solution to buffer the pH to ≈ 3.5 and 400 µl H_2O was added to bring the final volume up to 1.5

ml. Each sample was vortexed (~20 s) and the denatured protein was removed from the solution by centrifugation at 4 °C before HPLC was used to analyze 1 ml of the quenched reaction. HPLC was performed on a Waters system with a 1525 binary pump, 2487 dual wavelength UV/Vis detector, and an Agilent Zorbax SB C18 column (2.6 mm × 150 mm, 5 µm) with a gradient of 4 to 100% acetonitrile/0.1% formic acid over 7.5 min following an isocratic flow at 4% acetonitrile/0.1% formic acid for 2.5 min. The *cis*-diol products were detected by their optical absorption at 262 nm.

Catalase Assay for H_2O_2.

The enzyme catalase was used in several applications to assay for the presence of H_2O_2 at the end single-turnover and catalytic reactions. Catalase disproportionates H_2O_2 to H_2O and O_2 ($2\ H_2O_2 \rightarrow 2\ H_2O + O_2$). Catalase assays of catalytic turnover were done in a Hansatech Oxytherm oxygen electrode as outlined above for steady-state assays except that the NADH concentration was reduced so that it was the limiting reagent. After O_2 consumption had stopped, a catalytic amount of catalase was added (~ 5 µM) and the increase in O_2 concentration was monitored. Catalase assays for single-turnover reactions were done by transferring reneutralized acid or base quenched reactions to the oxygen electrode and monitoring the increase in O_2 concentration after adding a catalytic amount of catalase (~ 5 µM).

Fitting Procedures for Reaction Time Courses.

Nonlinear regression fitting of the kinetic traces of the Rieske oxidation reactions was performed using the Applied Photophysics Pro-Data Software Suite (version 4.2.12). For multistep reactions, the time course is expected to be described by an equation with the same number of exponential terms as reaction steps. The observed absorbance ($A_{t,obs}$) is given by: [109]

$$\boldsymbol{A_{t,obs} = A_{\infty} + \sum_{i=1}^{n} a_i e^{\left(-\frac{t}{\tau i}\right)}}$$

Equation 1

where $1/\tau_i$ is the reciprocal relaxation time of the phase in s^{-1}, a_i is the observed amplitude of phase i (of n) in absorbance units, t is time (s) and A_∞ is the final absorbance.

Stopped-flow data generated with Applied Photophysics instrumentation has two intrinsic data artifacts that must be avoided for repeatable and accurate data fitting (personal communication, Applied Photophysics). The stopped-flow instrumentation has a pressure hold option that, when activated, holds the drive-ram pressure throughout data collection. Due to potential breakage of the optical cuvette, pressure hold shots cannot exceed 10 seconds in length. When pressure hold is not in operation, the drive-ram cycle is complete in 0.05 seconds at which point pressure is released, and this causes an artifact within the data. To avoid this artifact during data fitting it is prudent not to fit nonpressure-hold time courses before 0.1 seconds. The second artifact occurs at very early times ≤ 0.01 seconds, and this appears to be caused by the dissolved gas that is required for the study of oxygenases. This artifact is less consistently observed than the one caused by the pressure release. To avoid this artifact is best not to fit data at times < 0.01 seconds.

Because of the variation in the number of phases and the magnitudes of the RRTs, multiple fitting procedures are required for the different substrates. The slowest substrate (3,4,5-FB) can be well fit with only a single 100 s nonpressure-hold time course. In this case, the RRTs of all the phases are slow enough that data before 0.1 seconds is not required. For the faster substrates (benzoate, 3,5FB, and 4-FB) the data between 0.01 and 0.1 s is required for accurate fitting of the faster phases, but data at times longer than 10 s is required for fitting the slower phases. In this case, both a 100 s nonpressure-hold and a 10 s pressure-hold time course must be collected. The magnitudes of the slower RRTs were first obtained from the 100 s time course. These values were then held constant while fitting the 10 s time course to obtain accurate values for the faster RRTs.

Authentic Standards of Dearomatized, 1,2-*cis*-Diol Products.

The 1,2 *cis*-diol products of benzoate and all fluorobenzoates in Table 1 were produced using *Ralstonia eutrophus* strain B9, a mutant that excretes the *cis*-diols into the media, and purified according to previously reported procedures. [51, 110, 111] Benzoate, 4-FB, and 3,5-FB *cis*-diols were obtained in high purity and characterized by ^{1}H- and, when applicable, ^{19}F-NMR. Residual proteated solvent (δ_H 3.31) was the reference compound for ^{1}H-NMR. These products were characterized and found to have the NMR spectral characteristics listed below. Using the methods referenced above, the 3,4,5-FB

cis-diol was obtained in moderate purity. Based on comparison with the other *cis*-diols, we assigned one observed multiplet (δ_H 5.37) to 3,4,5-FB *cis*-diol (500 MHz, CD_3OD). The amount of 3,4,5-FB *cis*-diol in the mixture was quantified by comparison to the ^{1}H-NMR integration values of a known amount of mesitylene.

(1*S*,6*R*)-1,6-*cis*-dihydroxycyclohexa-2,4-diene-1-carboxy acid (benzoate *cis*-diol). Off white solid: ^{1}H NMR (500 MHz, CD_3OD): δ_H 6.11 (1H, dd, J_1 = 9Hz, J_2 = 5Hz), 5.95-5.91 (1H, m), 5.80 (2H, br m), 4.85 (1H, s).

(1*S*,6*R*)-4-fluoro-1,6-*cis*-dihydroxycyclohexa-2,4-diene-1-carboxyic acid (4-FB *cis*-diol). Pink solid: ^{1}H NMR (500 MHz, CD_3OD): δ_H 6.08-6.04 (1H, m), 5.95 (1H, dd, J_1 = 10Hz, J_2 = 6Hz), 5.27 (1H, dt, , J_1 = 12 Hz, J_2 = 3 Hz), 4.83 (1H, q, J = 3 Hz). ^{19}F NMR (470 MHz, CD_3OD): δ_F -118.65 (1F, sextet, J_1 = 6 Hz).

(1*S*,6*S*)-3,5-difluoro-1,6-*cis*-dihydroxycyclohexa-2,4-diene-1-carboxyic acid (3,5-FB *cis*-diol). Off white solid: ^{1}H NMR (500 MHz, CD_3OD): δ_H 5.61(1H, t, J = 6 Hz), 5.20 (1H, d, J = 12 Hz), 4.93 (1H, s). ^{19}F NMR (470 MHz, CD_3OD): δ_F -111.17 (1F, t, J = 11 Hz), -111.28 (1F, m).

Results

Only Rieske Cluster Oxidation Contributes to the Optical Change During Single Turnover.

Both the reduced and oxidized Rieske clusters have optical absorbance spectra that cover the majority of the visible spectrum (Figure 2-1), but the spectrum of the oxidized Rieske clusters has a larger extinction coefficient at all wavelengths. As the Rieske cluster is oxidized during a single turnover, monitoring this optical change provides an important spectroscopic signal for mechanistic investigation. Several other iron/O_2 intermediates that may form during turnover also have absorbances within these wavelengths. Stopped-flow spectroscopy was used to investigate the time resolved optical changes during single turnovers with a large excess of substrate and O_2. As shown in Figure 2-1, the optical change appears to be a smooth transition between spectra of the reduced and oxidized Rieske cluster, and linear combinations of the fully oxidized and reduced Rieske cluster spectra recapitulate the observed spectra throughout turnover. This demonstrates that no chromophoric iron/O_2 intermediate(s) accumulate to detectable concentrations during single turnovers and the observed optical change is caused only by oxidation of the Rieske cluster. The Rieske cluster and mononuclear iron are separated by only 15 Å and a bridging aspartate residue provides a through-bond pathway to facilitate rapid intramolecular electron transfer directly between the Rieske cluster and the mononuclear iron (Figure 1-6). Taken together, these data suggest that Rieske cluster oxidation should occur as a single step process once the Michaelis complex (ESO_2 in the case of RDDs) is formed.

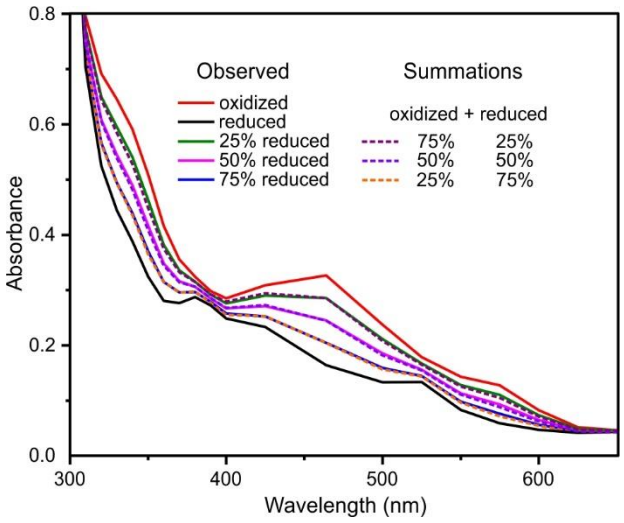

Figure 2-1: The optical changes during a single turnover with benzoate are well-accounted for by linear summations of the spectra of the reduced and oxidized Rieske cluster. Selected optical spectra observed after reduced BZDO (100 µM) was mixed with an O_2-saturated reaction buffer containing benzoate (20 mM) at 4 °C in a stopped-flow spectrophotometer. The spectra are combinations of 21 single wavelength time courses collected from 300 -725 nm. The simulated spectra where calculated by summing the indicated factions of the fully reduced and fully oxidized Rieske cluster spectra.

Rieske Cluster Oxidation During Single Turnover is a Multistep Process.

Figure 2-2a shows the optical time courses at 464 nm during single turnover reactions containing benzoate or one of several fluorinated benzoates selected for this study based on criteria described in the Research Directions (Chapter 1). Each reaction displayed two characteristics previously observed for the turnover of benzoate and meta-substituted substrate analogs (Figure 1-18).[8] First, a satisfactory simulation of the Rieske cluster oxidation time course under pseudo-first-order conditions requires more than one exponential phase term (Figure 2-2B). Second, the chemical nature of the substrate (in this case, the number and position of the fluorine aromatic substituents) changes the magnitudes of observed RRTs (Figure 2-2A and Table 2-1). The observation of multiphase Rieske cluster oxidation time course during single turnovers is not unique to BZDO, and has also been reported with phthalate and anthranilate dioxygenase.[74, 112]

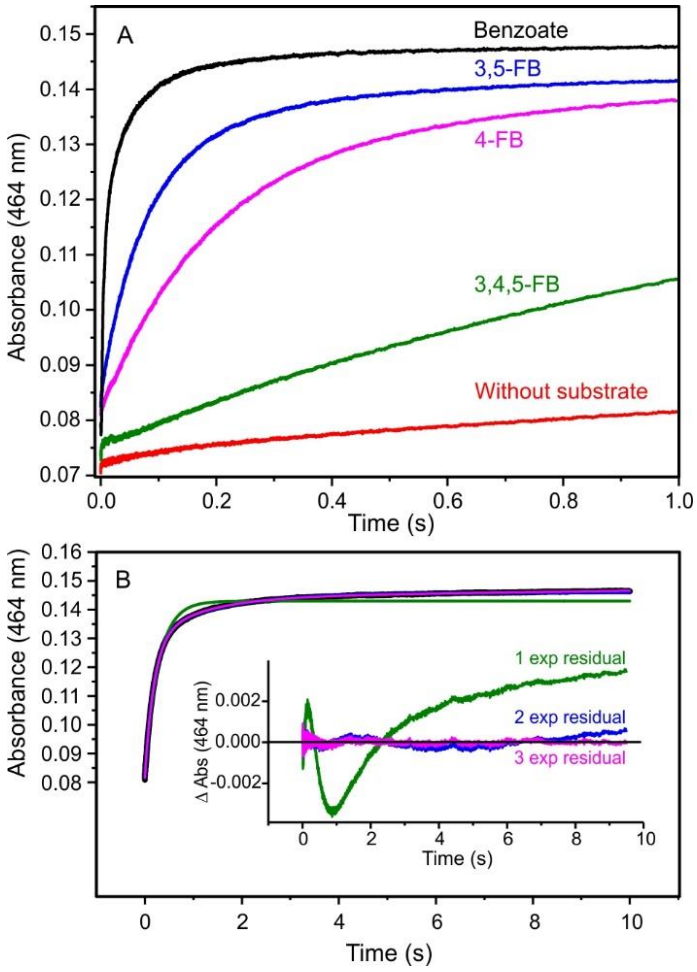

Figure 2-2: Rieske cluster oxidation rates during a single turnover depend upon the type of substrate present. (A) Optical change at 464 nm when reduced BZDO (60 µM) was mixed with an O_2 saturated reaction buffer containing the indicated substrate (5 mM) at 4 °C in a stopped-flow spectrophotometer. (B) The resulting optical change at 464 nm with 4-fluorobenzoate and residuals from single, double, and triple exponential function fits.

Table 2-1: Reaction kinetics and product formation during BZDO single turnover.[a]

		Steady State	Single Turnover								
Substrate		O_2 uptake	Product formation		Rieske re-oxidation (464 nm)						
					substrate coupled product forming oxidation		substrate coupled nonproduct forming oxidation				Slow oxidation phases[b]
	pK_a	k_{cat}(s^{-1})	k_{obs} (s^{-1})	Fractional Product Yield (%)	RRT-1 (s^{-1})	% Amp	RRT-2 (s^{-1})	% Amp	RRT-3 (s^{-1})	% Amp	% Amp
benzoate	4.2	4.4 ± 0.50	190 ± 50	47 ± 3	184 ± 23	49 ± 5	28 ± 3	32 ± 4	6.8 ± 1.0	14 ± 2	6 ± 2
4-fluoro-benzoate (4-FB)	4.14	0.48 ± 0.06	5.2 ± 1.2	62 ± 5	5.3 ± 0.2	70 ± 3	1.3 ± 0.3	19 ± 2			11 ± 2
3,5-difluoro-benzoate (3,5-FB)	3.5	1.0 ± 0.09	14.6 ± 0.6	63 ± 7	13 ± 1	66 ± 5	3.8 ± 0.6	22 ± 4			12 ± 2
3,4,5-trifluoro-benzoate (3,4,5-FB)	3.46	0.079 ± 0.01	0.70 ± 0.12	51 ± 8	0.86 ± 0.08	66 ± 4	0.28 ± 0.04	24 ± 3			10 ± 2

[a]Reduced BZDO was reacted with O_2 saturated buffer and the substrates shown. The steady state k_{cat}, rate constant and fractional yield of cis-diol product and RRTs and amplitudes from a multiexponential fit of the time course monitored at 464 nm were determined under the experimental conditions described in Experimental Procedures. [b]Two low-amplitude phases much slower than the k_{cat} were observed in most cases. The slowest phase has the same RRT as the substrate free reaction (0.1 s^{-1}). A slightly faster phase is observed only when a substrate is present, but exhibits no substrate concentration dependence.

The requirement of multiple exponentials phases during Rieske cluster oxidation is a kinetically intriguing but conceptually challenging observation. One analysis method for presteady-state kinetics relies on the ability to find analytical solutions via integration of the rate equations that describe the system. Analytical solutions do not exist for all systems, but do exist for a linear series of first-order or pseudo-first-order reactions. In these cases, the reaction time course is described by n summed exponential terms where n represent the total number of first-order or pseudo-first-order steps that occur in the reaction (Equation 1, Materials and Methods). The observation of multiple kinetic phases during single turnover of RDDs under pseudo-first-order concentrations of substrate and O_2 shows that there is more than one step in the Rieske cluster oxidation process, but it does not indicate whether the steps occur in sequence or in parallel, or whether all of the steps are catalytically relevant.

The catalytic relevance of the steps in a multistep reaction can sometimes be evaluated from the magnitudes of the RRTs in comparison to the k_{cat} values for the reactions. This is straightforward when the steps are irreversible, in which case the RRT of each exponential term is the rate constant for a specific step. When one or more of the (pseudo)first-order steps is reversible, the observed RRTs no longer reflect the rate constants of an individual step, but are instead combinations of multiple rate constants complicating the analysis. Fortunately, many of the steps in the current case are likely to be effectively irreversible: electron transfer across a substantial potential gradient, O-O bond cleavage, and *cis*-dihydroxylation.

Several experimental observations support the hypothesis that the electron transfer occurring between the Rieske cluster and mononuclear iron is effectively irreversible. In most characterized RDDs, the as-isolated state of the enzyme is composed of 100% oxidized Rieske cluster and 100% ferrous mononuclear iron (^{ox}RDD-Fe^{2+} in Figure 1-7).[11] No equilibrium is observed between the reduced mononuclear iron and the oxidized Rieske cluster showing that the reduction potentials are far enough apart that the electron transfer is effectively irreversible. This is supported by the reported reduction potentials for the Rieske cluster and mononuclear iron of a Rieske O-demethylase (Table 1-1, line 4) as 5 mV and ≥ 200 mV respectively.[29, 113]

Each substrate has more than one reoxidation step with RRTs dependent on the substrate concentration. All substrate-dependent phases exhibit a hyperbolic dependence. The mechanistic insights available from the hyperbolic dependence and the kinetic parameters that can be extracted from it are discussed in Chapter 3. With benzoate as the substrate, three substrate-dependent exponential phases are observed, while the reactions for the fluorobenzoates each exhibit only two substrate-dependent phases. All the substrate-dependent phases are faster than the respective k_{cat} values for the reactions, and thus all of the corresponding steps (assumed to be irreversible) must initially be considered relevant to the true catalytic process of the enzyme (Table 2-1). Turnover with each substrate also displayed one or more low amplitude substrate concentration independent phases with RRTs much slower than k_{cat} and are therefore not catalytically relevant. Despite the observation of at least two kinetically relevant phases, it is difficult to rationalize how a single, one electron, Rieske cluster oxidation event could occur in a multi-step sequential reaction. Thus, it is important to identify functionally relevant steps, which may be a subset of kinetically competent steps.

Product Formation Correlates with Only One Step of the Multi-step Rieske Cluster Oxidation Reaction.

One strategy that may distinguish functionally relevant from nonproductive Rieske oxidation steps is to determine the number of steps involved in product formation and their rate constant(s). Rapid chemical-quench samples taken at specific times during a single turnover under pseudo-first-order conditions were analyzed by HPLC to determine the rate constant(s) and fractional yield of product formation as shown in Figure 2-3 and summarized in Table 2-1**.** For each substrate, a single new HPLC peak appears at the same retention time as purified authentic standards of the *cis*-diol product (Figure 2-3, insets). In contrast to the time course for Rieske cluster oxidation, the accumulation of *cis*-diol products can be fit to a single exponential function (Figure 2-3). For each substrate, the k_{obs} for product formation is within experimental error of RRT-1 Table 2-1. Under the assumption of irreversible steps in the product formation process, this suggests that the product is formed in only one step of the Rieske oxidation reaction. If so, then the fraction of the overall amplitude of the Rieske oxidation represented in RRT-1 should correlate with the factional yield of each *cis*-diol product. It is shown in

Table 2-1 that this prediction is confirmed. These results strongly imply that the observed phases do not arise from a multistep, sequential process, but instead are the result of independent, parallel, substrate-triggered Rieske oxidation reactions. The reason that the slower substrate-dependent steps do not yield product remains unclear but several possibilities are considered in the discussion. However, the ability to consider the catalytically relevant product forming Rieske oxidations as a one-step process greatly simplifies further analysis of the mechanism of the *cis*-diol forming reaction conducted in Chapter 3.

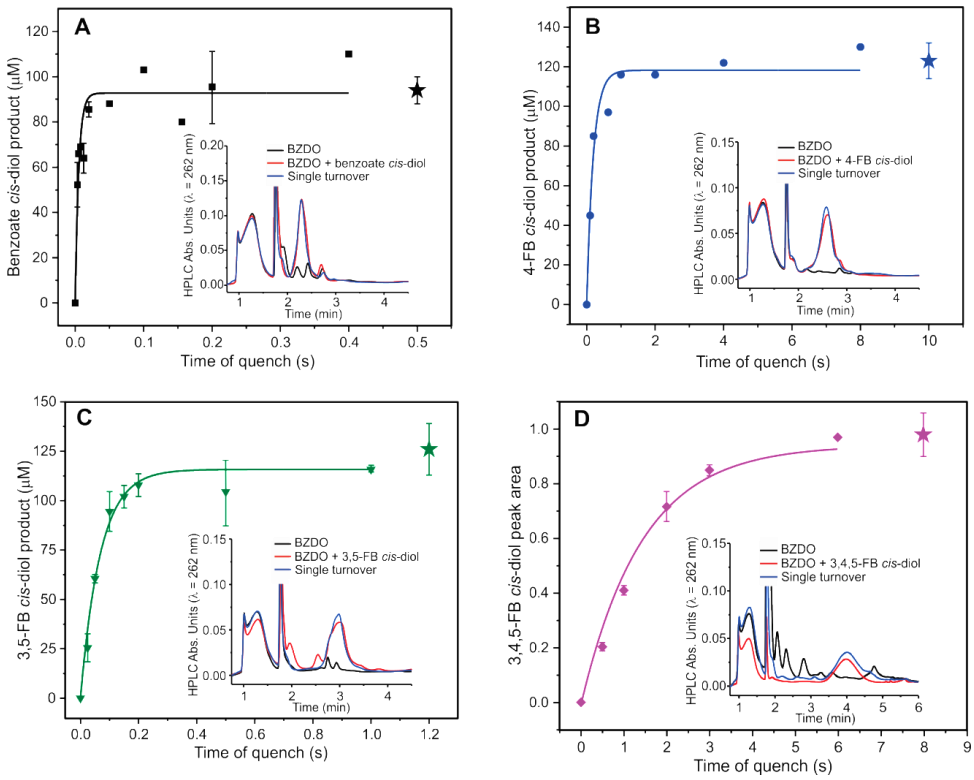

Figure 2-3: Product analysis of single turnover reactions shows a correlation with the fast phase of Rieske cluster oxidation. Reduced BZDO (400 μM) was rapidly mixed 1:1 with O_2 saturated reaction buffer containing 10 mM (A) benzoate, (B) 4-FB, (C) 3,5-FB, or (D) 3,4,5-FB and chemically quenched as described in the Materials and Methods. For each substrate, the yield at the end of the reaction (≥ 4 minutes) is shown by a star. The product formation time course can be fit to a single exponential equation for each substrate (solid line), yielding the k_{obs}. In each case, a single new HPLC peak consistent with an authentic standard of the *cis*-diol product is observed (insets). For replicated points, $n \geq 3$ and the errors bars represent 1 standard deviation of the mean.

Discussion

A long standing mystery in the study of BZDO is the cause of the multiphase Rieske cluster oxidation observed during single turnover.[8] This phenomenon has also been reported for other RDDs such as phthalate and anthranilate dioxygenases. [74, 112] Several hypotheses were proposed in these studies to account for the multiphase oxidation including (anti)cooperativity between the subunits of the enzymes, asymmetry caused by partially occupied metal sites, and multistep sequential reactions. The finding here that only the RRT and amplitude of the fastest phase correlate with the rate constant and overall yield of product formation during a single turnover argues against multistep sequential reactions and subunit (anti)cooperativity. Rather, the data support a model in which the Rieske cluster can oxidize in multiple, independent, one-step processes, only one of which is relevant to product formation. Furthermore, comparison of the kinetic parameters of product-coupled Rieske cluster oxidation and product formation provide information as to the location of the rate-limiting step of *cis*-dihydroxylation.

Electron Transfer and Product Formation are Rate Limited by the Same Step.

The results presented above give several important insights into what limits the rate of RDD single-turnover reactions. Even though it is Rieske cluster oxidation being monitored in the stopped-flow experiments, the electron transfer *per se* between the Rieske cluster and mononuclear iron site is highly unlikely to be rate-limiting. In all of the structurally characterized RDDs thus far, the electron transfer between the Rieske cluster and mononuclear iron occurs over a distance of ≤ 15 Å following a through-bond pathway[60, 72] with a considerable driving force caused by the difference in redox potentials of the metal sites.[29, 113] A rate constant for electron transfer of 2.2×10^6 s^{-1} was calculated from a theoretical study based on the NDO active site.[114] This rate constant is four orders of magnitude larger than those for single turnover with benzoate, the fastest substrate in this study. As a result, a step (or steps) in the formation of the chemically competent ESO_2 complex must be what actually limits the rate of electron transfer. Based on the observation that the RRT and amplitude of the fastest phase correlate with the rate constant and overall yield of product, it can be concluded that the

product forming steps occurring after electron transfer are not rate limiting. These results suggest that both Rieske cluster oxidation and product formation are rate-limited by the same step. If this model is correct, monitoring the Rieske cluster oxidation allows the rate-determining step in product formation to be characterized and its rate constant determined.

Possible Causes of the Substrate-dependent but Nonproduct-forming Steps.

Despite the observation that product is formed in only one of the multiple independent Rieske oxidation reactions, it is true that the rate constants for several of the nonproduct-forming reactions depend on both the type and concentration of substrate present. This implies substrate participation in each process, and consequently, a role for the mononuclear iron center where the substrate binds. The most straightforward explanation for this observation is that in each reaction an iron/O_2 species of some sort interacts with substrate to trigger the inter-subunit electron transfer. For the slower nonproduct-forming processes, the reaction apparently does not carry through to *cis*-diol formation. Indeed, after a single turnover of BZDO, all of the Rieske clusters and mononuclear irons are oxidized despite the less than stoichiometric product yield (Figure 2-3, Table 2-1).[8]

One possible explanation for the substrate-dependent but nonproduct-forming reactions is uncoupled oxygen activation resulting in release of H_2O_2 or other reduced oxygen species. Such uncoupling reactions are commonly observed in oxygenases under suboptimal conditions and have been reported for multiple RDD systems during catalytic turnovers. [27, 115, 116] Within this study, no significant amount of soluble H_2O_2 was detected from catalytic or single turnovers of BZDO using a catalase assay (see Materials and Methods). However, we have previously shown that BZDR/NADH and BZDO can each act as a catalase and this may lead to disproportion of H_2O_2 before it can be detected in the assay.[10, 100]. An alternative uncoupling pathway could involve formation of a side-on bound Fe^{3+}-peroxo species such that the formed peroxide is retained within the active site at the end of a single turnover. This species has been observed in multiple enzymes and model compounds, and is reported to be unreactive in regards to O-O bond cleavage and/or oxygen atom transfer reactions (compared to a

Fe^{3+}-(H)peroxo).[117] In an attempt to liberate and detect iron-bound peroxide, acid or base quenched single turnovers were readjusted to pH ~ 7 and assayed with catalase. Unfortunately, these experiments were ambiguous as control reactions demonstrated the decay of H_2O_2 during the quench. The side-on Fe^{3+}-peroxo intermediate could presumably be detected spectroscopically. Detection by EPR spectroscopy is complicated by the predicted low intensity spectra caused by the electronic environment of this ferric mononuclear iron species (see Chapter 4 for more details). Careful analysis by other techniques such as Mössbauer or a vibrational spectroscopy are more likely to reveal evidence of this proposed species.

An important question for future investigation is whether the multistep Rieske cluster oxidations observed during single-turnover reactions also occurs during catalytic turnover. If unique to *in vitro* single turnovers, this may indicate the choice of reductant affects the chemistry that occurs at the mononuclear iron. All single-turnover reactions reported in this chapter and this thesis used the chemical reductant dithionite for reduction of the enzyme. Catalytic turnovers *in vivo* use accessory proteins (Figure 1-4) and several reports have demonstrated that binding of an accessory protein can greatly influence the global structure and/or reactivity of an oxygenase.

Conclusions

This chapter provides new insights into the longstanding mystery of multiphase Rieske cluster oxidation and further defines the kinetics of BZDO single-turnover. The data support a model in which (1) the observed optical change during single-turnover reactions arises exclusively from Rieske cluster oxidation, (2) the Rieske cluster is oxidized in multiple independent and parallel steps, (3) product formation results from only one of the multiple Rieske cluster oxidation steps, and (4) product formation occurs rapidly after Rieske cluster oxidation.

A model for multistep Rieske cluster oxidation derived from the results in this chapter is illustrated in Figure 2-4. At the start of the single-turnover reaction, there is a mixed population of enzyme active sites, one that is capable of binding substrate and another that is not. It appears that the substrate binding population contributes to the

substrate-dependent steps because, even though not all of these steps form product, the binding of substrate still increases the rate constant for O_2 binding and Rieske oxidation, so many of the regulatory aspects of the reaction cycle are intact and functioning. To account for the substrate-dependent but non-product-forming pathways, we propose a bifurcation step occurring somewhere during the binding of substrate and/or O_2 or during the O_2 activation process after formation of the initial ESO_2 complex. The bifurcation would cause a fraction of the active population to form product (Figure 2-4, pathway A), while the remaining fraction would be unable to form product (Figure 2-4, pathway B). The exact mechanism of the bifurcation and what results from it are currently unknown, but formation a peroxo species of some kind is likely. The substrate independent and non-product-forming Rieske cluster oxidation steps (slow oxidation phases in Table 2-1) occur from a subpopulation of enzyme incapable of correctly binding the substrate. This subpopulation may be without mononuclear iron, or it have other active site damage (Figure 2-4, pathway C). For each substrate tested, these steps account for ≤ 12 % of the total Rieske cluster oxidation and in all cases have comparable rates to O_2-mediated Rieske cluster oxidation in the absence of substrate.

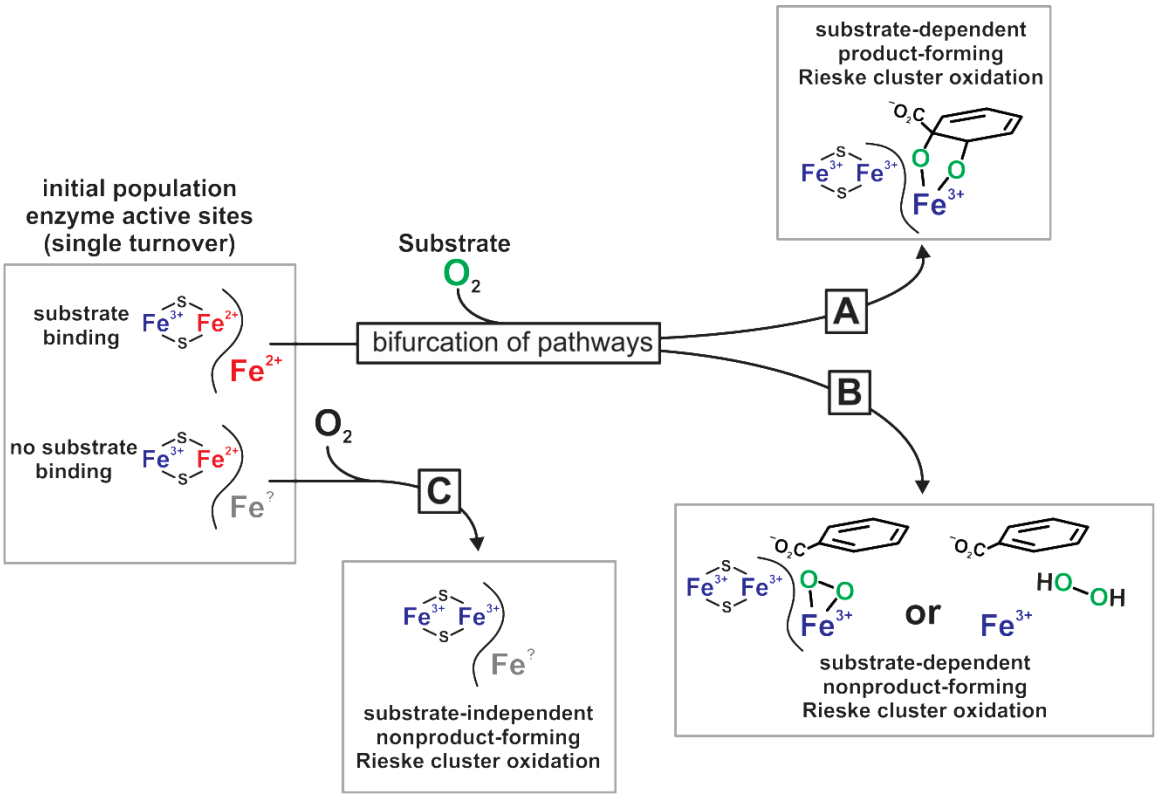

Figure 2-4: Proposed mechanism for the multistep Rieske cluster oxidation observed during single-turnover reactions.

Acknowledgments

I thank Dr. Melanie Rogers for her invaluable input and contributions as a collaborator on this project. I thank Prof. Simon E. Lewis for generously providing the *Ralstonia eutrophus* strain B9 used to make the *cis*-diol product standards and for providing us with an initial supply of the purified benzoate *cis*-diol product. I thank Prof Jung-Kul Lee for providing the pACYC-isc plasmid. I thank Johannes Klein for assistance with the NMR analysis.

Chapter 3

Kinetic Investigation of the Rate-limiting Step of Product Formation During Single Turnover of a Rieske Dearomatizing Dioxygenase with Native and Fluorinated Substrates

Note: This chapter is reprinted (adapted) with permission from Rivard, B. S., Rogers, M. S., Marell, D. J., Neibergall, M. B., Chakrabarty, S., Cramer, C. J., and Lipscomb, J. D. (2015) Rate-Determining Attack on Substrate Precedes Rieske Cluster Oxidation during Cis-Dihydroxylation by Benzoate Dioxygenase, Biochemistry 54(30), 4652-4664.

Summary

Rieske dearomatizing dioxygenases utilize a Rieske iron-sulfur cluster and a mononuclear Fe^{2+} located 15 Å across a subunit boundary to catalyze O_2-dependent formation of *cis*-dihydrodiol products from aromatic substrates. During catalysis, O_2 binds to the Fe^{2+} while the substrate binds nearby. Single turnover reactions have shown that one electron from each metal center is required for catalysis. This finding suggested that the reactive intermediate is Fe^{3+}-(H)peroxo or Fe^{5+}-oxo/hydroxo formed by O-O bond scission. Surprisingly, several kinetic phases were observed during the single turnover Rieske cluster oxidation. Chapter 2 shows that the rate constant for product formation correlates with only the fastest kinetic phase (RRT-1) for each substrate, suggesting that the slower phases are not mechanistically relevant. Here, the Rieske cluster oxidation step of a single turnover of benzoate 1,2-dioxygenase is investigated in depth using benzoate and three fluorinated analogs. The data presented provide further evidence that RRT-1 is strongly dependent on substrate type, suggesting a role for substrate in electron transfer from the Rieske cluster to the Fe^{2+} site. This insight, together with the substrate and O_2 concentration dependencies of RRT-1, indicates that a reactive species is formed after substrate and O_2 binding, but before electron transfer from the Rieske cluster. Computational studies show that RRT-1 is correlated with the electron density at the substrate carbon likely to be closest to the Fe^{2+}, consistent with initial electrophilic attack by an Fe^{3+}-superoxo-like intermediate. The resulting Fe^{3+}-peroxo-aryl radical species would then readily accept an electron from the Rieske cluster to complete the *cis*-dihydroxylation reaction.

Introduction

Rieske oxygenases catalyze a diverse repertoire of chemical reactions, but a subclass termed Rieske dearomatizing dioxygenases (RDDs) are the only known enzymes that catalyze dearomatizing *cis*-dihydroxylation of aromatic compounds (Table 1-1).[7] This reaction activates otherwise stable aromatic compounds, making RDDs effective agents for bioremediation.[46, 47] Another type of application stems from the ability of RDDs to produce large quantities of regio and stereospecific *cis*-diols as important synthetic building blocks for streamlining synthesis of drugs and antibiotics.[52] A complete understanding of the catalytic mechanism of RDDs will aid further development and utilization of these applications and provide guiding insights for mechanistic studies of the broad class of Rieske oxygenases.

Each RDD active site contains a [2Fe-2S] Rieske cluster and a nonheme mononuclear iron[66].[60] The conserved structure of RDDs places the Rieske cluster 15 Å away from its associated mononuclear iron.[60, 72] Substrates bind near (but not to) the mononuclear iron, showing that this is the site of O_2 activation and *cis*-dihydroxylation.[12, 68-70] Single turnover experiments have shown that reduction of both the Rieske cluster and the mononuclear iron is required for normal catalysis, and that one electron from each metal center is used during the *cis*-dihydroxylation reaction.[8] A conserved Asp residue links the two metal centers via hydrogen bonding and appears to mediate the electron transfer from the Rieske cluster to the mononuclear iron during the reaction. [72-74]

RDDs have characteristics that make them mechanistically distinct from other iron-dependent dioxygenases and monooxygenases (Table 1-2). For example, many non-heme dioxygenase classes that are reactive in the Fe^{2+} state utilize the 2-His-1-carboxylate facial triad iron binding ligation like the RDDs. [97] However, these dioxygenases extract all four electrons required for O_2 reduction from the substrate or co-substrate, whereas RDDs ultimately utilize two electrons from the substrate and two from NADH. Monooxygenases like methane monooxygenase or cytochrome P450, also extract two electrons from both substrate and NADH, but the products are oxidized substrate and water rather than a dihydroxylated substrate. [91-93] It is noteworthy that well-characterized Rieske monooxygenases exist which are structurally similar to RDDs, but exhibit the same NADH and O_2 stoichiometry and single oxygen atom incorporation

pattern as sMMO or cytP450.[14, 15] These similarities have led to mechanistic theories for RDDs along the lines of monooxygenase rather than dioxygenase enzymes.

A hypothesis for the mechanism of RDDs based on typical monooxygenase chemistry is shown in Figure 1-16.[8, 83, 85, 94-96] The results from experimental and computational approaches have supported the monooxygenase-like mechanism of RDD catalysis, but have not agreed on the identity of the reactive species performing the initial substrate oxidation.[7, 97] The focus on two-electron O_2 activation in RDDs has limited consideration of another commonly employed mechanistic strategy in the 2-His-1-carboxylate family involving one electron reduced O_2. Indeed, the initial attacking species in enzymes such as extradiol ring-cleaving dioxygenases[118, 119] and isopenicillin N-synthase [120] are proposed to be metal-bound superoxo moieties.

A potential difficulty with the monooxygenase-like mechanism derives from our past studies which showed that the rate of electron transfer from the Rieske cluster to the mononuclear iron site within BZDO is influenced by the functional groups on the aromatic ring of benzoate.[8] This observation might imply that the reaction of some type of iron/O_2 intermediate with substrate occurs before formation of a two-electron reduced reactive species proposed in the monooxygenase-like mechanism. Alternatively, it could reflect steric effects on the substrate position in the active site. Here, the transient kinetics of electron transfer within BZDO during a single turnover are examined for benzoate and a variety of fluorinated benzoates chosen to limit steric effects. It is shown that the step in which activated O_2 first attacks the substrate is rate limiting, and that this step is likely to involve a metal-bound species with superoxo character. The study provides new insight into the detailed steps of oxygen activation and reaction that ensure both specificity and efficient catalysis in Rieske dioxygenases.

Materials and Methods

Chemicals and Reagents.

Water used in all experiments was purified with a Millipore Super-Q system. All commercial reagents were purchased from standard vendors and used without further purification. Gases were purchased from Matheson. Unless noted, all enzymatic reactions were conducted in a standard reaction buffer of pH 6.9 MOPS (50 mM) and NaCl (100 mM).

Cloning, Heterologous Expression, and Purification of BZDO.

See the Materials and Methods section of Chapter 2.

Anaerobic Technique and Chemical Reduction of BZDO.

See the Materials and Methods section of Chapter 2.

Stopped-Flow Analysis of Single-turnover Reactions.

See the Materials and Methods section of Chapter 2.

Fitting Procedures for Substrate Concentration Dependencies.

For a two-step reaction where the first step is fast reversible binding, a hyperbolic dependence of the $1/\tau_{obs}$ on substrate or O_2 concentration may apply if the observable step that follows is comparatively slow: [121]

$$\mathrm{E} + \mathrm{ligand} \underset{k_{-1}}{\overset{k_1}{\rightleftarrows}} \mathrm{E{\cdot}ligand} \underset{k_{-2}}{\overset{k_2}{\rightleftarrows}} \mathrm{E\text{-}ligand'}$$

Plots of $1/\tau_{obs}$ versus either substrate, or oxygen, concentration were fit to the hyperbolic function below using Origin:

$$\frac{1}{\tau_{obs}} = \frac{k_2[\mathrm{ligand}]}{(\frac{k_{-1}}{k_1}) + [\mathrm{ligand}]} + k_{-2}$$

The parameters of the equation yield the apparent K_d for the binding reaction (k_{-1}/k_1) and forward and reverse rate constants for observable conversion which follows binding. The accuracy of the K_d value depends upon how closely the binding reaction approaches rapid equilibrium, and specifically, whether k_{-1} is >> than k_2.

Preparation of Nitric Oxide Adducts.

Reduced BZDO was prepared as above and substrate was anaerobically added to the concentration indicated for each experiment in the Figure legends. NO solutions were made by first removing O_2 from a sealed vial of reaction buffer by sparging with high purity argon gas dispensed through an additional O_2 scrubbing column (Agilent). The deoxygenated buffer was then sparged with NO gas (pretreated by passing through 6 N NaOH) in a fume hood until saturated. Gas-tight syringes were used to dilute the NO solution to the required concentration, and this solution was either directly added to reduced BZDO or loaded onto a deoxygenated stopped-flow instrument and rapidly mixed with reduced BZDO. It is important to note that two cautions be exercised when working with NO gas. First, it should only be handled in a fume hood as it poses a significant health risk if inhaled. Second, strict anaerobicity must be maintained in experimental solutions as exposure to O_2 in aqueous solution results in formation of nitrous acid.

Spectroscopy.

Electronic absorption spectra were recorded on either a Hewlett-Packard 8453 diode array spectrophotometer or an Agilent Technologies Cary 60 scanning spectrophotometer. X-band EPR spectra were recorded with a Bruker ELEXSYS E-500 system equipped with an Oxford ESR 910 liquid helium cryostat.

Computational Methods.

Molecular geometries for parent and various fluoro-substituted benzoic acids were optimized at the M06-2X level of density functional theory[122] employing the 6-311+(2df,p) basis set.[123] Both conjugate acid and conjugate base forms were considered in the optimizations, and the calculations were undertaken both in the gas phase and also including condensed phase effects using the SMD continuum aqueous solvation model.[124, 125] Charges were computed for the optimized structures at the same level of

theory employed for the optimizations, summing the charges for carbon atoms with those for attached H atoms in order to compute a net group partial charge for the C(2) C–H group. In the case of the conjugate acids, variations in this charge as a function of the position of the hydroxyl group of the carboxylic acid (distal or proximal to the carbon defined as C(2)) was in every instance 0.009 a.u. for gas-phase calculations, but no more than 0.001 a.u. with the SMD solvation model. Geometry optimizations were accomplished with the Gaussian09 suite of electronic structure programs[126] and CM5 charges were computed using CM5PAC.[127]

Results

Kinetic Investigation of Benzoate and Fluorobenzoate Binding During BZDO Single Turnover.

One possible explanation for the large difference in the rate constants of electron transfer during single turnovers with benzoate and the fluorobenzoates is that the fluorine substituent(s) interfere with substrate and /or O_2 binding despite the comparable van der Waals radii of hydrogen and fluorine. This possibility was examined by studying the substrate and O_2 binding kinetics of each reaction through monitoring the Rieske cluster oxidation time course under pseudo-first-order conditions in substrate and O_2.

The observed rate constants for all the substrate titrations exhibit a hyperbolic concentration dependence as shown in Figure 3-1. This result is consistent with a model in which the oxidation of the Rieske cluster is not rate-limited by substrate binding and substrate binding is reversibly connected to the true rate-limiting step. For this type of kinetic behavior (see Experimental Procedures), the K_d for the relatively fast (unobserved) binding reaction is given by the apparent K_d for the titration curve, and the extrapolated asymptotic maximum and y-intercept of the curve give information about forward ($k_{forward}$) and reverse ($k_{reverse}$) rate constants of the true rate-limiting step.

The kinetic parameters obtained from fitting the hyperbolic curves in Figure 3-1 are reported in Table 3-1. $k_{reverse}$ is not reported because the y-intercept is approximately zero for all substrates. This suggests that the rate-limiting reaction is effectively irreversible and supports the assumptions of irreversibility proposed in Chapter 2. The extrapolated maxima of the titration plots ($k_{forward}$) are all significantly different reflecting the substrate type-dependence of the true rate-limiting step. The K_d values for benzoate and 4-FB are approximately the same, showing that replacing hydrogen with a fluorine substituent at carbon 4 does not perturb the binding affinity (Figure 3-1 A). The apparent K_d values for the unobserved substrate binding step with 3,5-FB and 3,4,5-FB are an order of magnitude higher than those observed for benzoate and 4-fluorobenzoate (Figure 3-1 B). Apparently, the presence of fluorine at the 3 and/or 5 positions weakens the binding affinity slightly without causing a change in the product formed.

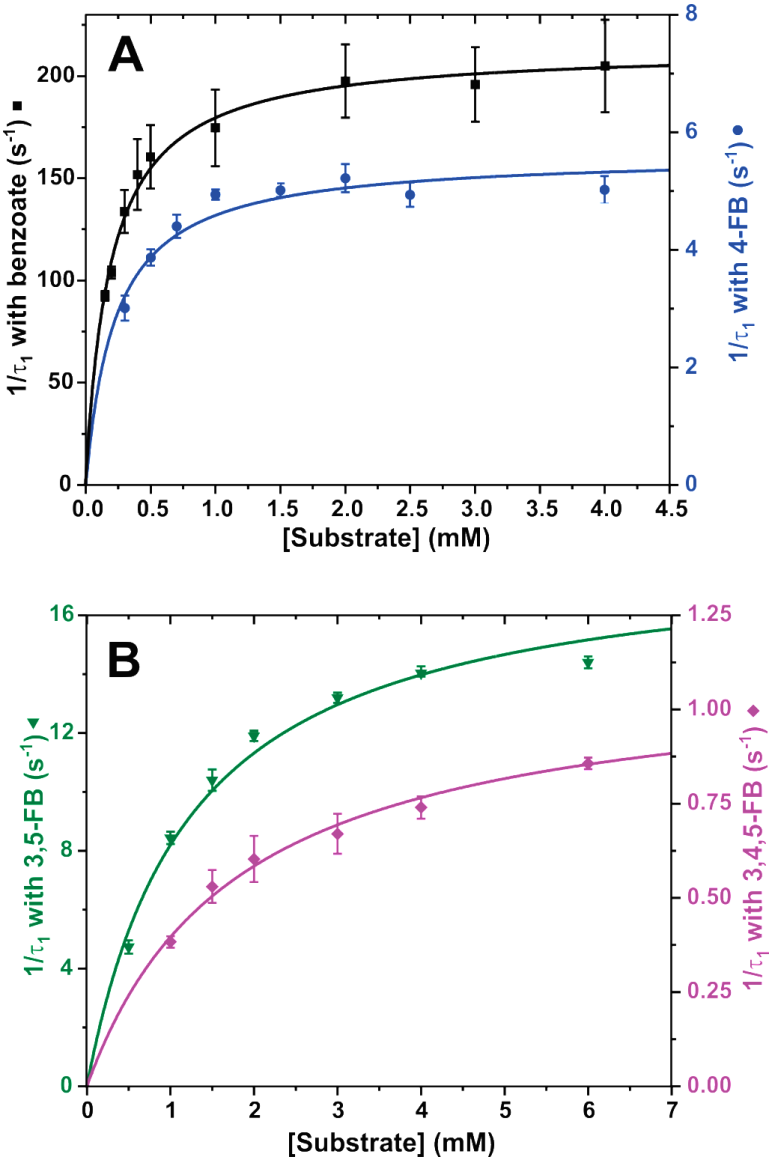

Figure 3-1: Substrate concentration dependence of RRT-1 reveals a subsequent slow step. Reduced BZDO (60 µM) was mixed 1:1 in a stopped-flow spectrophotometer with reaction buffer containing O_2 (saturated solution at 4 °C ≈ 1.8 mM) and varied concentrations of the indicated substrate. Reported error of each point (n ≥ 4) is one standard deviation of the mean. K_d and $k_{formation}$ values were determined by fitting the data to a hyperbolic function (solid curve) and are reported in Table 3-1.

Table 3-1: Kinetic parameters from substrate and O_2 concentration dependence of product coupled Rieske cluster oxidations (RRT-1).[a]

	$K_{d,substrate}$ (μM)	$k_{forward}$ (s^{-1})	$K_{d,O2}$ (μM)	$k_{forward}$ (s^{-1})
Benzoate	**191 ± 10**	**213 ± 4**	**135 ± 13**	**212 ± 6**
4-FB	**226 ± 40**	**5.6 ± 0.2**	**163 ± 12**	**6.4 ± 0.1**
3,5-FB	**950 ± 140**	**17 ± 1**	**150 ± 14**	**15 ± 0.4**
3,4,5-FB	**1800 ± 200**	**1.1 ± 0.1**	**152 ± 7**	**0.89 ± 0.02**

[a]Values determined from hyperbolic fits to the data shown in Figure 3-1 and Figure 3-2. The value for $k_{reverse}$ is approximately zero in all cases.

Kinetic Investigation of O_2 Binding During BZDO Single Turnover.

Earlier studies have shown that O_2 binding requires both reduction of the Rieske cluster and prior substrate binding. [8, 11] As shown in Figure 3-2, the rate constants for the catalytically relevant step preceding Rieske cluster oxidation reaction displays a hyperbolic O_2 concentration dependence under pseudo-first-order conditions for O_2 and each substrate. As described above for substrate binding, the hyperbolic plot shows that the initial O_2 binding reaction is not rate-limiting, but is reversibly connected to the rate-limiting step. The zero y-intercepts of the hyperbolic fits for all substrates further support a model in which the true rate-limiting reaction is effectively irreversible. The similar K_d values for all substrates shows that fluorine substituent(s) do not significantly affect initial O_2 binding affinity (Table 3-1). The $k_{forward}$ values of the fitted O_2 titration plots are different from each other, but similar to the respective values found for the substrate titration plots (Table 3-1). This suggests that the true rate-limiting step is substrate-type dependent, and that the rate constant for substrate and O_2 binding reactions are limited by the same downstream reaction.

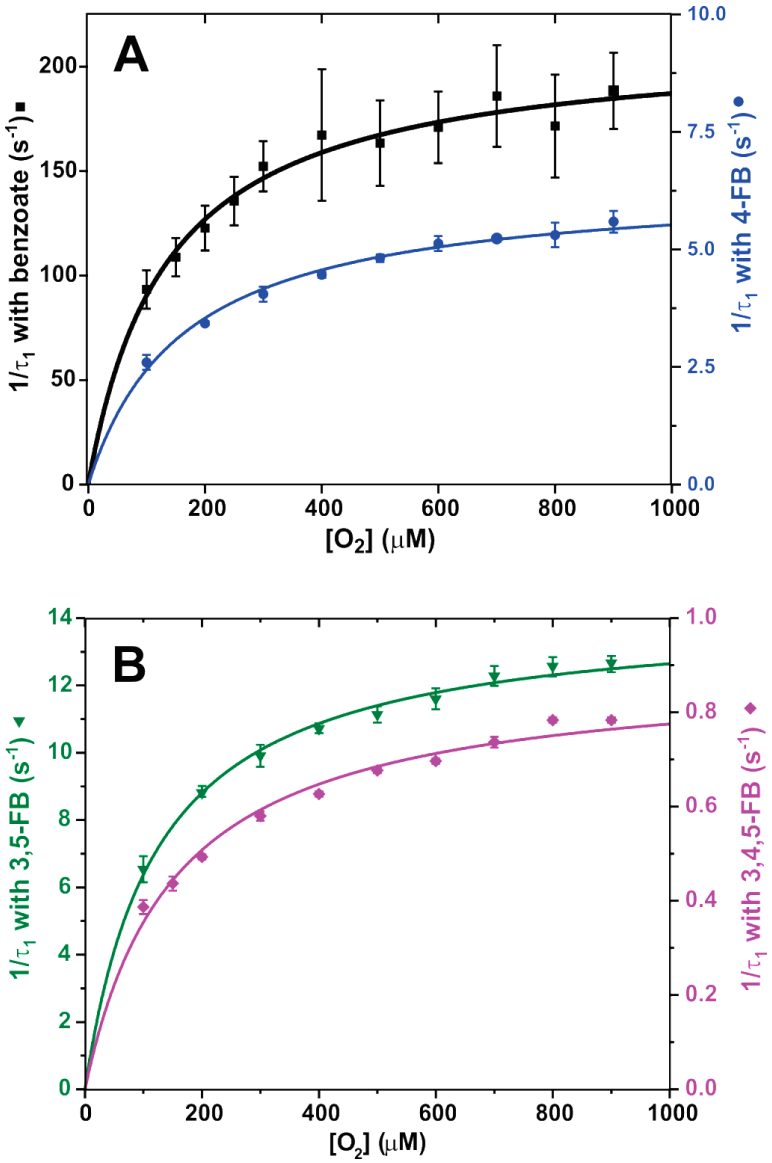

Figure 3-2: O_2 concentration dependence of RRT-1 reveals a subsequent slow step. Reduced BZDO (60 µM) was mixed 1:1 in a stopped-flow spectrophotometer with reaction buffer of varied O_2 concentration and 5 mM benzoate, 5 mM 4-FB, 20 mM 3,5-FB, or 20 mM 3,4,5-FB. Reported error of each point (n ≥ 4) is one standard deviation of the mean. K_d and $k_{formation}$ values were determined by fitting the data to a hyperbolic function (solid curve) and are reported in Table 3-1.

Binding of the O_2 Surrogate NO to the Mononuclear Fe^{2+} is Fast Relative to the Rate of Product Formation.

The kinetic information derived from the hyperbolic shape and K_d's of the above O_2 titrations only provide information about the initial binding step. Studies of other oxygenases have indicated that O_2 binding might proceed in several steps beginning with the formation of a complex in the active site but not yet with the metal center.[128-130] Indeed, a putative small molecule binding site has been identified in the active site of NDO.[131] As such, binding of O_2 to the mononuclear iron from an active site binding location might be rate-limiting. One means to directly observe small molecule binding to the metal center utilizes NO as an O_2 surrogate. [8, 132] The chemical and spatial environments of the spin-coupled Fe^{3+}-NO^- complex can be probed via its characteristic S = 3/2 EPR spectrum and broad optical spectrum.[133, 134] The optical spectra of reduced BZDO exposed to NO (~ 0.5 equivalents relative to active sites) with and without added benzoate or 4-FB are shown in Figure 3-3 A. In the absence of substrate, there is a large change in the intensity and shape of the optical absorption spectrum across the visible region, but a much smaller change in intensity and little change in spectral lineshape occurs in the presence of either substrate. The cause of this difference is revealed in EPR spectra (Figure 3-3 A inset) of identical samples. When NO was added to the reduced enzyme in the absence of substrate, the rhombic S = ½ EPR spectrum of the reduced Rieske cluster (g-values 2.01, 1.91, and 1.76)[8] was attenuated and a new species formed with spectral characteristics (g = 2.04) consistent with dinitrosyl iron complexes previously reported from reactions of biological Rieske clusters with NO.[135] When 4-FB was present, the predicted S =3/2 spectrum of a mononuclear Fe^{3+}-NO^- adduct appears without alteration of intensity or lineshape of the reduced Rieske cluster signal (Figure 3-3 A inset). This demonstrates that when substrate is present, NO binds preferentially to the mononuclear iron site, causing a broad increase in absorbance without significant change in the spectral line shape of the intense chromophore of the Rieske cluster.

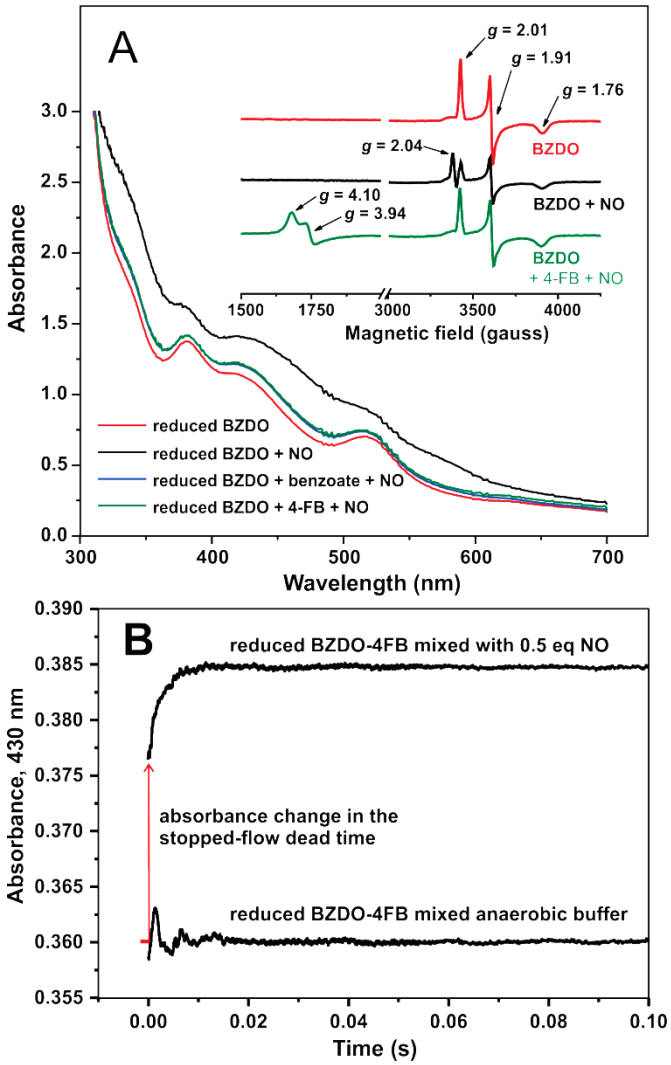

Figure 3-3: NO binds rapidly to the mononuclear Fe^{2+} center in the substrate complex. (A) The optical spectra of reduced BZDO (250 µM) with or without benzoate (50 mM) or 4-FB (50 mM) are shown 15 min after the addition of NO (~ 0.5 equivalents relative to BZDO sites). In the absence of substrate, the large change in electronic absorption is caused by NO binding to the Rieske cluster as can be observed by the attenuation of the S = ½ (g = 2.01, 1.91, and 1.76) EPR signal (inset) from the reduced Rieske cluster and formation of a new signal at g = 2.04. In the presence of benzoate or 4-FB, the NO adduct of the mononuclear iron is formed as shown by the appearance of the characteristic S =3/2 (g = 4.10 and 3.94) EPR signal. Conditions: microwave power, 0.2 mW; temperature, 20 K; microwave frequency, 9.64 GHz. (B) A solution of reduced BZDO (200 µM) and 4-FB (1 mM) was mixed 1:1 in a stopped-flow device with anaerobic reaction buffer or buffer containing NO (~ 0.5 equivalents relative to BZDO). Formation of the Fe^{3+}-NO^{-} adduct was monitored by the increase in absorption at 430 nm. The same experiment using benzoate in place of 4-FB gave indistinguishable results. Data collected by Dr. Melanie Rogers.

The optical changes observed upon binding of sub-stoichiometric NO exclusively to the mononuclear iron site in the presence of benzoate or 4-FB provide, in principle, a method to measure the rate constants for the binding reaction of NO, and by analogy O_2, to the metal. When sub-stoichiometric NO was rapidly mixed with solutions of reduced BZDO and benzoate or 4-FB (Figure 3-3 B), the change in absorbance occurred primarily in the dead time of the stopped-flow instrument (pseudo-first-order rate constant $\geq 600\ s^{-1}$). These results show that NO, and presumably O_2, in the presence of substrates bind with a much larger pseudo-first-order rate constant than the rate constant for the true rate-limiting step prior to the Rieske oxidation reaction.

The Rate Constant for the Rate-limiting Step Correlates with the Computed Atomic Charge at the Site of Substrate Attack.

An alternative explanation for the difference in single turnover rates of benzoate and the fluorobenzoates is that the electronegative fluorine aromatic substituents deactivate the substrates with respect to electrophilic attack on the aromatic ring. If this hypothesis is true, a relationship should exist that correlates the electronic changes within the fluorobenzoates and the rate constants for Rieske cluster oxidation ($k_{forward}$). As shown in Figure 3-4 A, this system is not described well by a Hammett σ plot. However, Hammett analysis is more typically successful for reactions occurring at benzylic positions than at aromatic ring centers themselves. A more direct approach to this analysis was adopted by calculating the partial atomic charges (CM5 partial charge) specifically at carbons 1 (the *ipso* carbon) and 2 for benzoate and the fluorobenzoates and then comparing these values to RRT-1 under saturating conditions for each substrate. While there is no trend associated with the CM5 partial charge for carbon 1 (nor is any trend apparent when correlating rates against computed frontier orbital energies), a linear relationship was observed between the observed rates and the CM5 partial group charge at carbon 2 (Figure 3-4 B), indicating that, as electron density is removed from carbon 2, the rate of electron transfer from the Rieske cluster decreases proportionally. The correlation in Figure 3-4 B is independent of whether the C(2)–H charges are computed for the conjugate acid (proximally or distally oriented) or base forms of the benzoates (R^2 values of 0.992 or higher), but the correlation *is* sensitive to

whether the charges are computed in the gas phase or including solvation effects. The correlation is significantly improved when using solvated values, as might be expected given the condensed-phase nature of the reaction.

The suggestion that the C(2)–H group is the site of initial reaction is supported by structural studies of NBDO, which is similar to BZDO in structure, substrate, and chemistry.[69] In NBDO, substrate carbon 2 is positioned closer to the mononuclear iron than carbon 1, and is thus the likely site of initial attack of the activated oxygen species. This result is consistent with the hypothesis that the decreased rate of turnover with the fluorobenzoates is caused by a change in electron density at the site of initial substrate oxidation.

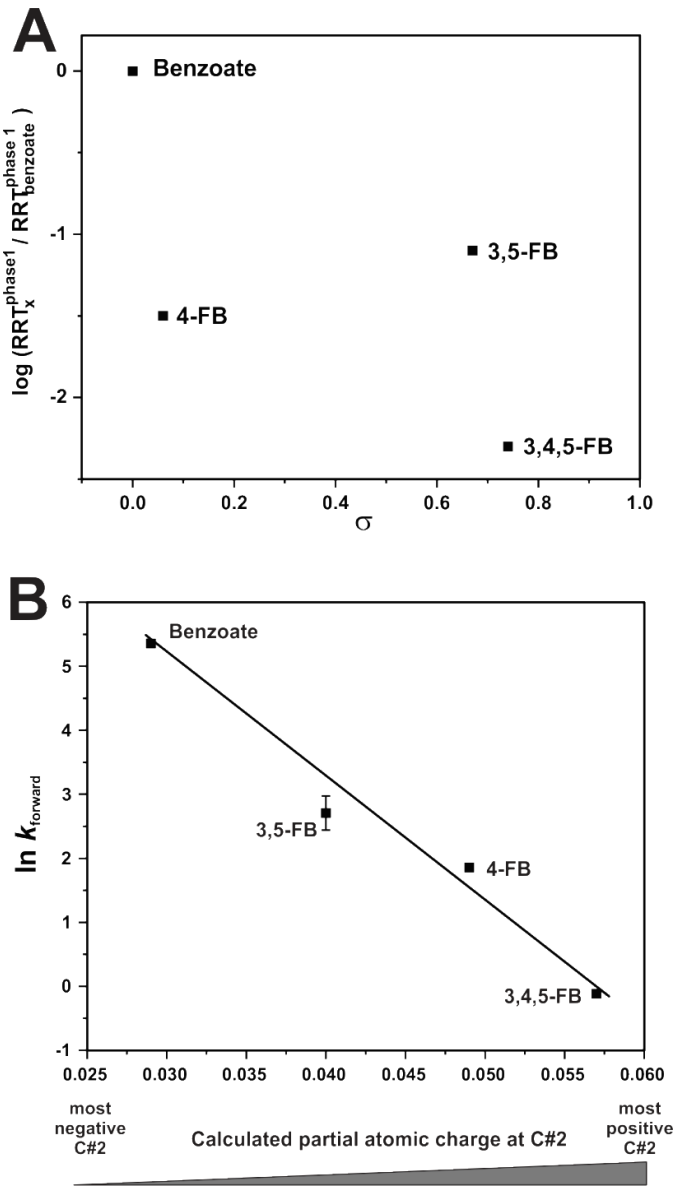

Figure 3-4: The natural logarithm of the rate of Rieske cluster oxidation is proportional to calculated partial group charge at C(2)–H of the substrates tested. (A) The Hammett plot for RRT-1 using the substrates investigated in this study shows no trend. (B) A linear trend is observed between the calculate CM5 partial charge at C(2)-H RRT-1. This trend shows that rate of Rieske cluster oxidation decreases as the electron density at the C(2)–H group is reduced. The observed substrate-type dependence of Rieske cluster oxidation is consistent with the predictions of the dioxygenase-like mechanism.

Discussion

The results presented in this chapter support a mechanistic model in which the rate-determining step of product formation in BZDO occurs after substrate and O_2 binding, but before transfer of an electron from the Rieske cluster to the mononuclear iron site. This observation is consistent with the dioxygenase-like model proposed in Chapter 1. This finding contradicts previous mechanistic theory for RDDs. [8, 11, 100, 114, 136] In these earlier studies, it was proposed the reactive species is an Fe^{3+}-(H)peroxo or Fe^{5+}-oxo-hydroxo which requires transfer of a Rieske electron prior to its formation. The new finding implies a new reactive species for RDDs and differentiates the potential mechanism from those proposed for other monooxygenases such as cytP450 and sMMO.[84, 85, 93, 137, 138]

A mechanistic model consistent with these new insights is presented in Figure 1-17. The current results show that substrate and O_2 binding occur rapidly to BZDO when both the mononuclear iron and Rieske cluster are reduced. After formation of the Fe^{2+}/O_2 adduct, an unknown chemical step(s) results in a one-electron oxidation of both the mononuclear iron and aromatic substrate yielding an Fe^{3+}-alkylperoxo-cation radical (alkyl$^{\bullet+}$peroxo). Formation of this species triggers Rieske cluster oxidation, forming a Fe^{2+}- alkyl$^{\bullet+}$peroxo that proceeds to product by an unknown pathway. The initial oxidation reaction in this model would depend strongly on the susceptibility of the aromatic ring to oxidation, specifically at the position of attack. The current results show that the presence of electron-withdrawing fluorine substituents on the ring deactivate the C(2) position for such an attack. Moreover, the computational evaluation of the effect of the numbers and positions of fluorine atoms on the charge density at the presumed position of attack, C(2), are consistent with this proposed mechanism.

Nature of the Reactive Species.

While informative in many regards, this data set lacks information regarding the exact nature of the initial substrate oxidation occurring after O_2 binding but before Rieske cluster oxidation and the product forming steps after electron transfer from the Rieske cluster. The later question is explored in the Perspective (Chapter 5) concluding this work, but possibilities for the former will now be explored.

Because of the formation of an Fe^{2+}-O_2 adduct, the isoelectronic Fe^{3+}-superoxo is a logical hypothesis for the initial oxidation. The reactivity of an Fe^{3+}-superoxo species directly with an aromatic ring has not been fully explored, but there are indications that some types of reactions are possible. For example, work from this lab and others has proposed that a metal-superoxo species can add to a catechol ring to form an alkyl-peroxo intermediate in the mechanism of extradiol ring-cleaving dioxygenases (Figure 3-5 A).[139] In this case, we also proposed that the reaction is promoted by electron transfer from the catechol to the iron, so that the iron and catechol have ferrous and radical character, respectively.[140] This, in turn, promotes recombination of the oxygen and substrate radicals to form the alkylperoxo intermediate. In the case of isopenicillin N-synthase, we and others have proposed that an Fe^{3+}-superoxo is capable of hydrogen atom abstraction from the β-carbon of the cysteinyl moiety of the δ-(L-α-aminoadipoyl)-L-cysteinyl-D-valine (ACV) substrate.[120, 141] The energy for such a reaction would be similar to that required for electron abstraction from an aromatic ring. Here again, the Fe^{3+}-superoxo species can be considered to be somewhat activated by a shift in electron density from the cysteinyl sulfur of ACV bound directly to the iron.

One particularly relevant example is found in the tryptophan 2,3-dioxygenase (TDO) and indolamine 2,3 dioxygenase (IDO) systems where electron abstraction from aromatic systems by Fe^{2+}-O_2 or Fe^{3+}-superoxo has been computationally and experimentally explored (Figure 3-5 B).[142-144] For this enzyme class, the iron-oxy system is not significantly activated, but initial attack involving 1- or 2-electron withdrawal from the heterocyclic indole ring, followed by recombination to form an alkylperoxo intermediate is predicted as a first step. Downstream reactions result in dioxygen insertion and indole ring cleavage. Lastly, radical reactions with aromatics have also been explored both experimentally and computationally using a diradical form of phthaloyl peroxide in which one radical moiety is proposed to attack an unactivated aryl moiety to form an ester-linked aryl radical with a moderate activation barrier of 10 kcal/mole (Figure 3-5 C).[145]

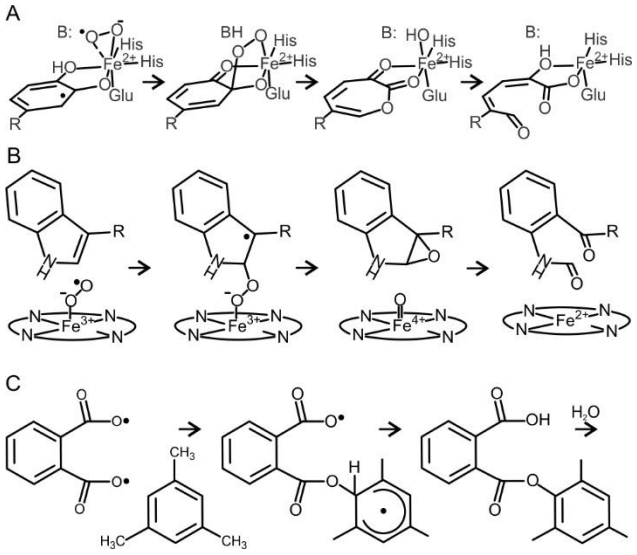

Figure 3-5: Key steps in reactions mechanisms invoking reactive iron-superoxide intermediates. The three examples provided are (A)Extradiol dioxygenase,[139] (B) Tryptophan 2,3-dioxygenase,[142-144] (C) phthaloyl peroxide reaction with unactivated aromatic compound. [145]

A conceptual problem exists if an Fe^{3+}-superoxo does form during RDD *cis*-dihydroxylation and the formation of a ferric mononuclear iron is the trigger for Rieske cluster oxidation. In this situation, it is a possibility that an Fe^{3+}-peroxo would form because the rate constant of the electron transfer *per se* is predicted to be much faster than that for the oxidation of the substrate. Fe^{3+}-peroxos are predicted to be unreactive, but protonation of the peroxo could result in a reactive species (Figure 3-6, pathway A). However, this returns the reaction coordinate to a monooxygenase-like mechanism (Figure 1-16) and is inconsistent with the results presented above showing that the rate constant for Rieske cluster oxidation is dependent on the substrates charge density.

If an Fe^{3+}-superoxo is the initial oxidant during RDD *cis*-dihydroxylation (Figure 3-6, pathway B), a yet unknown regulatory mechanism must keep the Rieske cluster from oxidizing prior to substrate oxidation. As an alternative to formation of a discrete Fe^{3+}-superoxo intermediate, a more concerted mechanism should also be considered

(Figure 3-6, pathway C). When the O_2 is correctly positioned between the mononuclear Fe and the substrate, incipient C-O and Fe-O bonds would form via simultaneous weakening of the O_2 double bond and oxidation of both the mononuclear iron and substrate. Rieske cluster oxidation is triggered when the mononuclear iron and substrate have been oxidized to the extent that the entire system is effectively equivalent to an Fe^{3+}- alkyl$^{\bullet+}$peroxo.

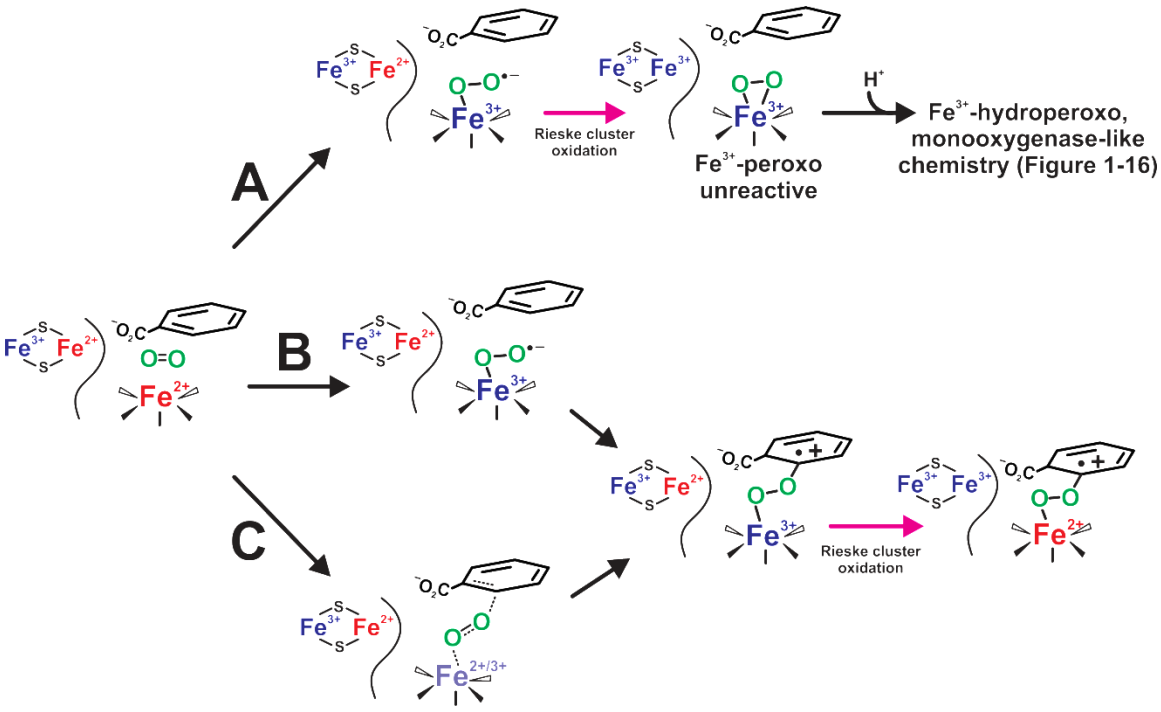

Figure 3-6: Possible on and off-pathway outcomes for the initial substrate oxidation based on an Fe^{3+}-superoxo intermediate.

Conclusions

The results presented in this chapter are consistent with a mechanism for *cis*-dihydroxylation in which (1) substrate and O_2 binding occur rapidly to BZDO when both the mononuclear iron and Rieske cluster are reduced, (2) the rate limiting step occurs after O_2 binding but before Rieske cluster oxidation, and (3) an Fe^{3+}-superoxo like species performs the initial substrate oxidation. In this scenario, the Fe^{3+}-superoxo like

species would have to have sufficient Fe^{2+} character to prevent electron transfer from the Rieske prior to rate limiting oxidation of the substrate. The initial oxidation of the aromatic substrate shown in Figure 3-6 would depend strongly on susceptibility of the aromatic ring to oxidation, specifically at the position of attack. The current results show that the presence of electron-withdrawing fluorine substituents on the ring deactivate the C(2) position for such an attack. Moreover, the computational evaluation of the effect of the numbers and positions of fluorine atoms on the charge density at the presumed position of attack, C(2), is consistent with this proposed mechanism.

Acknowledgments

I thank Dr. Melanie Rogers for her invaluable input and contributions as a collaborator on this project and for providing the data in Figure 3-3. I also thank Daniel Marell and Prof. Christopher Cramer for providing the computational aspects of the above work and for useful discussions in its interpretation.

Chapter 4

Characterization of the Fe^{3+}-hydroperoxo Species Formed During the BZDO Peroxide Shunt

Summary

Rieske dearomatizing dioxygenases catalyze a unique *cis*-dihydroxylation of aromatic compounds utilizing a nonheme mononuclear iron and a Rieske iron-sulfur cluster located 15 Å away in an adjacent subunit. RDDs can form the predicted *cis*-diol products via multiple pathways. During normal (O_2-driven) turnover, substrate and O_2 initially bind to a fully reduced form of the enzyme and the two metals centers are oxidized during product formation. Alternatively, the oxidized as-isolated form of the enzyme can utilize H_2O_2 as an oxidant in a peroxide shunt reaction. Spectroscopic analysis of the BZDO "peroxide shunt" has shown formation of a transient Fe^{3+}-hydroperoxo species preceding product formation. This species is analogous to the ferric peroxo complexes formed during O_2 and H_2O_2-driven turnover of the iron-dependent monooxygenases sMMO and cytP450. Initially, this was interpreted as (further) evidence of a shared mechanistic strategy between the monooxygenases and RDDs. The resulting hypothesis for RDD *cis*-dihydroxylation predicted that an Fe^{3+}-hydroperoxo or an Fe^{5+}-oxo/hydroxo (formed via heterolytic cleavage of the Fe^{3+}-hydroperoxo) was the common oxidant during both normal and H_2O_2-driven reactions. Chapter 3, however, provides evidence for a different mechanism during normal turnover in which the initial oxidant is a Fe^{3+}-superoxo-like species. Utilization of this reactive species significantly changes the predicted chemistry occurring during normal turnover and opens the possibility that multiple reaction coordinates may be used by RDDs depending on the redox state of the enzyme and the oxidant utilized. In this chapter, the H_2O_2-driven reaction of BZDO is further characterized by investigating several aspects of the $BZDO_P$ intermediate. The structure of $BZDO_P$ is probed via vibrational spectroscopy and the factors that regulate its formation are further defined. The results support the initial structural assignment of $BZDO_P$ as a side-on bound Fe^{3+}-hydroperoxo and show that this species can form in the absence of substrate.

Introduction

The experiments in Chapter 3 support a mechanistic hypothesis for RDD *cis*-dihydroxylation in which the initial substrate oxidation occurs before Rieske cluster oxidation.[9] This observation results in a significantly different mechanism (Figure 1-17) than the one first proposed based on canonical monooxygenase chemistry in which either an Fe^{3+}-(H)peroxo or Fe^{5+}-oxo-hydroxo performs the initial oxidations (Figure 1-16). The RDDs NDO and BZDO form the expected *cis*-diols products during peroxide shunt reactions starting from as-isolated enzyme (i.e. not fully reduced).[10, 100] Such reactions are generally considered evidence that a Fe^{3+}-(H)peroxo is an intermediate that forms during the optimized reaction (see Chapter 1).[98, 99] However, several complications prevent direct comparisons of the RDD peroxide shunt reactions to the corresponding reactions with sMMO or cytP450 where this prediction is supported (Figure 1-10and Figure 1-11).[10, 100]

The RDD peroxide shunt was first reported with NDO (Figure 4-1 A).[100] NDO is isolated as ^{ox}NDO-Fe^{2+} and has not yet been shown to be stable as ^{ox}NDO-Fe^{3+}.[11] Due to the ferrous mononuclear iron in the as-isolated state, an extra electron is available during the reaction, possibly changing the mechanism. The NDO peroxide shunt ends with a ferric mononuclear iron and product formed.[100] Because of the chemistry performed and the H_2O_2 oxidant, the mononuclear iron should not change oxidation state during the reaction. To account for this, it was proposed that the excess peroxide present during the reaction oxidizes the mononuclear iron prior to formation of an Fe^{3+}-(H)peroxo that either reacts directly with the substrate or cleaves heterolytically to form an Fe^{5+}-oxo-hydroxo.[100] This sequence is similar to the reported reactions of multiple biomimetic model compounds that start ferrous and have a H_2O_2 mediated oxidation step prior to formation of the on-pathway Fe^{3+}-(H)peroxo intermediates.[103]

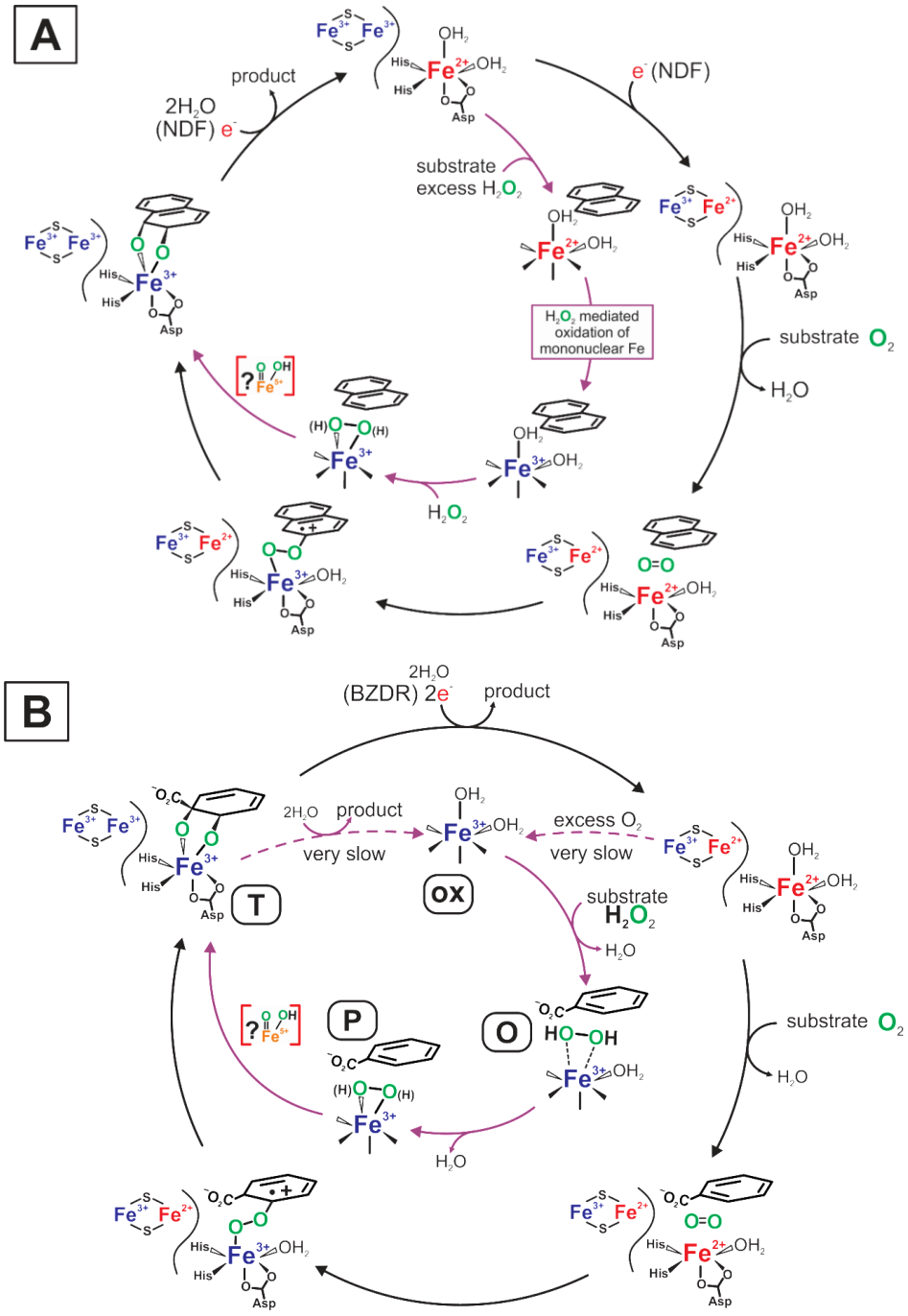

Figure 4-1: NDO (A) and BZDO (B) peroxide shunt reactions (inner cycles) compared to mechanism of optimized single turnover proposed in Chapter 3 (outer cycles).

The BZDO peroxide shunt reaction has several features that distinguish it from the analogous reaction in NDO, sMMO and cytP450. BZDO can be isolated in either the typical ^{ox}BZDO-Fe^{2+} (as with NDO and other RDDs) or a fully oxidized ^{ox}BZDO-Fe^{3+} state.[8] Importantly, the ^{ox}BZDO-Fe^{3+}resting state (hereafter $BZDO_{OX}$) is distinct from the fully oxidized BZDO formed within the catalytic cycle because product is not bound. $BZDO_{OX}$ forms very slowly (≫ 1 hour) by either product dissociation from the Fe^{3+}-product complex or slow O_2 mediated oxidation of the reduced enzyme (Figure 4-1 B, dashed lines).[8] $BZDO_{OX}$ does not form during normal turnovers because the reduction of the iron centers by BZDR and product release from reduced BZDO occur much faster than $BZDO_{OX}$ formation. As a result, the BZDO peroxide shunt does not bridge nonadjacent species within the normal catalytic cycle, as in sMMO and cytP450, and is not a true shunt.

Product formation during the BZDO peroxide shunt occurs over the course of ~ 90 minutes. This is significantly slower than product formation during normal single turnover and the NDO peroxide shunt which are complete in ≤ 0.2 and ≤10 seconds, respectively.[11, 100] The slow product formation during the BZDO peroxide shunt allowed two intermediates to be identified.[10] The spectroscopic analysis of these intermediates shows that the mononuclear iron is high-spin ferric, demonstrating that it does not change oxidation or spin state during the reaction (Table 4-1). Because of the likely similarity to the intermediates formed during sMMO turnover, an analogous naming scheme is used for the intermediates observed within the BZDO peroxide shunt. The proposed turnover cycle for the BZDO peroxide shunt is illustrated in Figure 4-1B. The cycle begins with the as-isolated form $BZDO_{ox}$. Addition of substrate to $BZDO_{OX}$ results in only minor changes to the observed EPR spectrum, but addition of substrate and H_2O_2 forms a new species ($BZDO_O$, Table 4-1). The spectroscopic parameters of $BZDO_O$ are distinct from, but very similar to $BZDO_{OX}$ and, based on this, it is likely that this species is formed by H_2O_2 binding near but not to the mononuclear iron. Over the course of ~ 5 min $BZDO_{OX}$ and $BZDO_O$ decay to a peroxo intermediate named $BZDO_P$. The unique spectroscopic features of $BZDO_P$ (*vide infra*) are consistent with Fe^{3+}-hydroperoxo complexes studied in the past (Table 4-1). The final species observed in the BZDO peroxide shunt is ferric product complex ($BZDO_T$). This species is

spectroscopically identical to the species observed at the end of regular single turnover, and the rate of its formation corresponds to the rate of product formation.[10]

The $BZDO_P$ intermediate has interesting spectroscopic parameters. The negative *D* value (Table 4-1) inverts the energies of the three Kramer's doublets (M_S = 1/2, 3/2 and 5/2) such that the usually excited M_S = 5/2 doublet is the ground state (Table 4-2).[10] Such a situation is called inverted zero-field splitting. The widely split *g*-values of the $BZDO_P$ ground state result in an extremely low transition probability for paramagnetic resonance, so the total intensity of the EPR spectrum decreases drastically. In this case, it is difficult to distinguish a highly anisotropic ferric ground state from an EPR silent ferrous center via EPR. Mössbauer spectroscopy was used to assign the oxidation state of $BZDO_P$ as a ferric center.[10] In order to gain more insights into the structure of $BZDO_P$ and to try to assign its structure based on the Mössbauer isomer shift (δ), a DFT study was conducted.[10] Models based on the NDO *in crystallo* iron\peroxo adduct were constructed.[12] The binding mode of the protein-derived carboxylate and the identity of the two exchangeable facial ligands were varied and the isomer shift calculated for each model. The calculated isomer shifts for Fe^{3+}-peroxo ligands were all ≥ 0.64, much larger than that spectroscopically observed for $BZDO_P$ (0.5, Table 4-1). In contrast to this, the calculated isomer shifts for both end-on (η^1) and side-on (η^2) Fe^{3+}-hydroperoxo complexes were within experimental error of that observed for $BZDO_P$. While the DFT calculations could not unambiguously assign the structure of $BZDO_P$, inverted zero field splitting (-*D* value in Table 4-1) is a characteristic shared with two other reported η^2 Fe^{3+}-peroxos models compounds.[117, 146] Taken together the available data support a structural model of $BZDO_P$ as a side-on bound Fe^{3+}-hydroperoxo.

Many questions remain to be answered regarding the mechanism of peroxide-driven *cis*-dihydroxylation by RDDs. Regarding BZDO specifically, the past studies provide an initial structural model for $BZDO_P$ but further characterization is required for unambiguous assignment. Also, it is unknown why the reaction of $BZDO_P$ with substrate is so slow compared to the peroxide shunt of NDO and single turnover reactions of both BZDO and NDO. The original hypothesis focused on slow substrate binding to the enzyme with a ferric mononuclear iron.[10] However, given the new mechanistic hypothesis proposed in Chapter 3, it is possible that the actual chemical steps involving $BZDO_P$ may be slow. The experiments reported below further investigate the BZDO

peroxide shunt by refining the structural assignment of $BZDO_P$ via vibrational spectroscopy and determining whether substrate is required for the formation of this reactive species.

Table 4-1: Ground state spin Hamiltonian parameters for high-spin ferric mononuclear centers of enzymes and model compounds.

	D (cm^{-1})	*E/D*	effective *g*-values (*gx*, *g*y, *g*z)	δ (mm/s)	ΔE_Q (mm/s)	ref
$BZDO_{OX}$	1.3	0.078	4.1, 7.7, 1.8	[a]	[a]	*10*
$BZDO_O$	[a]	0.072	4.3, 7.6, 1.8	[a]	[a]	*10*
$BZDO_P$	-1.5	0.12	0.07, 0.06, 9.9	0.50	0.5	*10*
$BZDO_T$	3.0	0.133	3.0, 8.5, 1.5	~ 0.45	~ 1.0	*8, 10*
$[Fe^{3+}(TMC)(\eta^2\text{- }O_2)]^+$	-0.91	0.28	0.59, 0.45, 9.8[b, c]	0.58	-0.91	*146*
$Fe^{3+}(TMC)(\mu\text{-}\eta^2\text{:}\eta^2\text{-}O_2)Sc^{3+}$	1.3	0.18	2.3, 9.1, 1.3[b,d]	0.47	0.50	*147*
$[Fe^{3+}(TMC)(\eta^1\text{-}OOH)]^{2+}$	2.5	0.097	3.4, 8.0, ~ 2	0.51	0.20	*146*
$[Fe^{3+}(N4Py)(\eta^2\text{- }O_2)]^+$	-1.0	0.11	~ 0.1, ~ 0.1, 9.9	0.61	1.11	*117*

[a] not reported; [b] values calculated based on the *E/D* value with the program visual RHOMBO available http://www.bt.tudelft.nl/biomolecularEPRspectroscopy; [c] the observed EPR signal arises from the middle state doublet (*S*= 3/2) with effective *g*-values of 4.2, ~ 4.1, 4.6; [d]The observed effective g-values (9.1, 5.1, 3.6, and ~ 2) are a combination of the ground and middle state doublets; TMC, tetramethylcyclam; N4Py, N,N-bis(2-pyridylmethyl-N-bis(2-pyridyl)methylamine

Table 4-2: Calculated[a] *g*-values for each Kramer's doublet of the BZDO peroxide shunt intermediates[b].

	Kramer's Doublet (M_S)	effective *g*-values (*gx*, *g*y, *g*z)
$BZDO_{OX}$	1/2	4.13, 7.66, 1.81
	3/2	1.83, 1.70, 5.80
	5/2	0.042, 0.039, 9.99
$BZDO_{O}$	1/2	4.27, 7.56, 1.84
	3/2	1.70, 1.59, 5.83
	5/2	0.036, 0.033, 9.99
$BZDO_{P}$	1/2	3.25, 8.32, 1.60
	3/2	2.65, 2.41, 5.57
	5/2	0.10, 0.090, 9.97
$BZDO_{T}$	1/2	3.01, 8.48, 1.53
	3/2	2.87, 2.59, 5.49
	5/2	0.13, 0.11, 9.96

[a] *g*-values calculated using the program Visual RHOMBO available at http://www.bt.tudelft.nl/biomolecularEPRspectroscopy; [b] the *E/D* value needed for each calculation was obtained from Table 4-1

Materials and Methods

Chemicals and Reagents.

Water used in all experiments was purified with a Millipore Super-Q system. All commercial reagents were purchased from standard vendors and used without further purification. Gases were purchased from Matheson. Unless noted, all enzymatic reactions were conducted in a standard reaction buffer of pH 6.9 MOPS (50 mM) and NaCl (100 mM).

Cloning, Heterologous Expression, and Purification of BZDO.

See the Materials and Methods section of Chapter 2.

Heterologous Expression and Purification of ^{57}Fe Enriched BZDO.

The heterologous expression and purification of ^{57}Fe enriched BZDO was essentially identical to the procedure above except the growth media used was a modified Hutner's mineral base.[148] The recipe for the defined media was followed as reported except natural abundance iron was not added to any of the media components. Instead, 3 mg/L (~ 60 µM) ^{57}Fe was added to each flask of growth media. The concentrated ^{57}Fe stock was made by dissolving an isotopically enriched iron powder (Cambridge Isotope Laboratories, ≥ 96% ^{57}Fe) in 4M HCl overnight. Filter sterilized Glucose (0.4% w/v) was used as the carbon source and was added from a 20% (w/v) stock.

Preparation of NRVS Samples.

To prepare the NRVS samples, ^{57}Fe enriched $BZDO_{OX}$ (used as purified) was first concentrated to ~ 5 mM. KCN (20 mM) and benzoate (50 mM) were added to the BZDO solution from a high concentration stocks to minimize dilution. KCN was included to suppress background catalase activity. Each NRVS sample was made by mixing 4 parts of the above enzyme solution with 1 part of reaction buffer supplemented as described below for each enzyme species. The mixed reactions were then injected into NRVS cells wrapped in Kapton tape (final volume ~ 50 µl) and frozen on a liquid nitrogen cooled aluminum block. $BZDO_{OX}$ samples were made with reaction buffer containing 50 mM benzoate. ^{16}O $BZDO_P$ samples were made with reaction buffer containing 50 mM benzoate and 250 mM H_2O_2. ^{18}O $BZDO_P$ samples were made with reaction buffer

containing 50 mM benzoate and 250 mM $H_2{}^{18}O_2$ (Cambridge Isotope Laboratories, 2-2.5% in water, ≥ 90% $^{18}O_2$). $BZDO_P$ samples were frozen 5 minutes after addition of the H_2O_2-containing buffer. ApoBZDO (without mononuclear iron) was prepared by overnight dialysis at 4 °C in reaction buffer containing 10 mM EDTA. Complete chelation of the mononuclear iron was verified by assaying steady-state activity with a Hansatech Oxytherm oxygen electrode. EDTA was removed by an additional overnight dialysis at 4 °C in reaction buffer without EDTA. A PD-10 desalting column (GE Healthcare) equilibrated in reaction buffer was used as a final step to remove trace residual EDTA. ApoBZDO NRVS samples were made with reaction buffer containing 50 mM benzoate. Analysis of the Rieske cluster by optical absorbance spectroscopy and EPR showed complete retention after dialysis.

Peroxide Dependent Reactions.

The peroxide dependent reactions reported below where initiated by 1:1 mixing of a solution of BZDO and reaction buffer containing 100 mM H_2O_2. The enzyme solution contained $BZDO_{OX}$ (1-2 mM) and KCN (20 mM) to suppress background catalase activity. When present, benzoate was added to a final concentration of 15 mM. At the indicated times, samples to be analyzed by EPR or Mössbauer spectroscopy were frozen in liquid nitrogen and samples to be analyzed by HPLC were acid quenched as described below. ^{57}Fe enriched BZDO was used for samples analyzed by Mössbauer spectroscopy.

Chemical Quench and HPLC Product Analysis.

Peroxide-driven reactions were quenched by adding a volume of 3% (v/v) trifluoroacetic acid equal to twice the reaction volume. Each sample was vortexed (~20 s) and the denatured protein was removed from the solution by centrifugation at 4 °C before HPLC was used to analyze 200 µl of the quenched reaction. HPLC was performed on a Waters system with a 1525 binary pump, 2487 dual wavelength UV/Vis detector, and an Agilent Zorbax SB C18 column (2.6 mm × 150 mm, 5 µm) with a gradient of 4 to 100% acetonitrile/0.1% formic acid over 7.5 min following an isocratic flow at 4% acentonitrile/0.1% formic acid for 2.5 min. The *cis*-diol products were detected by their optical absorption at 262 nm and quantified using a standard curve made from an authentic standard (see Materials and Methods, Chapter 2).

Spectroscopy

^{57}Fe NRVS spectra were recorded on multiple occasions at BL09XU at SPring-8 in Hyogo, Japan and at Beamline 3-ID-D at the Advanced Photon Source of the Argonne National Laboratory. Samples were maintained at 20K using a liquid helium cryostat. Spectra were collected between -25 and 85 meV. Scans were added together, and the total spectrum was converted to a partial-vibrational density-of-states spectrum using the PHOENIX program developed by Wolfgang Sturhahn.

X-band EPR spectra were recorded with a Bruker ELEXSYS E-500 system equipped with an Oxford ESR 910 liquid helium cryostat. Data was collected with the following conditions: temperature, 2.3 K; microwave frequency, 9.6 GHz; microwave power, 0.2 mW; modulation amplitude, 10 G; modulation frequency, 100 kHz.

Mössbauer spectra were recorded with a Janis Research Super-Varitemp cryostat with an external magnetic field (up to 8.0 T) applied parallel to the γ–radiation. The spectra were simulated using the WMOSS software package (SEE Co). The isomer shifts (δ) are reported relative to iron metal at 298 K.

Results

Vibrational Characterization of $BZDO_P$.

In order to further characterize $BZDO_P$, the technique of NRVS spectroscopy was used for vibrational characterization. In brief, NRVS is a synchrotron based vibrational technique that selectively enhances vibrational modes involving displacement of a Mössbauer active nucleus.[149, 150] The vibrational modes are inelastic sidebands of the Mössbauer nuclear transition and are detected by counting X-rays that are emitted from the sample as it relaxes to the ground state. Conveniently, the ^{57}Fe isotope is a Mössbauer active nucleus making NRVS a useful technique for the study of iron-containing enzymes. For NRVS spectroscopy, cells expressing BZDO were grown in a defined and ^{57}Fe-enriched medium, resulting in isotopic enrichment (>95%) of both the Rieske cluster and mononuclear iron.

Figure 4-2 shows the results from the NRVS experiment. The NRVS spectrum of apoBZDO (without mononuclear Fe) shows that the vibrational modes associated with the Rieske cluster occur between 0 and 450 cm^{-1}. The spectrum of $BZDO_{OX}$ is nearly identical to that of apoBZDO with the exception of a species at ~ 590 cm^{-1} likely arising from the vibrations of iron bound aqua ligands. Samples of $BZDO_P$ exhibit an isotope-sensitive vibration at 510 cm^{-1} that downshifts 14 wavenumbers when $H_2{}^{18}O_2$ is used. The isotope-sensitive nature of this vibration clearly shows that this feature arises from an interaction between the mononuclear iron and the H_2O_2.

The vibration at 510 cm^{-1} is within the range of reported iron/oxygen vibrational modes (ν(Fe-O)) from other high-spin ferric peroxo-, hydroperoxo-, and alkylperoxo-complexes (Table 4-3). The reported ν(Fe-O)'s of end-on (η^1) hydro and alkylperoxo complexes ranges from ~ 460 to 680 cm^{-1}, While the ν(Fe-O)'s of the side-on (η^2) peroxo complex are generally around 500 cm^{-1}. The lower ν(Fe-O) of $BZDO_P$ near 500 cm^{-1} is more consistent with an η^2 binding mode and supports a structural assignment of $BZDO_P$ as a side-on high-spin Fe^{3+}-hydroperoxo species.

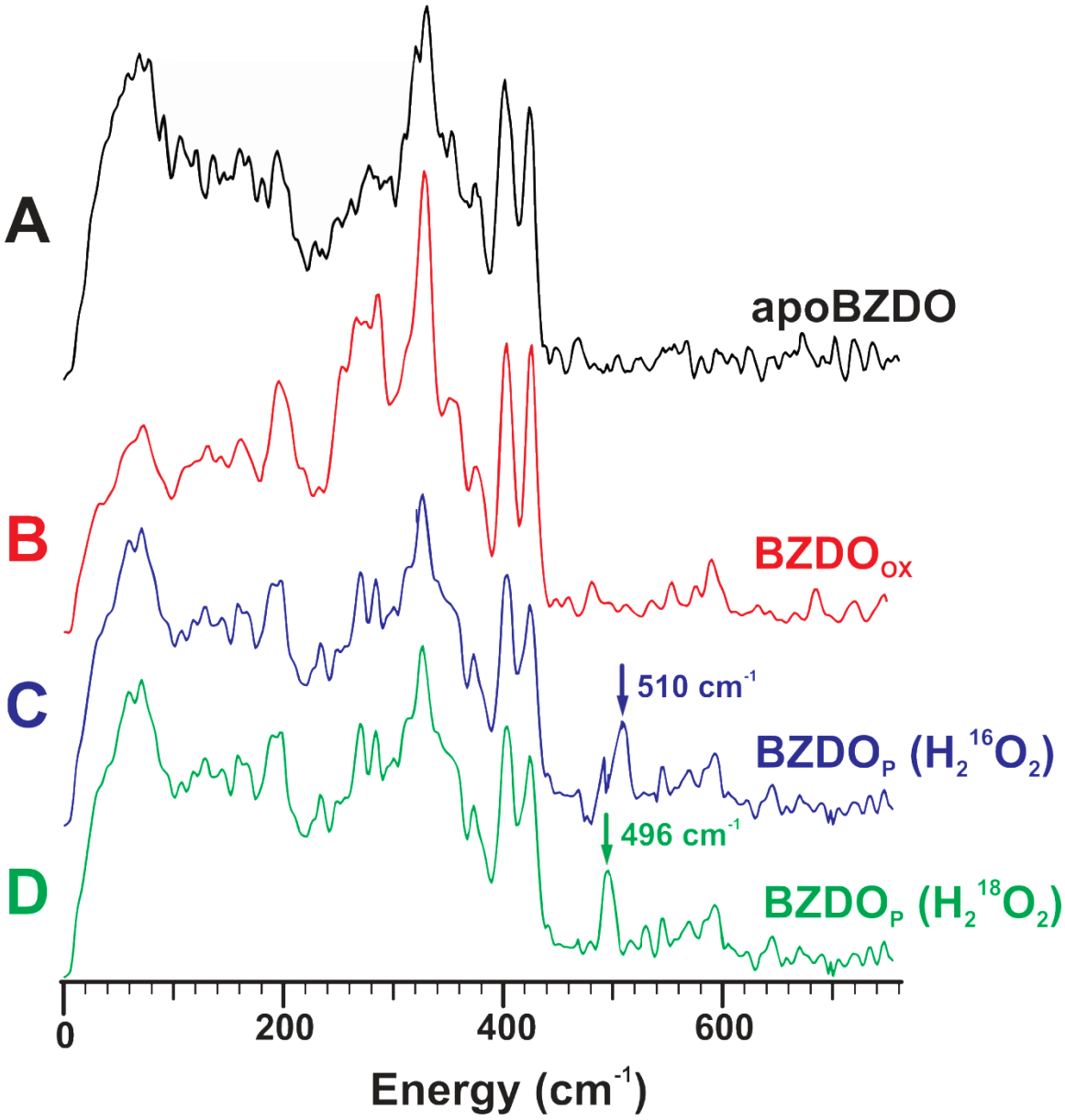

Figure 4-2: Characterization of $BZDO_P$ by NRVS. The enzyme solution used in each sample consisted of 4-5 mM ^{57}Fe enriched BZDO, 20 mM KCN, and 50 mM benzoate. The enzyme solution was mixed 4:1 with reaction buffer containing 50 mM benzoate and 0 mM H_2O_2 (A and B), 250 mM H_2O_2 (C), or 250 mM $H_2{}^{18}O_2$ (D). The $BZDO_P$ reactions were stopped by freezing to liquid nitrogen temperature five minutes after the addition of H_2O_2 or $H_2{}^{18}O_2$. Figure provided by Kyle Sutherlin (Stanford University) and modified by the author.

Table 4-3: Iron/oxygen vibrational modes for high-spin ferric peroxo-, hydroperoxo- and alkylperoxo- complexes

	ν(Fe-O), cm^{-1} (Δ ^{18}O)	ref
$BZDO_P$	510 (-14)	[a]
<u>end-on (η^1) hydroperoxo</u>		
$[Fe^{3+}(TMC)(\eta^1\text{-}OOH)]^{2+}$	676 (-24)	*146*
$[Fe^{3+}(TMC)(\eta^1\text{-}OOH)]^{2+}$	658 (-25)	*151*
$[Fe^{3+}(H_2bppa)(\eta^1\text{-}OOH)]^{2+}$	621 (-22)	*152*
oxyhemerythrin	503 (-24)	*153*
$[Fe^{3+}(cyclam\text{-}PrS)(\eta^1\text{-}OOH)]^{2+}$	419 (-19)	*154*
<u>end-on (η^1) alkylperoxo</u>		
$[Fe^{3+}(6\text{-}Me_3\text{-}TPA)(\eta^1\text{-}OO^tBu)]^{2+}$	637 (-25)	*155*
$[Fe^{3+}(H_2bppa)(\eta^1\text{-}OO^tBu)]^{2+}$	629	*156*
$[Fe^{3+}(15\text{-}TMC)(OTf)(\eta^1\text{-}OO^tBu)]^{2+}$	612 (-21)	*157*
$[Fe^{3+}(15\text{-}TMC)(SPh)(\eta^1\text{-}OO^tBu)]^{2+}$	584 (-19)	*157*
<u>side-on (η^2) peroxo</u>		
$Fe^{3+}(TMC)(\mu\text{-}\eta^2\text{:}\eta^2\text{-}O_2)Sc^{3+}$	543 (-23)	*147*
$[Fe^{3+}(N4Py)(\eta^2\text{-}O_2)]^{+}$	495 (-17)	*117*
$[Fe^{3+}(TMC)(\eta^2\text{-}O_2)]^{+}$	493 (-15)	*146*
$[Fe^{3+}(TMC)(\eta^2\text{-}O_2)]^{+}$	487 (-19)	*151*
$[Fe^{3+}(tmpIm)(\eta^2\text{-}O_2)]^{+}$	475 (-20)	*158*
E47A SOR	438 (-23)	*159*

[a] This work; TMC, tetramethylcyclam; H_2bppa, bis(6-pivalamido-2-pyridylmethyl)(2-pyridylmehyl)amine; SOR, superoxide reductase; cyclam-PrS-H, 1-(3'-mercaptopropyl)-1,4,8,11-tetraazacyclotetradecane; 6-Me_3-TPA, tris(6-methyl-2-pyridylmethyl)amine; ^{t}Bu, *tert*-butyl; 15-TMC, 1,4,8,12-tetramethyl-1,4,8,12-tetraazacyclo-pentadecane; N4Py, N,N-bis(2-pyridylmethyl-N-bis(2-pyridyl)methylamine; tmpIm, 5,10,15-tris(2',4',6'-trimethylphenyl)-20-(2'-(3'-imidazolylmethyl)-benzamido)phyenyl)porphyrinate dianion

The Reactivity of $BZDO_{OX}$ with Peroxide in the Absence of Substrate.

It was previously reported that H_2O_2 in the absence of substrate addition caused $BZDO_{OX}$ to decay without formation of the $BZDO_O$ or $BZDO_T$.[10] This observation may indicate that the reaction of H_2O_2 with the mononuclear iron is different without substrate. In the initial report, the reactivity of the species formed after $BZDO_{OX}$ was not tested, and further investigation was encouraged due to low iron content of the enzyme used and the subtle shifts in *g*-values between $BZDO_{OX}$ and $BZDO_O$. Heeding this warning, the experiment was repeated with enzyme of higher iron content (Figure 4-3). Addition of H_2O_2 to substrate-free $BZDO_{OX}$ resulted in formation of a second transient high-spin species. The *g*-value of the low field up-resonance is consistent with that of the $BZDO_O$ intermediate formed during the reaction in the presence of substrate. This species (putatively $BZDO_O$) then decays to another species (or multiple species) that exhibit no EPR signal or a resonance of low transition probability. No low field resonance characteristic of $BZDO_T$ was observed after longer incubation of this sample.

Given the similarities of the species formed during reactions of $BZDO_{OX}$ and H_2O_2 with and without substrate, it is possible $BZDO_P$ is forming. To test if a species capable of *cis*-dihydroxylation is forming in the absence of substrate, a set of reactions were analyzed with substrate added 4, 30, and 60 minutes after peroxide addition to $BZDO_{OX}$. Each reaction was acid quenched 60 minutes after substrate addition and the amount of *cis*-diol product quantified by HPLC. A sample with simultaneous addition of H_2O_2 and substrate served as the positive control, duplicating the conditions of a typical peroxide shunt reaction. The positive control sample and the sample with substrate added at 4 min each showed a 55 percent product conversion (relative to active sites that contain Rieske clusters). The product conversion then decreased to 6 and 0 % for the 30 and 60 min substrate addition samples, respectively. A follow-up experiment was conducted with more time points to obtain kinetic data on the decay of the reactive species. As shown in Figure 4-4, the amount of product formed decreases as a function of time and the data is well fit by a single exponential function with a reciprocal relaxation time (RRT) of 0.1 min^{-1}.

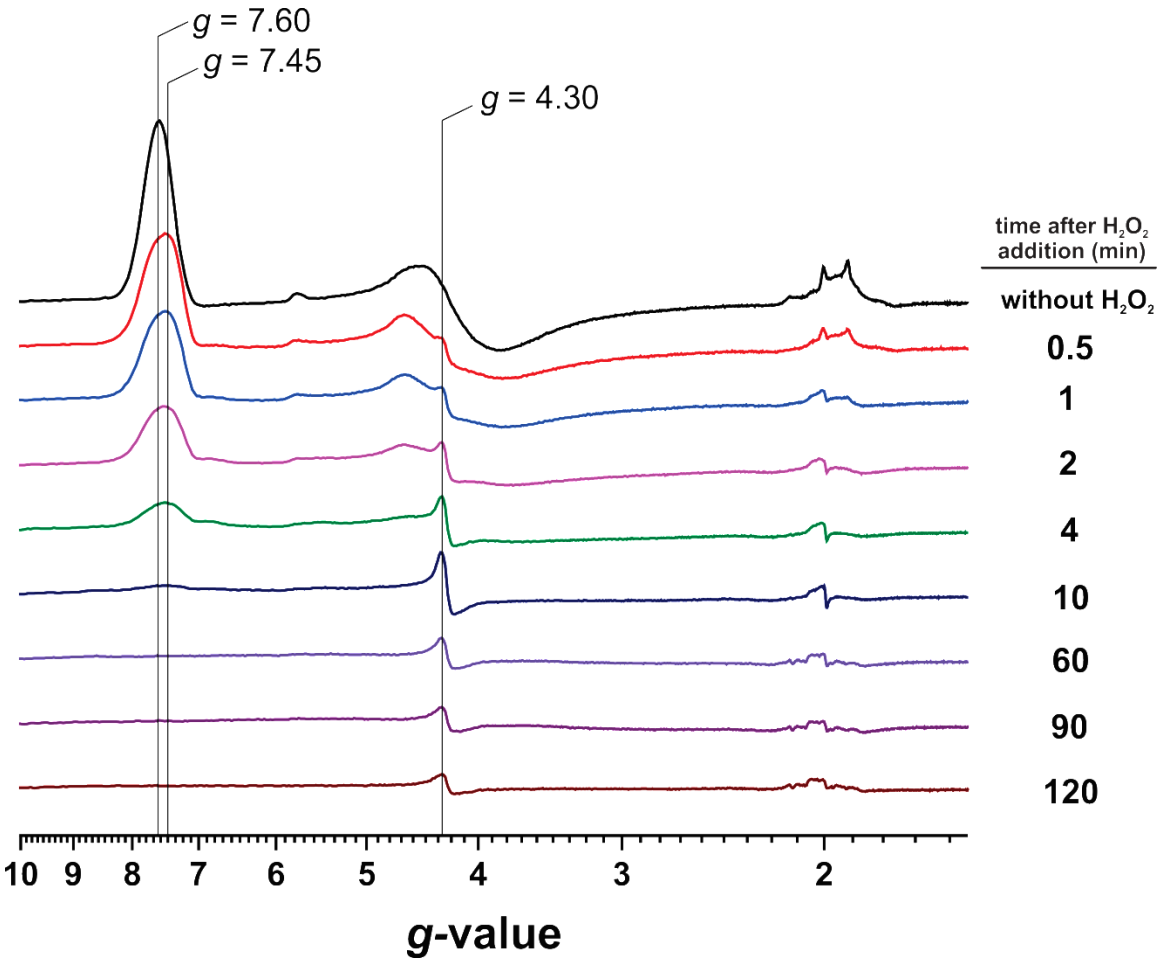

Figure 4-3: The reaction of $BZDO_{OX}$ and H_2O_2 in the absence of substrate. A solution of 1.2 mM $BZDO_{OX}$ and 20 mM KCN was mixed with an equal volume of pH 6.9 MOPS/NaCl buffer either with 100 mM H_2O_2, and the reactions frozen in liquid N_2 at the indicated times. X-band (9.6 GHz) EPR data was collected under the following conditions: temperature, 2.3 K; microwave power, 0.2 mW; modulation amplitude, 10 G; modulation frequency, 100 kHz.

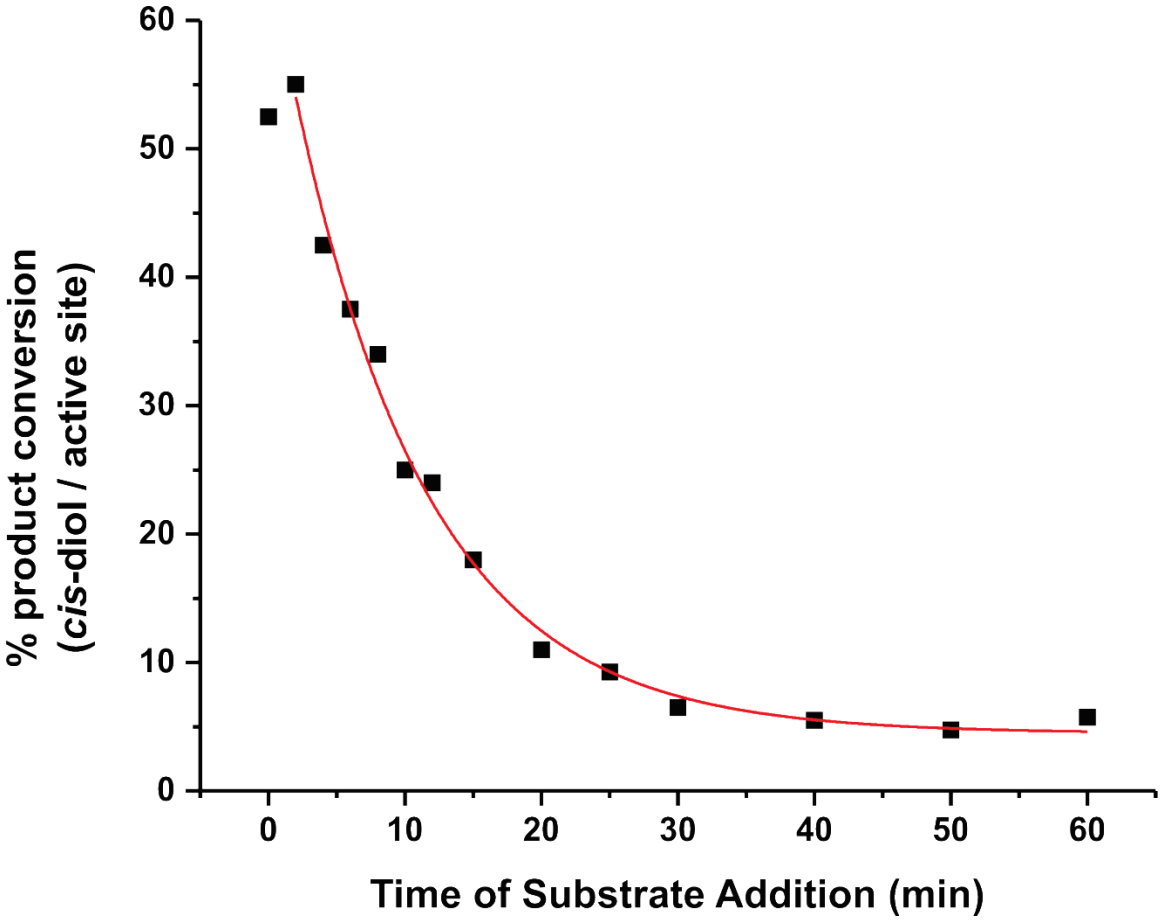

Figure 4-4: Time-dependent inactivation of $BZDO_{OX}$ after addition of H_2O_2. In these reactions, a 25 µl solution of 1.2 mM $BZDO_{OX}$ and 20 mM KCN was mixed with an equal volume of pH 6.9 MOPS/NaCl buffer containing 100 mM H_2O_2. Benzoate was added to 15 mM at the times indicated on the x-axis. 60 min after addition of the substrate, each reaction was quenched with 100 µl of 2% (v/v) trifluoroacetic acid. The *cis*-diol product formed was quantified by HPLC (Materials and Methods). The line is a single exponential fit with a reciprocal relaxation time of 0.1 min^{-1}.

The unidentified reactive species was further explored using EPR spectroscopy (Figure 4-5). Because only two additional electrons are required for breaking of a peroxide O-O bond and these electrons are supplied by the substrate during the BZDO peroxide shunt reaction, the Rieske cluster and the mononuclear iron need not change oxidation state during the reaction. As a consequence, the reactive mononuclear iron species will start and end the product forming chemistry in the same oxidation state. Addition of substrate five minutes after H_2O_2 results in the formation of the ferric $BZDO_T$ spectrum indicating formation of a ferric reactive species (Figure 4-5, species C).

However, not all of the initial $BZDO_{OX}$ (Figure 4-5, species A) was converted to the unidentified reactive species. Five minutes after addition of H_2O_2 and upon addition of substrate, there is a residual ferric signal composed of a mixture of spectra from $BZDO_{OX}$ and $BZDO_O$ (Figure 4-5, species B). This data is consistent with $BZDO_P$ forming, but does not clearly show how much is forming in the absence of substrate due to the residual amount of species B.

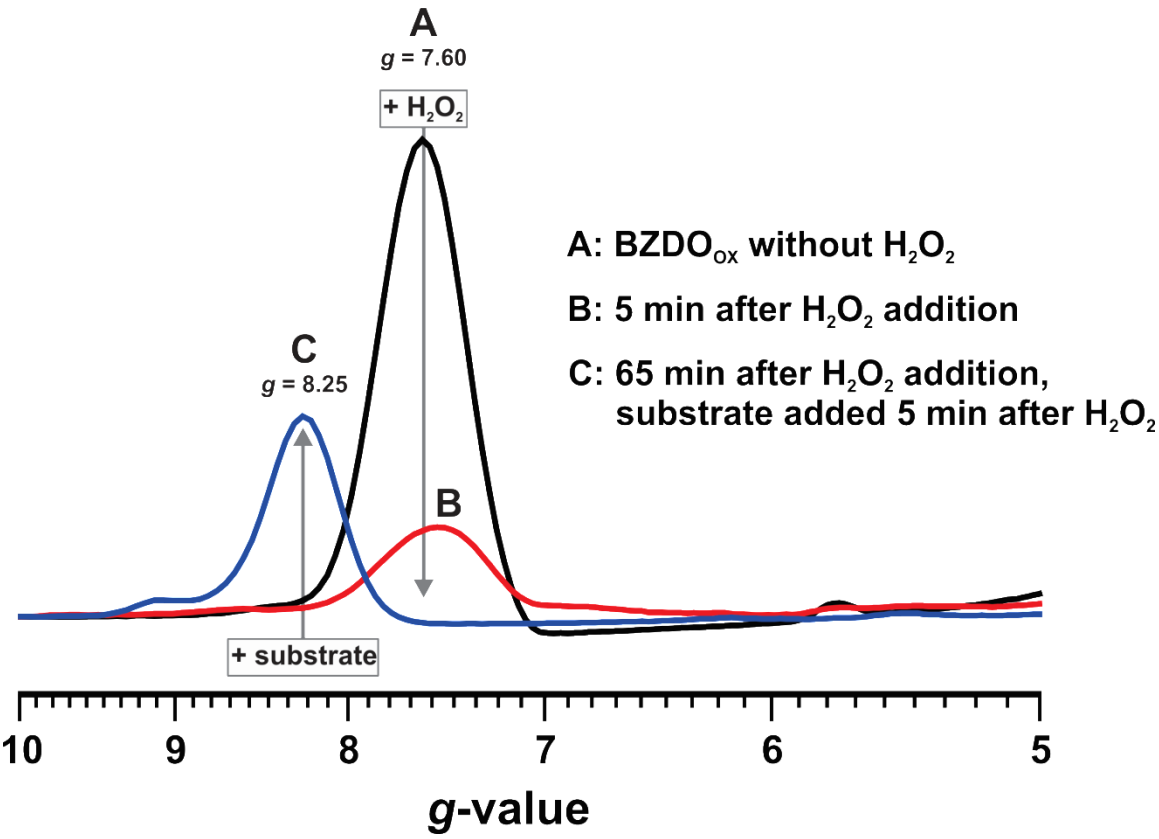

Figure 4-5: EPR analysis of samples with substrate added 5 min after H_2O_2. A solution of 1.8 mM $BZDO_{OX}$ and 20 mM KCN was mixed with an equal volume of reaction buffer containing either 0 mM (A) or 100 mM H_2O_2. The sample with H_2O_2 was allowed to react for 5 min (B). Benzoate (15 mM) was added to sample B and allowed to react for an addition 60 min (C). X-band (9.6 GHz) EPR data was collected under the following conditions: temperature, 2.3 K; microwave power, 0.2 mW; modulation amplitude, 10 G; modulation frequency, 100 kHz.

Mössbauer spectroscopy was used to further characterize the species that form after the addition of H_2O_2 to substrate free $BZDO_{OX}$. Mössbauer spectroscopy is ideally suited for investigation of iron-containing enzymes and complexes because all oxidation and spin states can be detected.[160] The samples in Figure 4-6 shows the Mössbauer spectrum of $BZDO_{OX}$. The spectrum is essentially identical to that previously reported for $BZDO_{OX}$.[8] Three iron species are present in the spectrum. The two large doublets near the middle of the spectrum arise from the two inequivalent irons of the Rieske cluster antiferromagnetically coupled to give an $S = 0$ spin state for the oxidized cluster. Simulation of the spectral contributions of the Rieske cluster irons (blue line in Figure 4-6) show each constitutes 36% of total iron. The Mössbauer spectrum of the mononuclear iron of $BZDO_{OX}$ exhibits the broad absorbances (with coincident attenuated intensity) typical of an $M_s = 1/2$ Kramers doublet of an $S = 5/2$ center with $E/D \approx 0.08$.[160] The spectral simulation of this iron (black line in Figure 4-6) shows that it constitutes 28% of the total iron. Figure 4-7 shows the Mössbauer spectra of substrate free $BZDO_{OX}$ five minutes after addition of H_2O_2. This spectrum shows no significant change to the Rieske clusters iron and no quadrupole doublets which would arise from the presence of ferrous mononuclear iron. The spectrum of the mononuclear iron has changed significantly and is consistent with that of $BZDO_P$, exhibiting the six sharp absorption lines typical of $M_s = 5/2$ Kramers doublet of an $S = 5/2$ center with $E/D < 0.15$. The simulation of this six-line spectrum shows that it constitutes 19% of the total iron. By comparison to the amount of mononuclear iron in the $BZDO_{OX}$ sample (28%, Figure 4-6) it can be estimated that ~ 70% of the available mononuclear iron has been converted to $BZDO_P$. This conclusively shows that not only does $BZDO_P$ form in the absence of substrate, but it accumulates to an equal (or possibly higher) concentration.

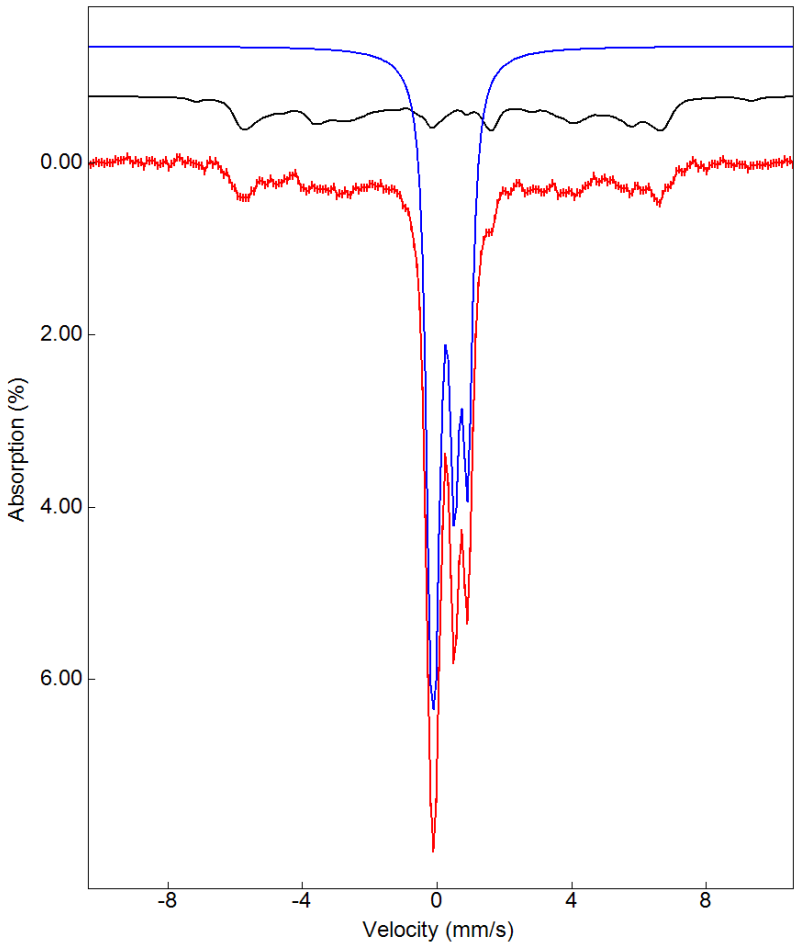

Figure 4-6: Mössbauer spectrum of $BZDO_{OX}$. A solution of 1.8 mM ^{57}Fe enriched $BZDO_{OX}$ and 20 mM KCN was mixed with an equal volume of reaction buffer. Mössbauer spectrum recorded at 4.2 K in a 0.45 T field.

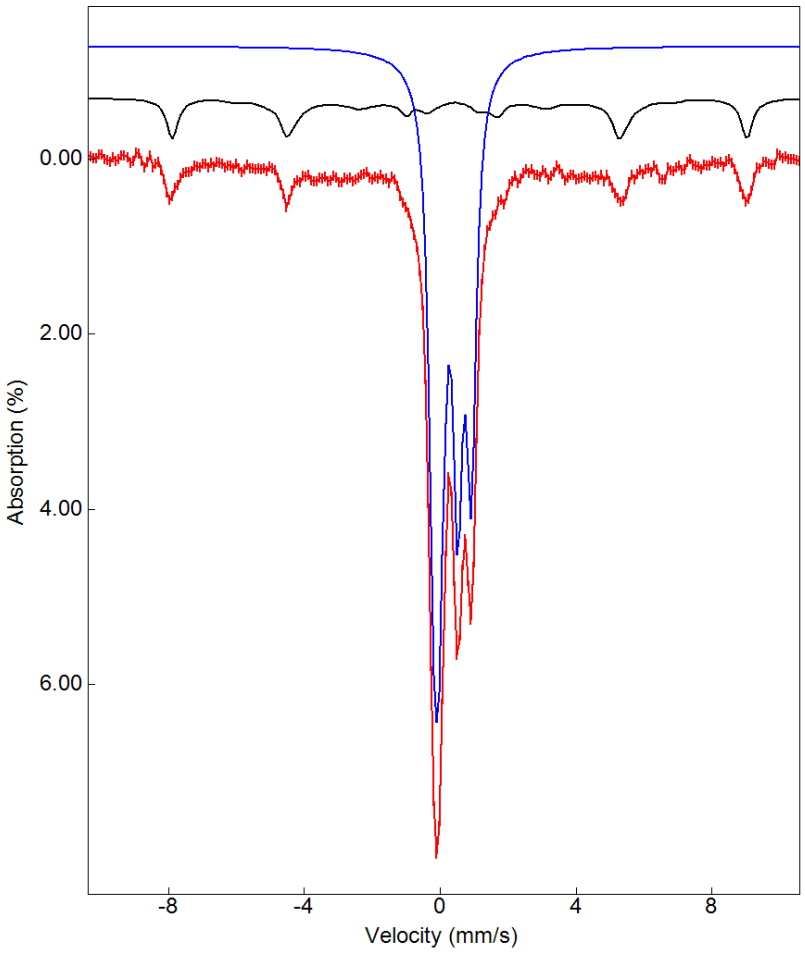

Figure 4-7: Mössbauer spectrum of substrate free $BZDO_{OX}$ five minutes after addition H_2O_2 addition shows formation of $BZDO_P$. A solution of 1.8 mM ^{57}Fe enriched $BZDO_{OX}$ and 20 mM KCN was frozen in liquid nitrogen five minutes after mixing with an equal volume of reaction buffer containing 100 mM H_2O_2. Mössbauer spectrum recorded at 4.2 K in a 0.45 T field.

Discussion/Conclusions

RDDs are unique enzymes that have characteristics of both monooxygenases and dioxygenases (Table 1-2). In addition to this, several reaction conditions can lead to formation of the correct *cis*-diol product. The various conditions are defined by the redox states of the active site metal centers and the oxidants utilized: (1) ^{red}RDD-Fe^{2+} with substrate and O_2, (2) ^{ox}RDD-Fe^{2+} with substrate and H_2O_2, and (3) ^{ox}RDD-Fe^{3+} with substrate and H_2O_2. These three combinations have been previously studied and are represented by: (i) the optimized single turnover reactions, (ii) the NDO peroxide shunt, and (iii) the BZDO peroxide shunt.[8-11, 100] It is currently not known how these reactions relate to one another. Of these three reactions, the BZDO peroxide shunt is by far the slowest.[10] The high rates of NDO peroxide shunt (complete in ≤ 10 seconds) and single turnover (complete in ~ 0.2 seconds) reactions do not allow the detection of intermediates for direct comparison. Working under the assumption of a monooxygenase-like mechanism, a $BZDO_P$-like intermediate (η^1 or η^2 Fe^{3+}-(H)peroxo) would be expected for each type of reaction, and thus the reactions would converge at the same reactive intermediate. In contrast, the data presented in Chapter 3 supports a dioxygenase-like mechanism in which the initial reactive species is superoxo in nature.[9] The dioxygenase-like reaction and the peroxide-driven reactions may still converge to a shared reaction coordinate, but they differ in the nature of the species that first attack the substrate. If so, then the RDD active site must be able to utilize several distinct pathways that lead to the same unique *cis*-diol product.

Structure of $BZDO_P$.

The NRVS data presented above provides the first vibrational characterization of $BZDO_P$. The initial characterization of $BZDO_P$ showed it was a high-spin ferric species with a negative zero-field splitting (*D* in Table 4-1).[10] Negative zero-field splitting is also displayed by several Fe^{3+}(η^2-peroxo) model complexes, but the isomer shift for these species is considerably higher than that observed for $BZDO_P$ (Table 4-1). A DFT analysis showed that protonation of the peroxo is consistent with a decreased isomer shift, supporting an Fe^{3+}(η^2-hydroperoxo) structure for $BZDO_P$.[10] In the same DFT study a nearly identical isomer shift for Fe^{3+}(η^1-hydroperoxo) complexes was calculated casting

some doubt on this initial assignment. The ν(Fe-O) mode obtained from the current study via NRVS (Figure 4-2) is most consistent with those reported for high-spin Fe^{3+}(η^2-peroxo) complexes (Table 4-3). This supports the initial structural assignment of $BZDO_P$ as a side-on Fe^{3+}-hydroperoxo. If this structural assignment is correct, $BZDO_P$ is (to our knowledge) the only reported metastable high-spin Fe^{3+}(η^2-hydroperoxo) species currently available for study.

$BZDO_P$ in the Absence of Substrate.

The results reported above show that $BZDO_P$ forms in the absence of substrate. The loss of EPR signal intensity upon addition of H_2O_2 to substrate-free $BZDO_{ox}$ is consistent with formation of $BZDO_P$, and the observed product formation provides further evidence for its formation. Analysis via Mössbauer spectroscopy (Figure 4-7) confirmed that $BZDO_P$ formed in the absence of substrate in yields equal to or greater than reactions carried out in the presence of substrate. The reaction of H_2O_2 with the mononuclear iron appears to be identical with or without substrate. In both cases, addition of H_2O_2 to $BZDO_{ox}$ results in conversion to $BZDO_o$ before formation of $BZDO_p$. In both cases, the kinetics of these processes appears to be comparable. Furthermore, the reactive intermediate formed makes the correct *cis*-diol product as confirmed by both HPLC analysis and the observation of the $BZDO_T$ spectrum via EPR. These observations suggest that the absence of substrate does not change the steps leading to, the structure of, or the reactivity of $BZDO_p$. The ability to generate $BZDO_P$ without substrate will aided further spectroscopic analysis because samples of higher purity can be made. With no product forming pathway, the amount of $BZDO_P$ formed will only depend on the rate constants for its formation and nonproduct-forming decay (Figure 4-4).

Mechanistic Significance of Substrate Independent $BZDO_P$ Formation.

It is possible that H_2O_2 reacts slowly with the mononuclear iron of $BZDO_{ox}$, and this may be one factor that contributes to slow product formation during the BZDO peroxide shunt. If so, this is different than observed for the other *cis*-diol forming reactions. During normal single turnover and the NDO peroxide shunt, the binding of the

oxidants and the conversion of this adduct to a reactive species occur on the sub-second rather than minutes time scale. Both of these reactions start from a form of the enzyme found in the normal catalytic cycle. As a result, some or all of the normal mechanisms for regulation of oxidant activation are likely to be operational (Figure 1-9). An important aspect of this regulatory mechanism for NDO is the coupling of substrate binding with the loss of an aqua ligand, changing the 6-coordinate mononuclear iron (unreactive) to 5-coordinate (reactive) state. The processes controlling $BZDO_p$ formation appear indifferent to substrate binding, suggesting that there is no substrate mediated modulation of the active site. This may mean that BZDO is regulated differently, but it is more likely that it reflects an inhibited access to the substrate binding pocket. Indeed, past experiments have provided evidence that the oxidation state of the mononuclear iron significantly impacts the ability of small molecule exchange showing increased access in the ferrous state. If substrate cannot access the active site with a ferric mononuclear iron, then it cannot prime the iron for peroxide binding. Thus, the mononuclear iron of $BZDO_{ox}$ could be locked in a 6-coordinate environment, inhibiting the initial binding of H_2O_2. Alternatively, substrate may be able to bind within the active site, but the mechanism of regulation is not operational in the $BZDO_{OX}$, a nonphysiological state of the enzyme and the mononuclear iron is again locked in 6-coordinate state. In either case, peroxide must be able to eventually access the mononuclear iron and/or directly displace water from the mononuclear iron site without the aid of substrate.

Even though the formation of $BZDO_P$ reaches a maximum ~ 5 minutes after addition of H_2O_2, product continues to accumulate for > 60 minutes. This shows there is an addition step(s) that limit the rate of the BZDO peroxide shunt after formation of $BZDO_P$. Several possible scenarios can be proposed to account for this. First, slow product formation may be caused by slow formation of a productive ES complex ($BZDO_{PS}$) with $BZDO_P$. Alternatively a slow step may occur after formation of $BZDO_{PS}$. The slow chemistry could be caused by either a slow oxidation of the substrate by the side-on Fe^{3+}-hydroperoxo species or a slow decay of this species to a different reactive species. One possibility for the latter is an Fe^{5+}-oxo/hydroxo that could then rapidly form product.

The ability to form $BZDO_P$ in the absence of substrate will greatly aid future kinetic studies testing the above scenarios as we continue to probe what contributes to the drastically slowed turnover during the BZDO peroxide shunt. Addition of substrate directly to a solution of preformed $BZDO_P$ will be a great advantage because the steps of $BZDO_O$ formation and decay can be circumvented, greatly simplifying the reaction that is being monitored.

Acknowledgments

I thank Kyle Sutherlin, Dr. Lei Liu, and Prof. Edward Solomon of Stanford University for collection and analysis of the NRVS data.

Chapter 5

Perspective

Towards a Complete Mechanism: Contributions of the Dynamic Protein.

The research regarding O_2 activation at iron center has revealed that multiple parameters simultaneously affect the chemistry that is performed by a given system in both subtle and drastic ways. Within an oxygenase active site, the accessible chemistry is expanded beyond the confines of a single gas or solution phase collision. Substrates and intermediates are bound and stabilized in specific orientations relative to a reactive species utilizing seeming infinite combinations of amino acid side chains. Going even beyond this, the enzyme active site is structurally dynamic and moves in stochastic and/or deterministic ways. Such dynamics appear to have a significant effect on the remarkable catalytic rate enhancement achieved in enzymes. The current body of RDD research indicates that structural changes, modulated by the oxidation state of the Rieske cluster, alter the distance between the mononuclear iron and substrate and this may contribute to the reactivity of the RDD reaction coordinate.

The crystal structure of BZDO has not been reported, making it impossible to explore theoretically any actual reaction coordinate with a requisite level of confidence, but structures of several other RDDs and some intermediates are known. This includes structures of the putative Fe^{3+}-(H)peroxo intermediate previously hypothesized to be the species that initially attacks the substrate.[12, 70] In all such structures, the distance between the mononuclear iron and the substrate carbon closest to the iron is 4-5 Å. This is the expected distance for formation of an aryl or alkyl-peroxo intermediate as proposed in the dioxygenase-like mechanism. After electron transfer from the Rieske cluster, the iron-bound oxygen would be approximately 2.5-3 Å from the nearest substrate carbon. This is not an unreasonable distance for a second attack on the activated (oxidized) substrate, but the reaction may be further promoted by the return of the Rieske cluster to the oxidized state. Structural studies of 2-oxoquinoline 8-monooxygenase and CarDO show that oxidation of the Rieske cluster forces the mononuclear iron to move approximately 0.5 Å toward the substrate. [14, 70] This compression of the active site would bring the iron-bound oxygen and activated substrate into closer proximity and may trigger rapid irreversible completion of the reaction once the electron from the Rieske cluster has been transferred. This structural rearrangement would make the rate-limiting formation of the Fe^{3+}- alkyl$^{\bullet+}$peroxo

intermediate appear to be irreversible, as we observe, even if it were in fact a reversible process.

Mechanistic Possibilities for the Product Forming Steps After Electron Transfer.

There are many mechanistic possibilities regarding the product forming steps occurring after Rieske cluster oxidation. Two general possibilities are now presented. Path A of Figure 5-1 illustrates a mechanism in which homolytic cleavage and epoxide formation precedes the active site compression. In this model, homolytic bond cleavage would be promoted by the two factors. First, the ferrous mononuclear iron can donate electron density via a π-interaction into the σ^* orbitals of the peroxide O-O bond and weaken it.[161] DFT calculations with models of the Fe^{2+}-pterin-peroxo of ADDs has concluded that the analogous electron transfer from the high-spin Fe^{2+} into the σ^* bonds of the pterin-peroxo occurs with a relatively low activation energy (computed $\Delta G^{\ddagger}$ = 4.8 kcal/mole).[162] Second, the radical cation on the substrate would act to abstract *a single* electron from the O-O bond (A1 in Figure 5-1).Substrate epoxidation and formation of an Fe^{3+}-hydroxide would occur after homolysis (A2 in Figure 5-1). The active site compression would then bring the substrate epoxide closer to the mononuclear iron such that a full or partial bond would form (A3 in Figure 5-1). Such an interaction may aid in opening of the epoxide, further facilitating the already favorable attack of the Fe^{3+}-hydroxide on the epoxide (A4 in Figure 5-1). An epoxide based mechanism was calculated to be the most energetically favorable pathway in a DFT study based on models of the NDO active site. The steps preceding epoxide formation are different from our model, but a similar iron mediated epoxide opening and Fe^{3+}-hydroxide attack was proposed with intermediates similar to A3 and A4 in Figure 5-1.[101] Opening of the iron-bond epoxide was calculated to be kinetically favorable and near thermoneutral ($\Delta G^{\ddagger}$ = 7.2 kcal/mole and ΔG = 1.2 kcal/mole). Attack of the Fe^{3+}-hydroxide on the iron-bound opened epoxide was calculated to be kinetically favorable and exothermic ($\Delta G^{\ddagger}$ = 2.4 kcal/mole and ΔG = -22.6 kcal/mole).

Path B of Figure 5-1 illustrated a second possible pathway in which active site compression would precede O-O bond cleavage. After active site compression, the substrate bound oxygen could form a partial bond with the mononuclear iron (B1 in

Figure 5-1). The Lewis acidity of the mononuclear iron would pull election density from the peroxide O-O bond onto the substrate bound oxygen. This would make the charge density of the two peroxo oxygens inequivalent, favoring heterolytic cleavage. The ability of the proposed η^2 Fe^{2+}- alkyl$^{\bullet+}$peroxo (B1 in Figure 5-1) to undergo heterolytic O-O bond cleavage may be well modeled by an η^2 Fe^{2+}-hydroperoxo. The reactivity of η^2 Fe^{2+}-hydroperoxo was computationally explored in the DFT study of NDO. The activation barrier ($\Delta G^{\ddagger}$) for heterolytic cleavage of high spin η^2 Fe^{2+}-hydroperoxo was calculated to be 16.4 kcal/mole suggesting this process is kinetically favorable vs the heterolytic cleavage of high-spin η^2 Fe^{3+}-hydroperoxo ($\Delta G^{\ddagger}$ of 26.5 kcal/mole).[101] Mechanistic evidence for heterolytic cleavage of an Fe^{2+}-hydroperoxo requiring two facial coordination sites has also been observed in studies with the hydrotris(3,5-diphenylpyrazolyl)borate ligand.[163] After O-O bond cleavage, product formation could occur via direct abstraction of the substrate radical by the resulting Fe^{4+}-oxo. Alternatively, the radical may reduce the mononuclear iron via the bound substrate C-O resulting in a cationic substrate and Fe^{3+}-hydroxide, an intermediate identical to that proposed in the homolytic pathway (A4 Figure 5-1).

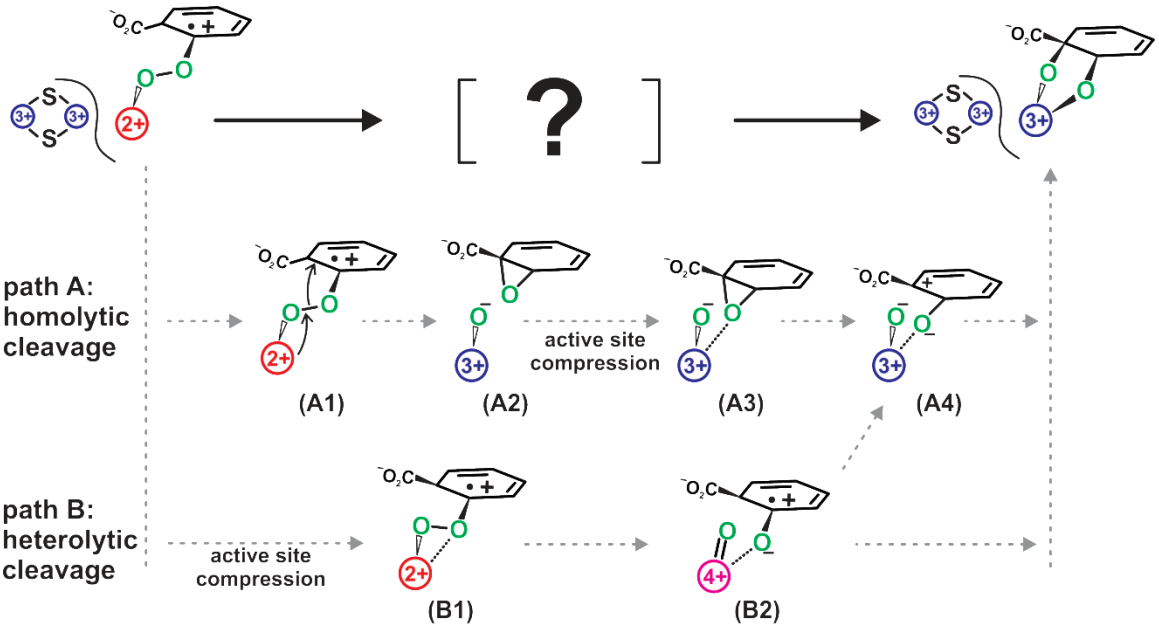

Figure 5-1: Possible pathways for O-O bond cleavage and product formation during *cis*-dihydroxylation by RDDs.

Consequences of a "Rieske" Mechanism: *cis*-Dihydroxylation vs. Ring Cleavage.

As proposed above, direct attack of a Fe^{3+}-superoxo-like intermediate on the aromatic substrate would yield an Fe^{3+}-alkyl$^{\bullet+}$peroxo analogous to the Fe^{3+}-peroxo-imidazole radical proposed as a feasible route for the TDO/IDO systems (Figure 3-5). [142-144] In the latter systems, the subsequent steps have been proposed to result in the formation of a substrate epoxide with coincident formation of an Fe^{4+}-oxo at the level of Compound II. Reaction of the high valent oxo species with the epoxide or the carbocation formed upon epoxide ring-opening would result in the dioxygenation reaction and ring opening. In contrast, the BZDO system is able to avoid ring cleavage. This can be achieved by controlling the source of the 2 electrons required for this phase of the reaction. Rather than utilizing 2 electrons from the sessile bond (as in the TDO/IDO case), our past results have shown that BZDO uses one from the iron and one from the Rieske cluster.[8, 11] We propose that the high potential Fe^{3+} formed concurrent with the formation of the putative Fe^{3+}-alkyl$^{\bullet+}$peroxo intermediate allows the transfer of

an electron from the Rieske cluster and promotes O-O bond cleavage with formation one of the intermediates proposed in Figure 5-1.

Concluding Summary

The observation that the apparent rate of the electron transfer from the Rieske cluster required to form the peroxo intermediate depends on the number and position of fluorines introduced into the substrate ring strongly suggests that there is a reaction with substrate prior to electron transfer. The dependence of the rate of this reaction on the electron density at the closest substrate carbon to the iron is consistent with the attacking species being an electrophilic Fe^{3+}-superoxo-like species. The result of this attack would be an Fe^{3+}- alkyl$^{\bullet+}$peroxo intermediate. While it is possible that the O-O bond cleavage occurs at this stage, we believe that it is unlikely because there is no detectable reaction of any type when only the mononuclear iron is reduced. However, it may also be that the presence of an oxidized Rieske cluster does not allow substrate and O_2 access to the active site to allow the reaction to initiate. Oxygen bond cleavage after electron transfer from the Rieske cluster would force the reaction onward irreversibly to product formation.

There is little doubt that RDD enzymes can stabilize a reactive Fe^{3+}-(H)peroxo species as demonstrated in both solution and crystallographic studies. [10, 14, 70] However, the current study suggests that this species is not accessed during normal turnover due to either kinetic or steric constraints. When the intermediate is formed during a single turnover peroxide shunt reaction of fully oxidized BZDO, the product formation reaction occurs on a minute rather than a millisecond time scale. [10]

NDO and other RDDs can catalyze both dioxygenase and adventitious monooxygenase reactions. [164] Use of a radical trap/clock molecule as a monooxygenase substrate for NDO unequivocally demonstrated that a radical intermediate was formed.[165] A radical is unlikely to arise from the attack of an Fe^{3+}-peroxo intermediate, but it might derive from attack by either an Fe^{3+}-superoxo-like species proposed here or an electrophilic Fe^{5+}-oxo/hydroxo species hypothesized previously. [165] Indeed, both types of chemistry might occur in the versatile RDD family

with the mechanism determined by the reaction type, the oxygen species supplied, and the kinetics of individual steps on the reaction coordinate.

References

[1] Hohmann-Marriott, M. F., and Blankenship, R. E. (2011) Evolution of photosynthesis, *Annu. Rev. Plant Biol. 62*, 515-548.

[2] Lyons, T. W., Reinhard, C. T., and Planavsky, N. J. (2014) The rise of oxygen in Earth's early ocean and atmosphere, *Nature 506*, 307-315.

[3] Wood, P. M. (1988) The potential diagram for oxygen at pH 7, *Biochem. J. 253*, 287-289.

[4] Hayaishi, O., and Hashimoto, K. (1950) Pyrocatecase a new enzyme catalizing oxidative breakdown of pyrocatechin, *Biochem. J. 37*, 371-374.

[5] Hayaishi, O., Katagiri, H., and Rothberg, S. (1955) Mechanism of the pyrocatechase reaction, *J. Am. Chem. Soc. 77*, 5450-5451.

[6] Mason, H. S., Fowlks, W. L., and Peterson, L. (1955) Oxygen Transfer and Electron Transport by the Phenolase Complex, *J. Am. Chem. Soc. 77*, 2914-2915.

[7] Barry, S., and Challis, G. L. (2013) Mechanism and catalytic diversity of Rieske non-heme iron-dependent oxygenases, *ACS Catal. 3*, 2362–2370.

[8] Wolfe, M. D., Altier, D. J., Stubna, A., Popescu, C. V., Münck, E., and Lipscomb, J. D. (2002) Benzoate 1,2-dioxygenase from *Pseudomonas putida*: Single turnover kinetics and regulation of a two-component Rieske dioxygenase, *Biochemistry 41*, 9611-9626.

[9] Rivard, B. S., Rogers, M. S., Marell, D. J., Neibergall, M. B., Chakrabarty, S., Cramer, C. J., and Lipscomb, J. D. (2015) Rate-determining attack on substrate precedes Rieske cluster oxidation during cis-dihydroxylation by benzoate dioxygenase, *Biochemistry 54*, 4652-4664.

[10] Neibergall, M. B., Stubna, A., Mekmouche, Y., Münck, E., and Lipscomb, J. D. (2007) Hydrogen peroxide dependent *cis*-dihydroxylation of benzoate by fully oxidized benzoate 1,2-dioxygenase, *Biochemistry 46*, 8004-8016.

[11] Wolfe, M. D., Parales, J. V., Gibson, D. T., and Lipscomb, J. D. (2001) Single turnover chemistry and regulation of O_2 activation by the oxygenase component of naphthalene 1,2-dioxygenase, *J. Biol. Chem. 276*, 1945-1953.

[12] Karlsson, A., Parales, J. V., Parales, R. E., Gibson, D. T., Eklund, H., and Ramaswamy, S. (2003) Crystal structure of naphthalene dioxygenase: Side-on binding of dioxygen to iron, *Science 299*, 1039-1042.

[13] Kurtz, D. M., Jr. (1999) Structure of an aromatic-ring-hydroxylating dioxygenase-naphthalene 1,2-dioxygenase, *Chemtracts 12*, 303-310.

[14] Martins, B. M., Svetlitchnaia, T., and Dobbek, H. (2005) 2-Oxoquinoline 8-monooxygenase oxygenase component: active site modulation by Rieske-[2Fe-2S] center oxidation/reduction, *Structure 13*, 817-824.

[15] Zhou, N.-Y., Al-Dulayymi, J., Baird, M. S., and Williams, P. A. (2002) Salicylate 5-hydroxylase from *Ralstonia* sp. strain U2: a monooxygenase with close relationships to and shared electron transport proteins with naphthalene dioxygenase, *J. Bacteriol. 184*, 1547-1555.

[16] Capyk, J. K., Casabon, I., Gruninger, R., Strynadka, N. C., and Eltis, L. D. (2011) Activity of 3-ketosteroid 9α-hydroxylase (KshAB) indicates cholesterol side chain and ring degradation occur simultaneously in *Mycobacterium tuberculosis*., *J. Biol. Chem. 286*, 40717-40724.

[17] Capyk, J. K., D'Angelo, I., Strynadka, N. C., and Eltis, L. D. (2009) Characterization of 3-ketosteroid 9a-hydroxylase, a Rieske oxygenase in the cholesterol

degradation pathway of *Mycobacterium tuberculosis*, *J. Biol. Chem. 284*, 9937-9946.
[18] Li, W., Estrada-de los Santos, P., Matthijs, S., Xie, G. L., Busson, R., Cornelis, P., Rozenski, J., and De Mot, R. (2011) Promysalin, a salicylate-containing *Pseudomonas putida* antibiotic, promotes surface colonization and selectively targets other Pseudomonas, *Chem. Biol. 18*, 1320-1330.
[19] Li, P., Wang, L., and Feng, L. (2013) Characterization of a novel Rieske-type alkane monooxygenase system in *Pusillimonas sp*. T7-7, *J. Bacteriol. 195*, in press.
[20] Schuster, J., Schäfer, F., Hübler, N., Brandt, A., Rosell, M., Härtig, C., Harms, H., Müller, R. H., and Rohwerder, T. (2012) Bacterial degradation of tert-amyl alcohol proceeds via hemiterpene 2-methyl-3-buten-2-ol by employing the tertiary alcohol desaturase function of the Rieske nonheme mononuclear iron oxygenase MdpJ., *J. Bacteriol. 194*, 972-981.
[21] Schäfer, F., Schuster, J., Würz, B., Härtig, C., Harms, H., Müller, R. H., and Rohwerder, T. (2012) Synthesis of short-chain diols and unsaturated alcohols from secondary alcohol substrates by the Rieske nonheme mononuclear iron oxygenase MdpJ., *Appl. Environ. Microbiol. 78*, 6280-6284.
[22] Kunugi, M., Takabayashi, A., and Tanaka, A. (2013) Evolutionary changes in chlorophyllide a oxygenase (CAO) structure contribute to the acquisition of a new light-harvesting complex in micromonas., *J. Biol. Chem. 288*, 19330-19341.
[23] Jiang, W., Wilson, M. A., and Weeks, D. P. (2013) O-demethylations catalyzed by rieske nonheme iron monooxygenases involve the difficult oxidation of a saturated C-H bond., *ACS Chem. Biol. 8*, 1687-1691.
[24] D'Ordine, R. L., Rydel, T. J., Storek, M. J., Sturman, E. J., Moshiri, F., Bartlett, R. K., Brown, G. R., Eilers, R. J., Dart, C., Qi, Y., Flasinski, S., and Franklin, S. J. (2009) Dicamba monooxygenase: Structural insights into a dynamic Rieske oxygenase that catalyzes an exocyclic monooxygenation, *J. Mol. Biol. 392*, 481-497.
[25] Dumitru, R., Jiang, W. Z., Weeks, D. P., and Wilson, M. A. (2009) Crystal structure of dicamba monooxygenase: A Rieske nonheme oxygenase that catalyzes oxidative demethylation, *J. Mol. Biol. 392*, 498-510.
[26] Priefert, H., Rabenhorst, J., and Steinbuechel, A. (1997) Molecular characterization of genes of *Pseudomonas sp*. strain HR199 involved in bioconversion of vanillin to protocatechuate, *J. Bacteriol. 179*, 2595-2607.
[27] Twilfer, H., Sandfort, G., and Bernhardt, F.-H. (2000) Substrate and solvent isotope effects on the fate of the active oxygen species in substrate-modulated reactions of putidamonooxin, *Eur. J. Biochem. 267*, 5926-5934.
[28] Bernhardt, F. H., Bill, E., Trautwein, A. X., and Twilfer, H. (1988) 4-Methoxybenzoate monooxygenase from *Pseudomonas putida*: isolation, biochemical properties, substrate specificity, and reaction mechanisms of the enzyme components, *Methods Enzymol. 161*, 281-294.
[29] Twilfer, H., Bernhardt, F. H., and Gersonde, K. (1985) Dioxygen-activating iron center in putidamonooxin. Electron spin resonance investigation of the nitrosylated putidamonooxin, *Eur. J. Biochem. 147*, 171-176.
[30] Bernhardt, F. H., Gersonde, K., Twilfer, H., Wende, P., Eckhard, B., Trautwein, A. X., and Pfleger, K. (1982) Dioxygen activation by putidamonooxin: substrate-modulated reaction of activated dioxygen, *Oxygenases Oxygen Metab., Symp. Honor Osamu Hayaishi*, 63-77.

[31] Twilfer, H., Bernhardt, F. H., and Gersonde, K. (1981) An electron-spin-resonance study on the redox-active centers of the 4-methoxybenzoate monooxygenase from Pseudomonas putida, *Eur. J. Biochem. 119*, 595-602.
[32] Wende, P., Pfleger, K., and Bernhardt, F. H. (1982) Dioxygen activation by putidamonooxin: substrate-modulated reaction of activated dioxygen, *Biochem. Biophys. Res. Commun. 104*, 527-532.
[33] Summers, R. M., Seffernick, J. L., Quandt, E. M., Yu, C. L., Barrick, J. E., and Subramanian, M. V. (2013) Caffeine junkie: an unprecedented GST-dependent oxygenase required for caffeine degradation by *P. putida* CBB5., *J. Bacteriol.*, JB.00585-00513-.
[34] Summers, R. M., Louie, T. M., Yu, C.-L., Gakhar, L., Louie, K. C., and Subramanian, M. (2012) Novel, highly specific N-demethylases enable bacteria to live on caffeine and related purine alkaloids., *J. Bacteriol. 194*, 2041-2049.
[35] Summers, R. M., Louie, T. M., Yu, C. L., and Subramanian, M. (2011) Characterization of a broad-specificity non-haem iron N-demethylase from *Pseudomonas putida* CBB5 capable of utilizing several purine alkaloids as sole carbon and nitrogen source, *Microbiology-(UK) 157*, 583-592.
[36] Gu, T., Zhou, C., Sørensen, S. R., Zhang, J., He, J., Yu, P., Yan, X., and Li, S. (2013) The novel bacterial N-demethylase PudmAB is responsible for the initial step of N,N-dimethyl-substituted phenylurea herbicides degradation, *Appl. Environ. Microbiol. 79*, 7846-7856.
[37] Daughtry, K. D., Xiao, Y., Stoner-Ma, D., Cho, E., Orville, A. M., Liu, P., and Allen, K. N. (2012) Quaternary ammonium oxidative demethylation: X-ray crystallographic, resonance Raman, and UV-visible spectroscopic analysis of a Rieske-type demethylase., *J. Am. Chem. Soc. 134*, 2823-2834.
[38] Najle, S. R., Nusblat, A. D., Nudel, C. B., and Uttaro, A. D. (2013) The sterol-C7 desaturase from the ciliate *Tetrahymena thermophila* is a Rieske oxygenase, which is highly conserved in animals., *Molecular biology and evolution 30*, 1630-1643.
[39] Wollam, J., Magomedova, L., Magner, D. B., Shen, Y., Rottiers, V., Motola, D. L., Mangelsdorf, D. J., Cummins, C. L., and Antebi, A. (2011) The Rieske oxygenase DAF-36 functions as a cholesterol 7-desaturase in steroidogenic pathways governing longevity, *Aging Cell 10*, 879-884.
[40] Yoshiyama-Yanagawa, T., Enya, S., Shimada-Niwa, Y., Yaguchi, S., Haramoto, Y., Matsuya, T., Shiomi, K., Sasakura, Y., Takahashi, S., Asashima, M., Kataoka, H., and Niwa, R. (2011) The conserved Rieske oxygenase DAF-36/Neverland is a novel cholesterol metabolizing enzyme, *J. Biol. Chem.*
[41] Lee, J., and Zhao, H. (2006) Mechanistic studies on the conversion of arylamines into arylnitro compounds by aminopyrrolnitrin oxygenase: identification of intermediates and kinetic studies., *Angew. Chem. Int. Ed. 45*, 622-625.
[42] Lee, J.-K., Ang, E.-L., and Zhao, H. (2006) Probing the substrate specificity of aminopyrrolnitrin oxygenase (PrnD) by mutational analysis., *J. Bacteriol. 188*, 6179-6183.
[43] Lee, J., Simurdiak, M., and Zhao, H. (2005) Reconstitution and characterization of aminopyrrolnitrin oxygenase, a Rieske N-oxygenase that catalyzes unusual arylamine oxidation., *J. Biol. Chem. 280*, 36719-36727.
[44] Sydor, P. K., Challis, G. L., and David, A. H. (2012) Oxidative tailoring reactions catalyzed by nonheme iron-dependent enzymes: Streptorubin B biosynthesis as an example, *Methods Enzymol. 516*, 195-218.

[45] Sydor, P. K., Barry, S. M., Odulate, O. M., Barona-Gomez, F., Haynes, S. W., Corre, C., Song, L., and Challis, G. L. (2011) Regio- and stereodivergent antibiotic oxidative carbocyclizations catalysed by Rieske oxygenase-like enzymes, *Nat. Chem. 3*, 388-392.
[46] Gibson, D. T., and Parales, R. E. (2000) Aromatic hydrocarbon dioxygenases in environmental biotechnology, *Curr. Opin. Biotechnol. 11*, 236-243.
[47] Aukema, K. G., Kasinkas, L., Aksan, A., and Wackett, L. P. (2014) Use of silica-encapsulated *Pseudomonas sp*. strain NCIB 9816-4 in biodegradation of novel hydrocarbon ring structures found in hydraulic fracturing waters, *Appl. Environ. Microbiol. 80*, 4968-4976.
[48] Sylvestre, M., Macek, T., and Mackova, M. (2009) Transgenic plants to improve rhizoremediation of polychlorinated biphenyls (PCBs), *Curr. Opin. Biotechnol. 20*, 242-247.
[49] Kolb, H. C., VanNieuwenhze, M. S., and Sharpless, K. B. (1994) Catalytic asymmetric dihydroxylation, *Chem. Rev. 94*, 2483-2547.
[50] Gally, C., Nestl, B. M., and Hauer, B. (2015) Engineering Rieske non-heme iron oxygenases for the asymmetric dihydroxylation of alkenes, *Angew. Chem. Int. Ed.*, n/a-n/a.
[51] Myers, A. G., Siegel, D. R., Buzard, D. J., and Charest, M. G. (2001) Synthesis of a broad array of highly functionalized, enantiomerically pure cyclohexanecarboxylic acid derivatives by microbial dihydroxylation of benzoic acid and subsequent oxidative and rearrangement reactions, *Org. Lett. 3*, 2923-2926.
[52] Lewis, S. E. (2014) Applications of biocatalytic arene ipso, ortho cis-dihydroxylation in synthesis, *Chem. Commun. 50*, 2821-2830.
[53] Charest, M. G., Lerner, C. D., Brubaker, J. D., Siegel, D. R., and Myers, A. G. (2005) A convergent enantioselective route to structurally diverse 6-deoxytetracycline antibiotics, *Science 308*, 395-398.
[54] Resnick, S. M., Lee, K., and Gibson, D. T. (1996) Diverse reactions catalyzed by naphthalene dioxygenase from *Pseudomonas sp.* strain NCIB 9816, *J. Ind. Microbiol. Biotechnol. 17*, 438-457.
[55] Kumar, P., Mohammadi, M., Dhindwal, S., Pham, T. T. M., Bolin, J. T., and Sylvestre, M. (2012) Structural insights into the metabolism of 2-chlorodibenzofuran by an evolved biphenyl dioxygenase., *Biochem. Biophys. Res. Commun. 421*, 757-762.
[56] Kumar, P., Mohammadi, M., Viger, J.-F., Barriault, D., Gomez-Gil, L., Eltis, L. D., Bolin, J. T., and Sylvestre, M. (2011) Structural insight into the expanded PCB-degrading abilities of a biphenyl dioxygenase obtained by directed evolution, *J. Mol. Biol. 405*, 531-547.
[57] Mohammadi, M., Viger, J.-F., Kumar, P., Barriault, D., Bolin, J. T., and Sylvestre, M. (2011) Retuning Rieske-type oxygenases to expand substrate range, *J. Biol. Chem. 286*, 27612-27621.
[58] Zhu, Y., Jameson, E., Crosatti, M., Schäfer, H., Rajakumar, K., Bugg, T. D. H., and Chen, Y. (2014) Carnitine metabolism to trimethylamine by an unusual Rieske-type oxygenase from human microbiota, *Proc. Natl. Acad. Sci. USA. 111*, 4268-4273.
[59] Fuchs, G., Boll, M., and Heider, J. (2011) Microbial degradation of aromatic compounds - from one strategy to four, *Nature Rev. Microbiol. 9*, 803-816.

[60] Ferraro, D. J., Gakhar, L., and Ramaswamy, S. (2005) Rieske business: Structure-function of Rieske non-heme oxygenases, *Biochem. Biophys. Res. Commun. 338*, 175-190.
[61] Jiang, H., Parales, R. E., and Gibson, D. T. (1999) The alpha subunit of toluene dioxygenase from *Pseudomonas putida* F1 can accept electrons from reduced FerredoxinTOL but is catalytically inactive in the absence of the beta subunit, *Appl. Environ. Microbiol. 65*, 315-318.
[62] Hurtubise, Y., Barriault, D., and Sylvestre, M. (1998) Involvement of the terminal oxygenase beta subunit in the biphenyl dioxygenase reactivity pattern toward chlorobiphenyls, *J. Bacteriol. 180*, 5828-5835.
[63] Ge, Y., and Eltis, L. D. (2003) Characterization of hybrid toluate and benzoate dioxygenases, *J. Bacteriol. 185*, 5333-5341.
[64] Parales, R. E., Emig, M. D., Lynch, N. A., and Gibson, D. T. (1998) Substrate specificities of hybrid naphthalene and 2,4-dinitrotoluene dioxygenase enzyme systems, *J. Bacteriol. 180*, 2337-2344.
[65] Capyk, J. K., and Eltis, L. D. (2012) Phylogenetic analysis reveals the surprising diversity of an oxygenase class, *J. Biol. Inorg. Chem. 17*, 425-436.
[66] Koehntop, K. D., Emerson, J. P., and Que, L., Jr. (2005) The 2-His-1-carboxylate facial triad: a versatile platform for dioxygen activation by mononuclear non-heme iron(II) enzymes, *J. Biol. Inorg. Chem. 10*, 87-93.
[67] Ohta, T., Chakrabarty, S., Lipscomb, J. D., and Solomon, E. I. (2008) Near-IR MCD of the nonheme ferrous active site in naphthalene 1,2-dioxygenase: Correlation to crystallography and structural insight into the mechanism of Rieske dioxygenases, *J. Am. Chem. Soc. 130*, 1601-1610.
[68] Carredano, E., Karlsson, A., Kauppi, B., Choudhury, D., Parales, R. E., Parales, J. V., Lee, K., Gibson, D. T., Eklund, H., and Ramaswamy, S. (2000) Substrate binding site of naphthalene 1,2-dioxygenase: Functional implications of indole binding, *J. Mol. Biol. 296*, 701-712.
[69] Friemann, R., Ivkovic-Jensen, M. M., Lessner, D. J., Yu, C.-L., Gibson, D. T., Parales, R. E., Eklund, H., and Ramaswamy, S. (2005) Structural insight into the dioxygenation of nitroarene compounds: the crystal structure of nitrobenzene dioxygenase, *J. Mol. Biol. 348*, 1139-1151.
[70] Ashikawa, Y., Fujimoto, Z., Usami, Y., Inoue, K., Noguchi, H., Yamane, H., and Nojiri, H. (2012) Structural insight into the substrate- and dioxygen-binding manner in the catalytic cycle of Rieske nonheme iron oxygenase system, carbazole 1,9a-dioxygenase, *BMC Structural Biology 12*, 15.
[71] Pabis, A., Geronimo, I., York, D. M., and Paneth, P. (2014) Molecular dynamics simulation of nitrobenzene dioxygenase using AMBER force field, *J. Chem. Theory Comput. 10*, 2246-2254.
[72] Kauppi, B., Lee, K., Carredano, E., Parales, R. E., Gibson, D. T., Eklund, H., and Ramaswamy, S. (1998) Structure of an aromatic-ring-hydroxylating dioxygenase-naphthalene 1,2-dioxygenase, *Structure 6*, 571-586.
[73] Parales, R. E., Parales, J. V., and Gibson, D. T. (1999) Aspartate 205 in the catalytic domain of naphthalene dioxygenase is essential for activity, *J. Bacteriol. 181*, 1831-1837.
[74] Beharry, Z. M., Eby, D. M., Coulter, E. D., Viswanathan, R., Neidle, E. L., Phillips, R. S., and Kurtz, D. M., Jr. (2003) Histidine ligand protonation and redox potential in the Rieske dioxygenases: Role of a conserved aspartate in anthranilate 1,2-dioxygenase, *Biochemistry 42*, 13625-13636.

[75] Batie, C., Ballou, D. P., and Correll, C. C. (1991) Phthalate dioxygenase reductase and related flavin-iron-sulfur containing electron transferases, In *Chemistry and Biochemistry of Flavoenzymes* (Müller, F., Ed.), pp 543-556, CRC Press, Boca Raton, Fl.
[76] Werlen, C., Kohler, H. P., and van der Meer, J. R. (1996) The broad substrate chlorobenzene dioxygenase and cis-chlorobenzene dihydrodiol dehydrogenase of *Pseudomonas sp.* strain P51 are linked evolutionarily to the enzymes for benzene and toluene degradation, *J. Biol. Chem. 271*, 4009-4016.
[77] Nam, J.-W., Nojiri, H., Yoshida, T., Habe, H., Yamane, H., and Omori, T. (2001) New classification system for oxygenase components involved in ring-hydroxylating oxygenations, *Biosci. Biotechnol. Biochem. 65*, 254-263.
[78] Kweon, O., Kim, S.-J., Baek, S., Chae, J.-C., Adjei, M., Baek, D.-H., Kim, Y.-C., and Cerniglia, C. (2008) A new classification system for bacterial Rieske non-heme iron aromatic ring-hydroxylating oxygenases, *BMC Biochemistry 9*, 1-20.
[79] Solomon, E. I., Light, K. M., Liu, L. V., Srnec, M., and Wong, S. D. (2013) Geometric and electronic structure contributions to function in non-heme iron enzymes, *Acc. Chem. Res. 46*, 2725-2739.
[80] Yang, T.-C., Wolfe, M. D., Neibergall, M. B., Mekmouche, Y., Lipscomb, J. D., and Hoffman, B. M. (2003) Substrate binding to NO-ferro-naphthalene 1,2-dioxygenase studied by high-resolution Q-band pulsed ^{2}H-ENDOR spectroscopy, *J. Am. Chem. Soc. 125*, 7056-7066.
[81] Yang, T.-C., Wolfe, M. D., Neibergall, M. B., Mekmouche, Y., Lipscomb, J. D., and Hoffman, B. M. (2003) Modulation of substrate binding to naphthalene 1,2-dioxygenase by Rieske cluster reduction/oxidation, *J. Am. Chem. Soc. 125*, 2034-2035.
[82] Poulos, T. L. (2014) Heme enzyme structure and function, *Chem. Rev. 114*, 3919-3962.
[83] Denisov, I. G., Makris, T. M., Sligar, S. G., and Schlichting, I. (2005) Structure and chemistry of cytochrome P450, *Chem. Rev. 105*, 2253-2277.
[84] Wallar, B. J., and Lipscomb, J. D. (1996) Dioxygen activation by enzymes containing binuclear non-heme iron clusters, *Chem. Rev. 96*, 2625-2657.
[85] Tinberg, C. E., and Lippard, S. J. (2011) Dioxygen activation in soluble methane monooxygenase, *Acc. Chem. Res. 44*, 280-288.
[86] Banerjee, R., Meier, K. K., Münck, E., and Lipscomb, J. D. (2013) Intermediate P* from soluble methane monooxygenase contains a diferrous cluster, *Biochemistry 52*, 4331-4342.
[87] Fielding, A. J., Lipscomb, J. D., and Que, L. J. (2014) A two-electron-shell game: intermediates of the extradiol-cleaving catechol dioxygenases, *J. Biol. Inorg. Chem. 19*, 491-504.
[88] Knoot, C. J., Purpero, V. M., and Lipscomb, J. D. (2015) Crystal structures of alkylperoxo and anhydride intermediates in an intradiol ring-cleaving dioxygenase, *Proc. Natl. Acad. Sci. USA 112*, 388-393.
[89] Martinez, S., and Hausinger, R. P. (2015) Catalytic mechanisms of Fe(II)- and 2-oxoglutarate-dependent oxygenases, *J. Biol. Chem. 290*, 20702-20711.
[90] Roberts, K. M., and Fitzpatrick, P. F. (2013) Mechanisms of tryptophan and tyrosine hydroxylase, *IUBMB Life 65*, 350-357.
[91] Dalton, H. (1980) Oxidation of hydrocarbons by methane monooxygenase from a variety of microbes, *Adv. Appl. Microbiol. 26*, 71-87.

[92] Tyson, C. A., Lipscomb, J. D., and Gunsalus, I. C. (1972) The role of putidaredoxin and $P450_{cam}$ in methylene hydroxylation, *J. Biol. Chem. 247*, 5777-5784.
[93] Ortiz de Montellano, P. R. (1995) *Cytochrome P450 : Structure, Mechanism, and Biochemistry*, Plenum Press, New York.
[94] Liu, K. E., Valentine, A. M., Wang, D. L., Huynh, B. H., Edmondson, D. E., Salifoglou, A., and Lippard, S. J. (1995) Kinetic and spectroscopic characterization of intermediates and component interactions in reactions of methane monooxygenase from *Methylococcus capsulatus* (Bath), *J. Am. Chem. Soc. 117*, 10174-10185.
[95] Lee, S. K., and Lipscomb, J. D. (1999) Oxygen activation catalyzed by methane monooxygenase hydroxylase component: Proton delivery during the O-O bond cleavage steps, *Biochemistry. 38*, 4423-4432.
[96] Davydov, R., Makris, T. M., Kofman, V., Werst, D. E., Sligar, S. G., and Hoffman, B. M. (2001) Hydroxylation of camphor by reduced oxy-cytochrome $P450_{cam}$: Mechanistic implications of EPR and ENDOR studies of catalytic intermediates in native and mutant enzymes, *J. Am. Chem. Soc. 123*, 1403-1415.
[97] Kovaleva, E. G., and Lipscomb, J. D. (2008) Versatility of biological non-heme Fe(II) centers in oxygen activation reactions, *Nat. Chem. Biol. 4*, 186-193.
[98] Andersson, K. K., Froland, W. A., Lee, S.-K., and Lipscomb, J. D. (1991) Dioxygen independent oxygenation of hydrocarbons by methane monooxygenase hydroxylase component, *New J. Chem. 15*, 411-415.
[99] Hrycay, E. G., Gustafsson, J. A., Ingelman-Sundberg, M., and Ernster, L. (1976) The involvement of cytochrome P-450 in hepatic in hepatic microsomal steroid hydroxylation reactions supported by sodium periodate, sodium chlorite, and organic hydroperoxides, *Eur. J. Biochem. 61*, 43-52.
[100] Wolfe, M. D., and Lipscomb, J. D. (2003) Hydrogen peroxide-coupled *cis*-diol formation catalyzed by naphthalene 1,2-dioxygenase, *J. Biol. Chem. 278*, 829-835.
[101] Bassan, A., Blomberg, M. R. A., and Siegbahn, P. E. M. (2004) A theoretical study of the *cis*-dihydroxylation mechanism in naphthalene 1,2-dioxygenase, *J. Biol. Inorg. Chem. 9*, 439-452.
[102] Pabis, A., Geronimo, I., and Paneth, P. (2014) A DFT study of the cis-dihydroxylation of nitroaromatic compounds catalyzed by nitrobenzene dioxygenase, *J. Phys. Chem. B 118*, 3245-3256.
[103] Chen, K., Costas, M., Kim, J., Tipton, A. K., and Que, L., Jr. (2002) Olefin cis-dihydroxylation versus epoxidation by non-heme iron catalysts: two faces of an Fe^{III}-OOH coin, *J. Am. Chem. Soc. 124*, 3026-3035.
[104] Prat, I., Mathieson, J. S., Guell, M., Ribas, X., Luis, J. M., Cronin, L., and Costas, M. (2011) Observation of Fe(V)=O using variable-temperature mass spectrometry and its enzyme-like C-H and C=C oxidation reactions, *Nat. Chem. 3*, 788-793.
[105] Oloo, W. N., Fielding, A. J., and Que, L., Jr. (2013) Rate-determining water-assisted O-O bond cleavage of an Fe(III)-OOH intermediate in a bio-inspired nonheme iron-catalyzed oxidation, *J. Am. Chem. Soc. 135*, 6438-6441.
[106] Liu, L. V., Hong, S., Cho, J., Nam, W., and Solomon, E. I. (2013) Comparison of high-spin and low-spin nonheme Fe(III)-OOH complexes in O-O bond homolysis and H-atom abstraction reactivities., *J. Am. Chem. Soc. 135*, 3286-3299.
[107] Meier, K. K., Rogers, M. S., Kovaleva, E. G., Mbughuni, M. M., Bominaar, E. L., Lipscomb, J. D., and Münck, E. (2015) A long-lived Fe(III)-(hydroperoxo)

intermediate in the active H200C variant of homoprotocatechuate 2,3-dioxygenase: Characterization by Mössbauer, electron paramagnetic resonance, and density functional theory methods, *Inorg. Chem. 54*, 10269-10280.
[108] Tiwari, M. K., Lee, J. K., Moon, H. J., and Zhao, H. (2011) Further biochemical studies on aminopyrrolnitrin oxygenase (PrnD), *Bioorg Med Chem Lett 21*, 2873-2876.
[109] Vergé, D., and Arrio-Dupont, M. (1981) Interactions between apoaspartate aminotransferase and pyridoxal 5'-phosphate. A stopped-flow study, *Biochemistry 20*, 1210-1216.
[110] Reiner, A. M., and Hegeman, G. D. (1971) Metabolism of benzoic acid by bacteria. Accumulation of (-)-3,5-cyclohexadiene-1,2-diol-1-carboxylic acid by mutant strain of *Alcaligenes eutrophus*, *Biochemistry 10*, 2530-2536.
[111] Jenkins, G. N., Ribbons, D. W., Widdowson, D. A., Slawin, A. M. Z., and Williams, D. J. (1995) Synthetic application of biotransformations: absolute stereochemistry and Diels-Alder reactions of the (1S,2R)-1,2-dihydroxycyclohexa-3,5-diene-1-carboxylic acid from *Pseudomonas putida*, *J. Chem. Soc., Perkin Trans. 1*, 2647-2655.
[112] Tarasev, M., Rhames, F., and Ballou, D. P. (2004) Rates of the phthalate dioxygenase reaction with oxygen are dramatically increased by interactions with phthalate and phthalate oxygenase reductase, *Biochemistry 43*, 12799-12808.
[113] Bernhardt, F. H., Ruf, H. H., and Ehrig, H. (1974) A 4-methoxybenzoate monooxygenase system from *Pseudomonas putida*. Circular dichroism studies on the iron--sulfur protein, *FEBS Lett. 43*, 53-55.
[114] Bassan, A., Blomberg, M. R. A., Borowski, T., and Siegbahn, P. E. M. (2004) Oxygen activation by Rieske non-heme iron oxygenases, a theoretical insight, *J. Phys. Chem. B 108*, 13031-13041.
[115] Lee, K. (1999) Benzene-induced uncoupling of naphthalene dioxygenase activity and enzyme inactivation by production of hydrogen peroxide, *J. Bacteriol. 181*, 2719-2725.
[116] Perez-Pantoja, D., Nikel, P. I., Chavarria, M., and de Lorenzo, V. (2013) Endogenous stress caused by faulty oxidation reactions fosters evolution of 2,4-dinitrotoluene-degrading bacteria, *PLoS Genet. 9*, e1003764.
[117] Roelfes, G., Vrajmasu, V., Chen, K., Ho, R. Y. N., Rohde, J.-U., Zondervan, C., la Crois, R. M., Schudde, E. P., Lutz, M., Spek, A. L., Hage, R., Feringa, B. L., Münck, E., and Que, L., Jr. (2003) End-on and side-on peroxo derivatives of non-heme iron complexes with pentadentate ligands: Models for putative intermediates in biological iron/dioxygen chemistry, *Inorg. Chem. 42*, 2639-2653.
[118] Mbughuni, M. M., Chakrabarti, M., Hayden, J. A., Meier, K. K., Dalluge, J. J., Hendrich, M. P., Münck, E., and Lipscomb, J. D. (2011) Oxy-intermediates of homoprotocatechuate 2,3-dioxygenase: Facile electron transfer between substrates, *Biochemistry 50*, 10262-10274.
[119] Mbughuni, M. M., Chakrabarti, M., Hayden, J. A., Bominaar, E. L., Hendrich, M. P., Münck, E., and Lipscomb, J. D. (2010) Trapping and spectroscopic characterization of an Fe^{III}-superoxo intermediate from a nonheme mononuclear iron-containing enzyme, *Proc. Natl. Acad. Sci. USA 107*, 16788-16793.
[120] Brown, C. D., Neidig, M. L., Neibergall, M. B., Lipscomb, J. D., and Solomon, E. I. (2007) VTVH-MCD and DFT studies of thiolate bonding to $\{FeNO\}^7/\{FeO_2\}^8$ complexes of isopenicillin N synthase: Substrate determination of oxidase versus oxygenase activity in nonheme Fe enzymes, *J. Am. Chem. Soc. 129*, 7427-7438.

[121] Whittaker, J. W., and Lipscomb, J. D. (1984) Transition state analogs for protocatechuate 3,4-dioxygenase. Spectroscopic and kinetic studies of the binding reactions of ketonized substrate analogs, *J. Biol. Chem. 259*, 4476-4486.
[122] Zhao, Y., and Truhlar, D. G. (2008) The M06 suite of density functionals for main group thermochemistry, thermochemical kinetics, noncovalent interactions, excited states, and transition elements: two new functionals and systematic testing of four M06-class functionals and 12 other functionals, *Theor. Chem. Acc. 120*, 215-241.
[123] Hehre, W. J., Random, L., Schleyer, P. v. R., and Pople, J. A. (1986) *Ab Initio Molecular Orbital Theory*, Wiley, New York.
[124] Marenich, A. V., Cramer, C. J., and Truhlar, D. G. (2009) Universal solvation model based on solute electron density and on a continuum model of the solvent defined by the bulk dielectric constant and atomic surface tensions, *J. Phys. Chem. B 113*, 6378-6396.
[125] Marenich, A. V., Jerome, S. V., Cramer, C. J., and Truhlar, D. G. (2012) Charge model 5: An extension of Hirshfeld population analysis for the accurate description of molecular interactions in gaseous and condensed phases, *J. Chem. Theory Comput. 8*, 527-541.
[126] Frisch, M. J., Trucks, G. W., Schlegel, H. B., Scuseria, G. E., Robb, M. A., Cheeseman, J. R., Scalmani, G., Barone, V., Mennucci, B., Petersson, G. A., Nakatsuji, H., Caricato, M., Li, X., Hratchian, H. P., Izmaylov, A. F., Bloino, J., Zheng, G., Sonnenberg, J. L., Hada, M., Ehara, M., Toyota, K., Fukuda, R., Hasegawa, J., Ishida, M., Nakajima, T., Honda, Y., Kitao, O., Nakai, H., Vreven, T., Montgomery, J. A., Peralta, J. E., Ogliaro, F., Bearpark, M., Heyd, J. J., Brothers, E., Kudin, K. N., Staroverov, V. N., Kobayashi, R., Normand, J., Raghavachari, K., Rendell, A., Burant, J. C., Iyengar, S. S., Tomasi, J., Cossi, M., Rega, N., Millam, J. M., Klene, M., Knox, J. E., Cross, J. B., Bakken, V., Adamo, C., Jaramillo, J., Gomperts, R., Stratmann, R. E., Yazyev, O., Austin, A. J., Cammi, R., Pomelli, C., Ochterski, J. W., Martin, R. L., Morokuma, K., Zakrzewski, V. G., Voth, G. A., Salvador, P., Dannenberg, J. J., Dapprich, S., Daniels, A. D., Farkas, Ö., Foresman, J. B., Ortiz, J. V., Cioslowski, J., and Fox, D. J. (2010) Gaussian 09, Revision C.01, Gaussian Inc., Wallingford, CT.
[127] Marenich, A. V., Cramer, C. J., and Truhlar, D. G. (2011) CM5PAC, University of Minnesota, Minneapolis.
[128] Liu, Y., Nesheim, J. C., Lee, S.-K., and Lipscomb, J. D. (1995) Gating effects of component B on oxygen activation by the methane monooxygenase hydroxylase component, *J. Biol. Chem. 270*, 24662-24665.
[129] DuBois, J. L., and Klinman, J. P. (2005) The nature of O_2 reactivity leading to topa quinone in the copper amine oxidase from *Hansenula polymorpha* and its relationship to catalytic turnover, *Biochemistry 44*, 11381-11388.
[130] Orville, A. M., Lipscomb, J. D., and Ohlendorf, D. H. (1997) Crystal structures of substrate and substrate analog complexes of protocatechuate 3,4-dioxygenase: endogenous Fe^{3+} ligand displacement in response to substrate binding, *Biochemistry 36*, 10052-10066.
[131] Karlsson, A., Parales, J. V., Parales, R. E., Gibson, D. T., Eklund, H., and Ramaswamy, S. (2005) NO binding to naphthalene dioxygenase, *J. Biol. Inorg. Chem. 10*, 483-489.

[132] Orville, A. M., and Lipscomb, J. D. (1993) Simultaneous binding of nitric oxide and isotopically labeled substrates or inhibitors by reduced protocatechuate 3,4-dioxygenase, *J. Biol. Chem. 268*, 8596-8607.
[133] Arciero, D. M., Lipscomb, J. D., Huynh, B. H., Kent, T. A., and Münck, E. (1983) EPR and Mössbauer studies of protocatechuate 4,5-dioxygenase. Characterization of a new Fe^{2+} environment, *J. Biol. Chem. 258*, 14981-14991.
[134] Schenk, G., Pau, M. Y. M., and Solomon, E. I. (2004) Comparison between the geometric and electronic structures and reactivities of $\{FeNO\}^7$ and $\{FeO_2\}^8$ complexes: A density functional theory study, *J. Am. Chem. Soc. 126*, 505-515.
[135] Tinberg, C. E., Tonzetich, Z. J., Wang, H., Do, L. H., Yoda, Y., Cramer, S. P., and Lippard, S. J. (2010) Characterization of iron dinitrosyl species formed in the reaction of nitric oxide with a biological Rieske center, *J. Am. Chem. Soc. 132*, 18168-18176.
[136] Bugg, T. D. H., and Ramaswamy, S. (2008) Non-heme iron-dependent dioxygenases: unravelling catalytic mechanisms for complex enzymatic oxidations, *Curr. Opin. Chem. Biol. 12*, 134-140.
[137] Shaik, S., Cohen, S., Wang, Y., Chen, H., Kumar, D., and Thiel, W. (2010) P450 enzymes: Their structure, reactivity, and selectivities modeled by QM/MM calculations, *Chem. Rev. 110*, 949-1017.
[138] Kovaleva, E. G., Neibergall, M. B., Chakrabarty, S., and Lipscomb, J. D. (2007) Finding intermediates in the O_2 activation pathways of non-heme iron oxygenases, *Acc. Chem. Res. 40*, 475-483.
[139] Lipscomb, J. D. (2008) Mechanism of extradiol aromatic ring-cleaving dioxygenases, *Curr. Opin. Struct. Biol. 18*, 644-649.
[140] Kovaleva, E. G., and Lipscomb, J. D. (2007) Crystal structures of Fe^{2+} dioxygenase superoxo, alkylperoxo, and bound product intermediates, *Science 316*, 453-457.
[141] Lundberg, M., Siegbahn, P. E. M., and Morokuma, K. (2008) The mechanism for isopenicillin N synthase from density-functional modeling highlights the similarities with other enzymes in the 2-His-1-carboxylate family, *Biochemistry 47*, 1031-1042.
[142] Capece, L., Lewis-Ballester, A., Yeh, S.-R., Estrin, D. A., and Marti, M. A. (2012) Complete reaction mechanism of indoleamine 2,3-dioxygenase as revealed by QM/MM simulations, *J. Phys. Chem. B 116*, 1401-1413.
[143] Chung, L. W., Li, X., Sugimoto, H., Shiro, Y., and Morokuma, K. (2010) ONIOM study on a missing piece in our understanding of heme chemistry: Bacterial tryptophan 2,3-dioxygenase with dual oxidants, *J. Am. Chem. Soc. 132*, 11993-12005.
[144] Basran, J., Efimov, I., Chauhan, N., Thackray, S. J., Krupa, J. L., Eaton, G., Griffith, G. A., Mowat, C. G., Handa, S., and Raven, E. L. (2011) The mechanism of formation of N-formylkynurenine by heme dioxygenases, *J. Am. Chem. Soc. 133*, 16251-16257.
[145] Yuan, C., Liang, Y., Hernandez, T., Berriochoa, A., Houk, K. N., and Siegel, D. (2013) Metal-free oxidation of aromatic carbon-hydrogen bonds through a reverse-rebound mechanism., *Nature 499*, 192-196.
[146] Li, F., Meier, K. K., Cranswick, M. A., Chakrabarti, M., Van Heuvelen, K. M., Münck, E., and Que, L., Jr. (2011) Characterization of a high-spin non-heme Fe^{III}−OOH intermediate and its quantitative conversion to an Fe^{IV} = O complex, *J. Am. Chem. Soc. 133*, 7256-7259.

[147] Li, F., Van, H. K. M., Meier, K. K., Münck, E., and Que, L., Jr. (2013) Sc^{3+}-triggered oxoiron(IV) formation from O_2 and its non-heme iron(II) precursor via a Sc^{3+}-peroxo-Fe^{3+} intermediate, *J. Am. Chem. Soc. 135*, 10198-10201.
[148] Cohen-Bazire, G., Sistrom, W. R., and Stanier, R. Y. (1957) *J. Cell. Physiol. 49*, 25-68.
[149] Liu, L. V., Bell, C. B., III, Wong, S. D., Wilson, S. A., Kwak, Y., Chow, M. S., Zhao, J., Hodgson, K. O., Hedman, B., and Solomon, E. I. (2010) Definition of the intermediates and mechanism of the anticancer drug bleomycin using nuclear resonance vibrational spectroscopy and related methods, *Proc. Natl. Acad. Sci. USA 107*, 22419-22424.
[150] Scheidt, W. R., Durbin, S. M., and Sage, J. T. (2005) Nuclear resonance vibrational spectroscopy - NRVS, *J. Inorg. Biochem. 99*, 60-71.
[151] Cho, J., Jeon, S., Wilson, S. A., Liu, L. V., Kang, E. A., Braymer, J. J., Lim, M. H., Hedman, B., Hodgson, K. O., Valentine, J. S., Solomon, E. I., and Nam, W. (2011) Structure and reactivity of a mononuclear non-heme iron(III)-peroxo complex, *Nature 478*, 502-505.
[152] Wada, A., Ogo, S., Nagatomo, S., Kitagawa, T., Watanabe, Y., Jitsukawa, K., and Masuda, H. (2002) Reactivity of hydroperoxide bound to a mononuclear non-heme iron site, *Inorg. Chem. 41*, 616-618.
[153] Shiemke, A. K., Loehr, T. M., and Sanders-Loehr, J. (1984) Resonance Raman study of the m-oxo-bridged binuclear iron center in oxyhemerythrin, *J. Am. Chem. Soc. 106*, 4951-4956.
[154] Kitagawa, T., Dey, A., Lugo-Mas, P., Benedict, J. B., Kaminsky, W., Solomon, E., and Kovacs, J. A. (2006) A functional model for the cysteinate-ligated non-heme iron enzyme superoxide reductase (SOR), *J. Am. Chem. Soc. 128*, 14448-14449.
[155] Zang, Y., Kim, J., Dong, Y. H., Wilkinson, E. C., Appelman, E. H., and Que, L., Jr. (1997) Models for nonheme iron intermediates: Structural basis for tuning the spin states of Fe(TPA) complexes, *J. Am. Chem. Soc. 119*, 4197-4205.
[156] Wada, A., Ogo, S., Watanabe, Y., Mukai, M., Kitagawa, T., Jitsukawa, K., Masuda, H., and Einaga, H. (1999) Synthesis and characterization of novel alkylperoxo mononuclear iron(III) complexes with a tripodal pyridylamine ligand: a model for peroxo intermediates in reactions catalyzed by non-heme iron enzymes, *Inorg. Chem. 38*, 3592-3593.
[157] Namuswe, F., Hayashi, T., Jiang, Y., Kasper, G. D., Sarjeant, A. A. N., Moenne-Loccoz, P., and Goldberg, D. P. (2010) Influence of the nitrogen donors on nonheme iron models of superoxide reductase: High-spin FeIII-OOR complexes, *J. Am. Chem. Soc. 132*, 157-167.
[158] Liu, J.-G., , Ohta, T., Yamaguchi, S., Ogura, T., Sakamoto, S., Maeda, Y., and Naruta, Y. (2009) Spectroscopic characterization of a hydroperoxo–heme intermediate: Conversion of a side-on peroxo to an end-on hydroperoxo complex, *Angew. Chem. Int. Ed. 48*, 9262-9267.
[159] Mathe, C., Mattioli, T. A., Horner, O., Lombard, M., Latour, J.-M., Fontecave, M., and Niviere, V. (2002) Identification of iron(III) peroxo species in the active site of the superoxide reductase SOR from *Desulfoarculus baarsii*, *J. Am. Chem. Soc. 124*, 4966-4967.
[160] Münck, E. (2000) Aspects of ^{57}Fe Mössbauer spectroscopy, In *Physical Methods in Bioinorganic Chemistry* (Que, L., Jr, Ed.), pp 287-319, University Science Books, Sausalito, CA.

[161] Lehnert, N., Fujisawa, K., and Solomon, E. I. (2003) Electronic structure and reactivity of high-spin iron-alkyl- and -pterinperoxo complexes, *Inorg. Chem. 42*, 469-481.
[162] Bassan, A., Blomberg, M. R. A., and Siegbahn, P. E. M. (2003) Mechanism of dioxygen cleavage in tetrahydrobiopterin-dependent amino acid hydroxylases, *Chem. Eur. J. 9*, 106-115.
[163] Paria, S., Que, L., Jr., and Paine, T. K. (2011) Oxidative decarboxylation of benzilic acid by a biomimetic iron(II) complex: evidence for an iron(IV)-oxo-hydroxo oxidant from O_2, *Angew. Chem. Int. Ed. 50*, 11129-11132.
[164] Gibson, D. T., Resnick, S. M., Lee, K., Brand, J. M., Torok, D. S., Wackett, L. P., Schocken, M. J., and Haigler, B. E. (1995) Desaturation, dioxygenation, and monooxygenation reactions catalyzed by naphthalene dioxygenase from *Pseudomonas sp*. strain 9816-4, *J. Bacteriol. 177*, 2615-2621.
[165] Chakrabarty, S., Austin, R. N., Deng, D., Groves, J. T., and Lipscomb, J. D. (2007) Radical intermediates in monooxygenase reactions of Rieske dioxygenases, *J. Am. Chem. Soc. 129*, 3514-3515.